2013

Development of a Mathematical Model for Electrically Assisted Oil Transport in Porous Media

Ehsan Ghazanfari
Lehigh University

DEVELOPMENT OF A MATHEMATICAL MODEL FOR ELECTRICALLY ASSISTED OIL TRANSPORT IN POROUS MEDIA

by

Ehsan Ghazanfari

Presented to the Graduate and Research Committee
of Lehigh University
in Candidacy for the Degree of
Doctor of Philosophy

in
Civil Engineering

Lehigh University
(September 2013)

Approved and recommended for acceptance as a dissertation in partial fulfillment of the requirement for the degree of Doctor of Philosophy.

_____

Accepted Date

Committee Members:

_____

Sibel Pamukcu (Ph.D. Advisor)

Professor, Department of Civil and Environmental Engineering
Lehigh University

_____

Muhannad T. Suleiman (Committee Chair)

Assistant Professor, Department of Civil and Environmental Engineering
Lehigh University

_____

Philip A. Blythe
Professor, Department of Mechanical Engineering and Mechanics
Lehigh University

_____

Akram N. Alshawabkeh
Professor, Department of Civil and Environmental Engineering
Northeastern University

_____

Mesut Pervizpour
Assistant Professor, Department of Civil and Environmental Engineering
Lafayette College

_____

George Chilingar
Distinguished Emeritus Professor, Department of Civil and Environmental Engineering
University of Southern California

Acknowledgments

I would like to express the deepest appreciation to my advisor, Professor Pamukcu, who has the attitude and the substance of a genius: she continually and convincingly conveyed a spirit of adventure in regard to research and scholarship, and an excitement in regard to teaching. Without her guidance and persistent help this dissertation would not have been possible.

I would like to thank my Graduate Committee members, Professor Suleiman, Professor Blythe, Professor Alshawabkeh, Professor Pervizpour, and Professor Chilingar for their intellectual support through the years of my doctoral study. I also wish to thank Dr. Wittle for his support and valuable comments and discussions throughout this research study.

My heartfelt thanks to my parents for supporting me throughout my life. Finally, my loving thanks to my wife, Samaneh, who has endlessly and patiently supported me in finishing my doctoral study.

Contents

List of Tables

List of Figures

Abstract

In this study, it was attempted to develop a mathematical model for electrically assisted oil transport in porous media. The main implementation of the model would be in predicting the oil recovery in electrically enhanced oil recovery method. First, the contributing factors to the electrically assisted oil transport in porous media were investigated through laboratory experiments. Some of these contributing factors were found to be (i) viscous drag of oil with electro-osmosis of the water phase, primarily controlled by the oil/water ratio and the hydraulic and electro-osmotic permeability of the formation; (ii) reduction of oil-water interfacial tension due to electrochemical transformation of oil that affect its viscosity, hence increases its mobility, and (iii) increase in the permeability of the formation rock under applied electric field.

A mathematical model that couples the pressure and electric gradients applied to the porous medium and incorporates the viscous drag of water on the oil phase under applied electric gradient was developed. Implicit Pressure Explicit Saturation (IMPES) solution strategy was used to solve the set of governing equations and Finite Volume Method (FVM) was used to solve the model numerically and to run several simulations. One of the most important constitutive relationships necessary for solution of the model, relative permeability coefficients as a function of water saturation, were introduced and evaluated under applied electric field in this study.

Although it was attempted to capture the most important parameters in the development of the mathematical model, to have a model that more realistically represent the electrically assisted oil recovery phenomena in reservoir scale, the transient change in the viscosity of formation oil and the non-isothermal effects should also be considered in the model for future researches.

Chapter 1

Introduction

The theoretical development of electrokinetic transport has a long and distinguished tradition, which includes the works of Helmholtz [50], Nernst [81], Planck [89], and Warburg [107]. The theoretical understanding has been applied successfully in many electrochemical systems in different areas such as: energy storage and conversion, water treatment, microfluidics, metallurgy and semiconductor and MEMs devices. Among these, electrokinetically driven mass transport in porous medium has been of special interest to soil scientists, environmental and geotechnical engineers because of its ability to help strip and extract contaminating chemicals from low permeability clay soils.

Electrically assisted mass transport of hydrocarbon compounds in natural porous media has gained much attention not only for environmental mitigation of contaminating oils, but also recovery of reservoir oils over the last two decades [4, 9, 10, 27, 28, 41, 42, 59, 82, 83, 84, 91, 109, and 112]. Applying a direct current (DC) to activate ElectroKinetic (EK) phenomena near the solid-liquid interfaces inside the porous media constitutes the basic concept of this method. As a result, the water, solutes, micelles and colloids that reside in the pore space or in the vicinity of the pore walls are transported from one electrode to the other where they can be collected, immobilized, treated or transformed.

The remediation of oil-contaminated soils is a challenging area in geo-environmental engineering, which often requires a thorough knowledge of the contamination history and its distribution, and reliable mathematical models to predict the transport of the oil in multi-phase flow. The mathematical models of electrokinetically driven contaminant migration, which

emerged in early 90s focused mostly on the charged, ionic or dissolved compounds in the pore fluid [1, 2, 7, 8, 35, and 102]. Sites with high groundwater tables have shown to respond well to electrokinetic treatment of hydrocarbon compounds [22, 51, 64, 68, 69, 83, and 112], but the predictive capabilities that integrate multi-phase flow with electrokinetic transport and recovery of the hydrocarbon mass is lacking. In electrically enhanced oil recovery applications, the phenomenon leads to oil transport under an applied electric field in reservoirs [4, 41, 47, 63, 109, and 110]. Although there are numerous multi-phase flow models used to predict oil recovery rate under applied and reservoir pressures in petroleum engineering [13, 16, 30, 37, and 46], there is no working model of this transport under an electrical gradient.

1.1. Scope

Mathematical modeling of electrically assisted oil transport in porous media necessitates incorporating different contributing factors. Better understanding of the contributing factors to the oil recovery in this method necessitates a comprehensive experimental program to first understand the physics involved in the phenomena, and then to capture the essential parameters that impact the flow and oil recovery, and finally incorporate the variables and parameters in a mathematical model.

This study includes an experimental program to determine the underlying parameters contributing to electrically enhanced oil recovery, the mathematical modeling of the two phase flow under applied hydraulic and electrical gradients, and numerical simulation of the two phase flow based on the developed model. The model attempts to couple equations that govern electrosmotic flow transport with those of two-phase flow for a well-defined porous system.

The multi-physic nature of the problem in hand makes it very challenging to incorporate the effect of all the physical phenomena through variables and parameters in the mathematical model.

The experimental part of this study revealed that changes in the permeability of the formation under applied electric field has a great influence on the oil recovery in this method. Also, electrochemical reactions taking place in the formation under applied direct current promote transformation of formation oil, which in turn lowers the viscosity of the formation oil over time. The non-isothermal effects resulting from temperature increase in the formation due to resistivity of the formation under applied electric field result in transient changes in thr viscosity of the formation.

The developed model does not address these phenomena and instead focuses on the coupling of applied electric gradient (through electroosmotic drag) with pressure gradient which is believed to be the most important contributing factor in electrically enhanced oil recovery. Implicit Pressure Explicit Saturation (IMPES) solution strategy is implemented to solve the system of governing equations. The model is solved numerically using finite volume method.

1.2. Contents

Chapter 2 provides background information on classical treatise of electrically assisted mass transport in porous media, relevant models of oil transport in porous media, and laboratory and field experimental results conducted in this study to investigate the contribution of different underlying mechanism to the oil recovery under applied electric field.

Chapter 3 discusses the set of governing equations for single phase flow, two phase flow under applied pressure and electrical gradients, contribution of viscous coupling in two phase flow, solution techniques for the set of governing equations, and the up-scaling issues in modeling of the phenomena.

The experimental and analytical evaluation of transport coefficients under applied direct current which are required for numerical modeling of the phenomena are discussed in chapter 4. The scaling issues in evaluation of electroosmotic transport coefficients are also discussed in this chapter.

Implementation of Finite Volume Method (FVM) for numerical modeling of the single phase flow, and two phase flow under applied pressure and electric gradients are discussed in chapter 5. The discretization of pressure and saturation equations and the implicit and explicit solvers are also discussed in this chapter.

Several simulations for single and two phase flow under applied pressure and electrical gradients are performed using finite volume method in chapter 6. Finally, chapter 7 provides the summary and conclusions of this study.

Chapter 2

Background and Experimental Results

2.1 Classical treatise of electrically assisted mass transport

As in many electrochemical systems, flow of electric current through a network of a multi-phase system occurs in different phases simultaneously, in the bulk liquid (electrolyte in the pores), on the surface of the solid (clay particles), and in the interface layer(s) between the solid and the liquid. Flow of the current can be achieved by ionic conduction through the liquid phase and electronic conduction through the solid phase and the interface layer(s). The electronic conduction orthogonal to and along the interface layer(s) takes place via charge transfer. In the classical treatise of "electrokinetic phenomenon" in colloidal systems [54, and 75] it is this interface, known as the electric double layer which plays a critical role in the coupling between the ion motion and the fluid flow. The double layer intrinsically connects the solid and the liquid phase, and mediates the relative motion between the liquid and solid phase through (i) accumulation of charge density; (ii) transport of charge and ions along surface; and (iii) passage of charge to the surrounding electrolyte [14].

The bulk transport of ions in electrochemical systems without the contribution of advection is described by Poisson-Nernst-Planck (PNP) equations [93]. The well-known Nernst-Planck equation describes the processes of diffusion: the process that drives the ions from regions of higher concentration to regions of lower concentration; and electromigration (also referred to as migration), the process that launches the ions in the direction of the electric field [14]. Since the ions themselves contribute to the local electric potential, Poisson's equation that relates the electrostatic potential to local ion concentrations is solved simultaneously to describe this effect.

The electroneutrality assumption simplifies the mathematical treatise of bulk transport in most electrochemical systems. Nevertheless, this "no charge density accumulation" assumption does not hold true at the interface regions of electric double layer between the solid and liquid, hence become the cause of most electrokinetic phenomenon in clay-electrolyte systems, as summarized below.

Electroosmosis:

Electroosmosis is the fluid movement with respect to a solid wall as a result of an applied electric potential gradient. Fluid flux due to the applied electric gradient is given by the Helmholtz- Smoluchowski theory as:

$$J_w^e = k_{eo} \nabla(-E) \tag{2.1}$$

Where, k_{eo} $(k_{eo} = \frac{\varepsilon \xi}{\mu})$ is electroosmosis permeability, ε is permittivity of the medium, ξ is zeta potential, E is electric potential, and μ is dynamic viscosity of pore fluid. Electrosmotic flow is believed to be the main driving force in electrically assisted transport of hydrocarbon compounds in porous media.

Electromigration:

Electromigration is the migration of the ionic components between the anode and the cathode under the applied electric field. Most organic compounds in oil bearing formations are non-polar/non-ionic or form neutral micelles and surface coated colloids and could not be transported by electromigration. However, in cases when organic compounds are ionized or form acid and base complexes, they would migrate under the applied electric field [84]. Mass flux due to ion migration is given as:

$$J_i = -u_i c_i \frac{\partial E}{\partial x} \quad (2.2)$$

$$u_i = \frac{D_i Z_i F}{RT} \quad (2.3)$$

Where,

u_i is the effective ionic mobility of species i at infinite dilution ($L^2\ T^{-1}V^{-1}$)

Z_i is the charge of the ith species (Coulomb)

F is Faraday's constant (96,485 C/mo1 electrons)

R is the universal gas constant (8.3144 J/Kmol)

T is the absolute temperature (K)

Electrophoresis:

Electrophoresis induces movement of the charged colloidal particles or surface charged micelles free to move in the pore liquids. Organic compounds with relatively large molecular structures tend to form colloidal electrolytes or ionic micelles that could be transported by electrophoresis [55]. Figure 2.1 shows a schematic of micro-scale pore processes involved in electrically assisted hydrocarbon transport in porous media.

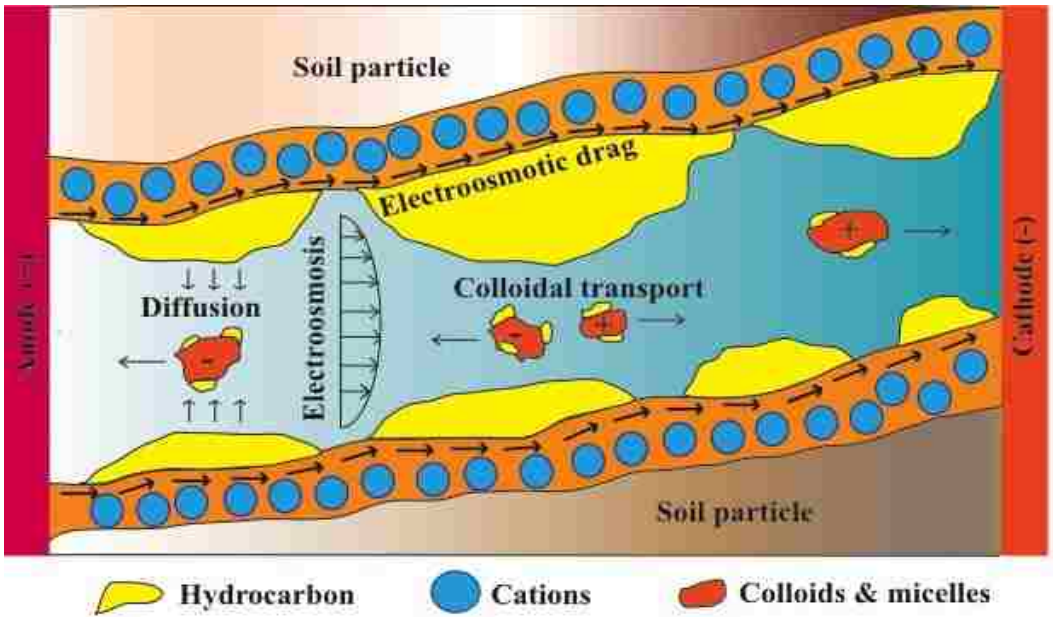

Figure 2.1. Pore processes in electrically assisted oil transport

2.2 "Electroosmotic pump" analogy in soils

Soils subjected to electrokinetic mass transport through their porous structure can be regarded as "electroosmotic (EO) pumps." Electroosmosis is the bulk motion of an electrolyte caused by electric forces acting on regions of net charge in a micro-channel or capillary. Fabricated mostly of porous glass or fused silica with deprotonated silanol groups on the surface (SiO^-), EO pumps use this effect to generate both flow and pressure differentials under a DC electric field [106, and 113]. The performance of EO pumps have been reported to depend on the porosity, tortuosity, pore size of the matrix, and the pH and ionic concentration of the electrolyte [106, and 113]. Figure 2.2 shows a depiction of net flow in a micro-channel of a porous glass type electroosmotic pump and the theoretical determination of flow rate due to the electrical (v_{eo}) and pressure (v_p) gradients.

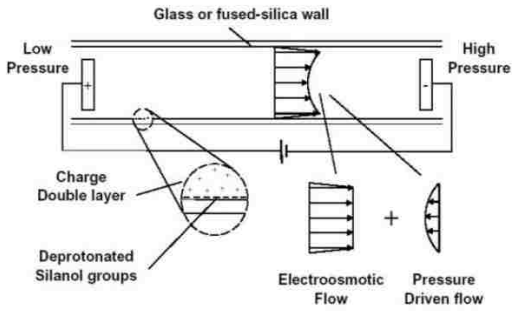

$$v_{eo} = -\frac{\varepsilon\xi}{\mu}\frac{dE}{dx}$$

$$v(r) = v_{eo} + v_p = k_{eo}\frac{dE}{dx} - \frac{dp}{dx}\frac{(a^2 - r^2)}{4\mu}$$

$$k_{eo} = \frac{\varepsilon_s\xi}{\mu}$$

ε is permittivity

ξ is zeta potential

μ is dynamic viscosity of fluid

dE/dx is electrical field strength along channel length

P is pressure along channel length

a is channel radius

Figure 2.2. "Frustrated" flow of EO pump [106]

Electrically assisted flow in porous media that behave as electrosmotic pumps had led to the advent of microfluidic fabrication technologies. These technologies implement electroosmosis as a unique tool to control the fluids in microfluidic chips [95]. The tool has been reported to offer unique advantages in microfluidics, such as low hydrodynamic dispersion, no moving parts, electrical actuation and sensing, and easy integration with microelectronics [20]. Treating electroosmotic flow as flow through a large number of idealized tortuous micro-channels in parallel in soil matrices, the analytical expressions developed for electroosmotic pumps may be used to model the EO transport in terms of flow rate, current, and pressures generated.

Recent studies have shown that pressures generated in clay matrices indeed influence the electroosmotic transport [79]. In addition, similar to the EO pumps, the EO transport efficiency in

soils depend upon the pH and bulk ionic concentration of the electrolyte, which in turn determines the zeta potential and the redox transformations near the electrical double layer interface [84, and 87].

Figure 2.3 shows the temporal variation of the voltage gradients and the subsequent water pressures at adjacent measurement locations in kaolinite clay under constant DC electric field. In this particular case, the temporal and spatial variation of the voltage gradient is believed to cause the buildup of the pressure gradients resulting in stagnant zones of pressure and no flow. According to the EO pump analogy, the flow is maximized (Q_{max}) in the absence of pressure, and the pressure (ΔP) is maximized in the absence of flow as given by the following equations:

$$Q_{max} = k_{eo} \frac{dE}{dx} A \tag{4}$$

$$Q = \int v.dA = 0 \rightarrow \Delta P = \frac{8.\mu.E}{a^2} \tag{5}$$

where, E is the electrical potential difference; μ is dynamic viscosity of the fluid, and a is pore radius.

The development of backpressure and its spatial variability in pore channels is of particular interest to transport of organic and non-polar molecules which depend on electrosmotic advection more so than other electrokinetic mechanisms in soils [106].

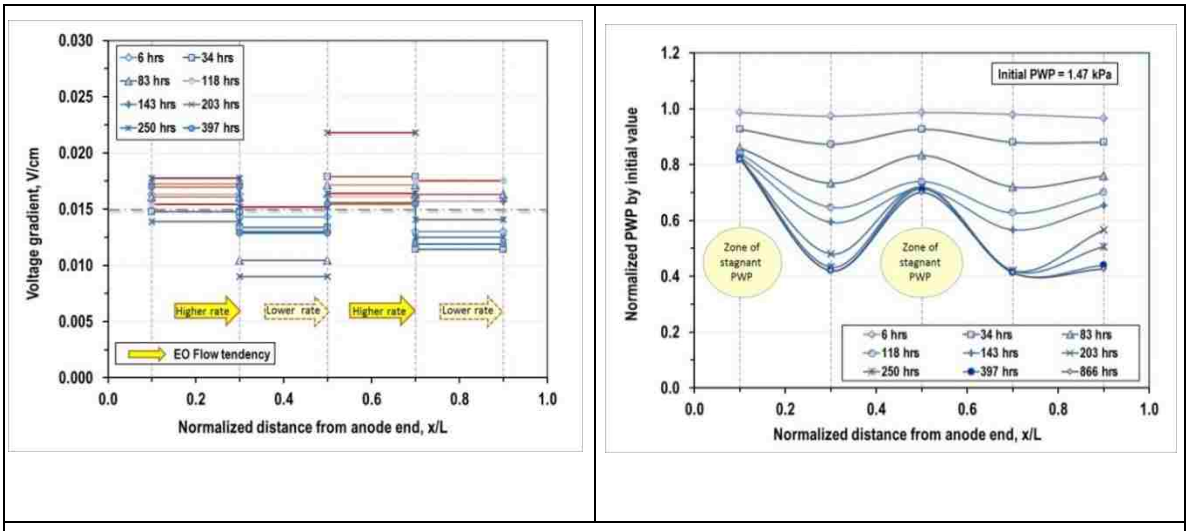

Figure 2.3. Temporal and spatial distribution of voltage and pressure gradients in clay [79]

2.3 Electrically assisted transport of hydrocarbons in porous media

Enhanced Oil Recovery (EOR) is referred to those techniques used for enhancing the amount of crude oil that can be extracted from an oil field. Using EOR, 30-60 % or more of a reservoir's original oil can be extracted compared to the 20-40% using primary and secondary recovery [103]. Enhanced oil recovery is achieved by water flooding, gas injection, chemical injection, microbial injection, or thermal recovery, which includes cyclic steam, steam flooding, and fire flooding [16, and 25] . Water flooding still remains the most universally accepted method for enhancing oil recovery after initial natural pressure depletion [16].

For heavy oils (i.e., less than 17˚ API gravity) enhanced recovery is more of a challenge since extraction of high viscosity liquids from low permeability oil reservoirs involves many difficulties. Movement of heavy molecule hydrocarbons in low permeability reservoirs requires a driving force that most of conventional oil recovery techniques are not able to provide.

The electrically assisted transport of hydrocarbons has great potential to be exploited as a viable energy resource recovery application. Based on few available reports, it has emerged to have advantages as a non-drilling operation and reduced oil viscosity compared to other conventional methods [111]. Upon application of direct current, Electrokinetic phenomenon is activated near the solid-liquid interfaces inside the pores and a multiphase flow is generated and sustained by the electrically assisted transport.

2.4 Relevant models of oil transport in porous media

In petroleum engineering, most of the models of the transport of hydrocarbons in porous media employ fundamentals of multiphase flow [5, 13, 16, 30, 31, and 66]. However, none of these models consider an applied electric field as the driving force of hydrocarbons. In geo-environmental remediation, different electrokinetic models have been developed to predict the mass transport of chemical species and contaminants in soil under applied electric field [1, 2, 7, 8, 24, 58, and 100]. However, none of these models consider multi-phase transport.

In this section, some of the relevant models dealing with electrokinetic and multi-phase mass transport will be introduced. The mathematical descriptions of these models including the assumptions and the derivations of the governing equations are provided in appendix A.

2.4.1 Electrokinetic mass transport models

Several mathematical models have been developed to predict contaminant transport by electrokinetics [7, 8, 24, 78, and 100]. In the following section, three of the models will be discussed. All three models incorporate the electrical and chemical gradient contributing to the mass transport of ionic species under applied electric field.

Alshawabkeh and Acar model (1992)

This is a general model of mass transport in soil under applied direct current. The model incorporates electric, hydraulic, and chemical gradients as well as chemical reactions. The governing equation of one dimensional mass transport is obtained considering the conservation of mass and charge.

Shapiro and Probstein model (1993)

The one dimensional model was developed to predict the removal rate of contaminants from saturated clay. The model incorporates ion diffusion, migration, and electroosmotic advection and assumes incompressible soil medium (constant hydraulic head distribution). Electroosmotic flux is calculated by averaging the electrical gradient and zeta potential across the soil sample. First order sorption and water dissociation are included as geochemical reactions.

Cao and Pamukcu model (1997)

The model was developed to investigate multispecies transport under transient electric field as an extension to the Alshawabkeh and Acar model. The model incorporates chemical reactions such as sorption and aqueous phase reactions.

2.4.2 Multiphase flow models in enhanced oil recovery

There are numerous mathematical models developed for enhanced oil recovery applications. In the following sections three of the most relevant models used in enhanced oil recovery applications are introduced.

Buckley-Leverett model (1942)

The simple model is developed for two-phase flow in porous medium. The model has been used frequently in petroleum engineering since gas and water injection are among the

common methods of oil recovery. The model considers the simplest multiphase flow in porous media in which two fluids flow simultaneously but do not exchange mass or react with the solid matrix. The model provides the phase saturation, pressure, and flow rate but neglects the capillary pressure gradient.

Black oil model (1948)

Black oil model is a multiphase fluid flow model through porous media. The model is a special case of general compositional equations that allow limited inter-phase mass transfer. The premise of the black oil model is that a highly simplified three species system could be implemented as a model representing complex mixtures of brine and hydrocarbon in oil reservoirs. The model provides phase saturation, pressure, and flow rate.

EEOR model (1986)

The model is a three dimensional reservoir simulator that models the electrically enhanced oil recovery process [63]. The basic assumption in the model is that upon application of electric current between to two adjacent wells, the conductive oil bearing formation between the wells is heated due to the electrical dissipation and results in reduced oil viscosity. The model is a non-isothermal, multicomponent, multiphase reservoir simulator that solves for temperature, saturation, mole fraction, pressure, and electric potential in the reservoir.

2.4.3 Simplified models of multiphase fluid flow with flow induced charge

In order to couple the electric potential gradient and fluid pressure gradient, several researchers [56, 57, and 94] tried to use the bundle of capillary tubes model (where a porous medium is depicted as composite of a bundle of capillaries entering a unit volume cube on one

face and emerging on the opposite face). In this section several of these models that deal with single and multiphase flows are introduced.

Ishido and Mizutani (1981)

Ishido and Mizutani [57] used a capillary model to derive an explicit expression for the coupling term between the electric potential gradient and the fluid pressure gradient for a general porous medium. Although the real structure of a porous medium is not as simple as that described by the capillary model, the model may be sufficient for the first order of approximation. The model incorporates electric and pressure gradients and provides the fluxes of electric current density and fluid volume flow density.

Jackson model (2007)

Jackson [56] tried to define the streaming potential coupling coefficient (C) in multiphase flow using bundle of capillary tubes. This model is an extension of the bundle of capillary tubes approach [57]. Each capillary can have a different radius (r_c) and all capillaries have the same orientation and there is no intersection between capillaries. The model assumption is that the small capillaries are occupied by the wetting phase and large capillaries are occupied by the non-wetting phase, because the capillary entry pressure for the non-wetting phase increases with decreasing capillary radius. Also, the model assumes that the surface charge is constant in capillaries occupied by a given phase. The model provides the streaming potential coupling coefficient.

Saunders model (2008)

Saunders and coworkers [97] developed a model combining both multiphase flow and electrokinetic components to investigate the behavior of streaming potential during oil production.

When the soil particle surface becomes electrically charged, the diffuse double layer is formed in the adjacent fluid and contains excess counter charge. When the fluid is induced to flow (by an external hydraulic potential), some of the excess charge within the boundary layers is transported with the flow. Thus, there is a rise in streaming current and accumulation of charge associated with the diversity of the streaming current density results in streaming potential [56].

The model introduces a saturation dependent relative coupling term to account for partial saturation of the wetting phase. The electrical term is coupled to fluid term using the electrokinetic coupling term. Saunders and co-workers used finite element scheme to solve the fluid flow and charge flow equations with no external current source.

Pore network models

In addition to capillary tube models, several pore network structure models have been developed during the past decades to model the immiscible displacement in porous media [32, 60, 67, and 71]. However, implausible assumptions associated with these models (equal viscosity for two fluids, or sand pack media) inhibit widespread use of these models in multiphase flow cases. Most importantly, none of these models incorporate any applied electric gradient that drive the transport to be considered as an appropriate model for the goals of this research work.

2.4.4 Summary of the mathematical models

Among the enhanced oil recovery models (Buckley Leverret, Black oil, and EEOR) only the EEOR model incorporates the additional applied electric term, but it does not consider the flow of phases due to the applied electric gradient. The model considers the role of the applied electric field as a heating source which results in enhanced oil production due to reduced oil viscosity. Indeed, the model does not consider any mass transport resulting directly from the applied current or electrical field. The electrokinetic transport models do not consider the mass

transport in two phase flow explicitly. They are developed to predict the transport of the ionic constituents and the water soluble portion of the organic compounds. The pore network structure models do not incorporate the applied electric field as one of the driving forces of the fluid flow.

The multiphase, non-isothermal electrokinetic models by [56] and Saunders [97] are closer models of the electrically assisted oil transport in porous media. In these models, the term containing the streaming potential coefficient is developed to couple the fluid potential driving the fluid flow with the electrical potential driving the charge flow. However, no external current source is considered in their governing equations.

2.5. Laboratory and field studies of the electrically assisted oil transport

Chilangar and co-workers investigated the use of electrokinetics to augment reservoir energy during petroleum production [9, 10, 27, and 28]. They found that application of direct electric current resulted in several fold increase in the flow rate of oil and water (as much as 34 fold) in both synthetic and natural sandstone cores. Synthetic cores were prepared using various percentages of different types of clay admixed with 200 mesh size silica or $CaCO_3$ powder. Also, it was found that the effective permeability to kerosene of core samples containing connate water (entrapped water in the pores when the rocks were formed) was increased by 50 percent on temporary application of direct potential gradient.

Pamukcu and co-workers [83, and 84] investigated the role of electrokinetics in transporting Polynuclear Aromatic Hydrocarbon (PAH) compounds in contaminated soils. They investigated the feasibility of electrokinetic treatment of clay mixtures containing multiple organic compounds found in retrieved soil specimens from a gas plant site and also in laboratory prepared contaminated specimens. Electroosmosis was found to be the dominant mechanism of transport, though electromigration and electrophoresis played minor roles in transport of some

PAHs. The PAH compounds with higher water solubility (i.e.,Naphtalene) was found to be transported by electroosmosis without the aid of surface tension reducing agents, which was necessary for higher molecular compounds such as penanthrene. Also, it was found that electrokinetically enhanced transport of targeted PAH compounds was at average of 44 to 70 percent upon 2 to 9 pore volumes of electroosmotic water flow through the soil specimens.

Successful field pilot tests have been reported on application of EEOR (Electrically Enhanced Oil Recovery) in heavy oil fields in the Santa Maria (California) basin and the Eastern Alberta Plains [110, and 111]. In these pilot tests, the EEOR was found to be more efficient than other conventional heavy oil recovery methods including steam flood or cyclic stream flood. Also, these field pilot studies demonstrated the capability of EEOR in cracking heavy oil in-situ, reducing water cut and increasing oil production rates. The field tests in California demonstrated up to ten folds increase in the oil production from a field containing 8˚ API gravity oil.

Haroun and coworkers [47] reported the results of DC application, concurrently with water-flood recovery in mobilizing the connate water and the trapped oil through core-flood studies. In the first set of experiments, DC was applied after ultimate water-flood recovery and in the second set of experiments the DC was applied on oil saturated core plugs concurrently with water flood from the beginning of the test. Comparison of the two processes revealed that application of DC concurrently with water flooding at the beginning of the process recovered approximately 1.5 - 4% more oil and reduced water requirement by 15 – 22% in comparison with the water flooding process alone [4, and 47]. However, application of DC on a completely water swept core was found to recover 3-9 % additional oil. Also, on repeat application DC, up to 30% increase in permeability of cores was reported which was attributed to clay dislodgement due to electrophoresis mechanism involved in EEOR.

Jihong and coworkers [59] reported that application of DC concurrently with water flooding on core samples containing oil with viscosity of 8 MPa.s, increased the oil recovery rate by more than 5%. Also, the apparent viscosity of the oil was found to decrease as the electric field strength was increased.

2.6. Laboratory and field experimental Results in this study

2.6.1. Laboratory scale tests on natural cores

A series of laboratory experiments and pilot field applications were conducted to investigate the contribution of some of the mechanisms and physical conditions on the electrically induced transport and recovery of oil, including: (i) electro-osmotic drag of oil phase that results in oil production, (ii) increase in the hydraulic permeability of the porous media with the application of electric field, (iii) the oil production regime under combined application of pressure injection and direct current in a field application.

Natural oil bearing sandstone core specimens

Oil-bearing rock core specimens retrieved from a shallow oil formation in Kentucky were used to test for oil extractability and change in permeability under applied electric field. The physical properties of the three core specimens are given in Table 2.1. The physical properties of the natural oil in the rock cores and the brine solution used in the experiments as the surrogate formation water are given in Table 2.2. The core specimens were tested in EK cells as shown in Figure 2.4. The core compartments of these cells were 10 cm long and 3.6 cm in diameter. Platinum mesh electrodes were placed adjacent to the rock core in the cell. Glass frits separated the core compartment of the cell from the liquids in the catholyte and anolyte reservoirs. The liquid levels in the stand tubes were monitored and adjusted to prevent hydraulic pressure

difference across the core. The applied current density was selected as 1Amp/m^2 in accordance with the achievable current densities of 1.0-1.5 Amp/m^2 in practical applications in the field [107]. To achieve a current density of about 1 Amp/m^2, a constant voltage gradient of 12V/cm was applied across the Kentucky cores. The total flow generated in each phase (oil and water) was measured periodically for 120 hours. The pre- and post-test hydraulic permeability of the cores were measured in a tri-axial cell under backpressure with saturation (ASTM D5567-94).

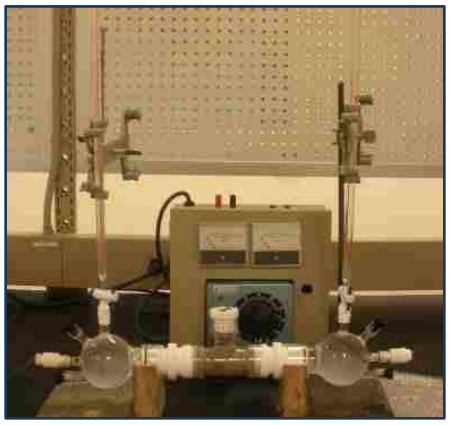

Figure 2.4. Electrokinetic reactor apparatus used in the experiments

Table 2.1. Physical properties of the natural sand stone cores (Kentucky field)

Core	Porosity (%)	Bulk wet density (gr/cm^3)	Residual oil (%) (by volume)	Residual water (%) (by volume)	Hydraulic Permeability (mD)
KY1	10.2	2.48	12.9	61	2.67
KY2	13.6	2.39	28.1	43.9	11.59
KY3	14.7	2.37	30.2	33.9	41.88

Table 2.2. Physical properties of the formation oil and surrogate water (Kentucky field)

fluid	Properties
Natural formation oil	API 22; Dynamic viscosity = 66.5 cP Specific gravity =0.92 at 20°C
Electrolyte solution (Surrogate formation water)	Salinity= 33,000 ppm Major elements: Na, Cl, Mg, S, K, Ca, Br Electrical conductivity = 45,000 µS pH = 7.50

Table 2.3 presents the oil recovery results for the three Kentucky core, KY1, KY, and KY3. The oil separation and analysis were conducted using standard techniques [41]. As observed, most of the oil recovered was produced at the catholyte, while the oil recovered at the anolyte was negligible. The total oil recovered was in the range of 5 to 11% by mass of the initial oil content in the cores.

Table 2.3. Oil recovery results of the natural sand stone cores (Kentucky field)

Core	Recovered oil at the anolyte (ml)	Recovered oil at the catholyte (ml)	Total recovered oil (%)
KY1	0.000	0.021	5.1
KY2	0.005	0.104	9.9
KY3	0.002	0.157	11.4

The oil recovery results suggest that the higher initial oil content of the formation results in higher oil recovery. Modeling studies on two-phase EO flow have revealed that the drag force

exerted by the mobile water phase on the oil phase increases with availability of water up to about 50% of water saturation in the pore, and it starts to decrease when water saturation is above 50% and oil saturation drops below 50% [42]. The higher recovery of oil with higher initial oil/water ratio is attributed to the availability of more oil.

The hydraulic permeability of the cores (pre- and post-EK test) and the *equivalent EO* permeability, k_{eh} ($k_{eh}= k_{eo}* \nabla E$) are presented in Figure 2.5. As observed, the equivalent EO permeability is at least one order of magnitude higher than the hydraulic permeability for all three cores. Other researchers have reported similar findings, where up to 50 percent increase in effective permeability to kerosene was observed in sandstone core samples with a short term application of DC potential [27]. Important to note is the marked change in the permeability of the core specimens after EK tests, as shown in Figure 2.5. The hydraulic permeability of the cores KY1, KY2, and KY3 increased about 28%, 57%, and 37%, respectively, after the EK tests. Although EO permeability is not dependent on the pore structure as per Helmholtz-Smoluchowski equation (Eq. 2.1), it appears from the results that the higher the hydraulic permeability of the core the higher the oil recovery. One plausible explanation for this finding is that the larger pore throat sizes in higher permeability core specimens help efficient transport of the oily micelles that may otherwise clog the smaller pores.

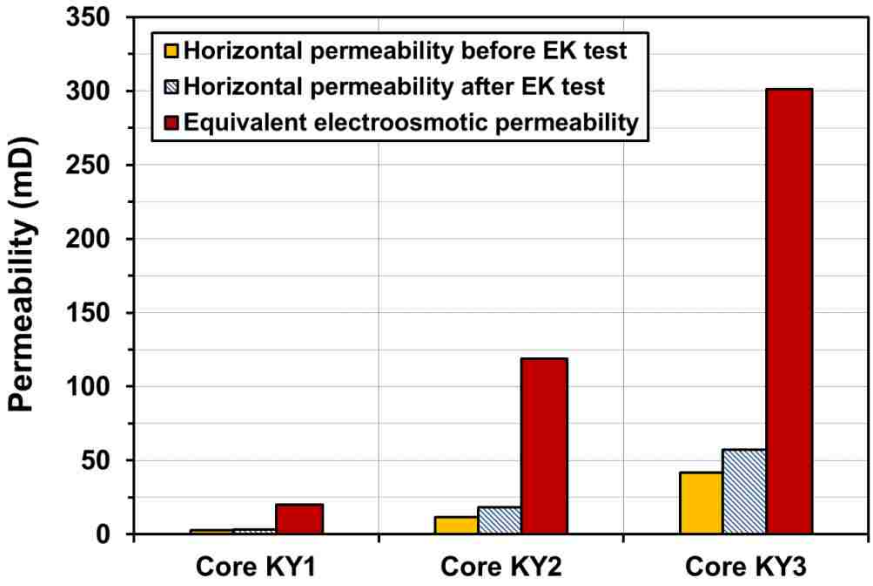

Figure 2.5. Changes in the permeability of the cores (Kentucky field)

The increased hydraulic permeability of the cores in the aftermath of electrically enhanced flow of mass can be attributed to two contributing processes. First, the electrophoretic transport of colloidal particles, lining the walls of the capillaries, would empty out the pores hence result in enlargement of the pore throat diameter. Others made similar observations in the field [4, and 47] and in lab tests where up to 30% increase in permeability of sandstone cores was reported upon repeat application of direct current. This increase in permeability was attributed to colloid dislodgement in the pore space due to the mass transport. Second, owing to the electrolysis reactions, the acidification of the pore fluid would result in collapse of the clay EDL lining of the pores. In very low permeability formations where the pore size distribution are mostly in capillary range, the potential collapse or shrinkage of EDL can result in widening of the pore diameter [83].

In order to verify that the increased permeability of the cores was due to the applied electric field rather than any disturbance to its internal structure due to pressure injection, multiple sequential hydraulic permeability tests were performed on KY1 and KY 2 cores. These tests were conducted under different injection pressures before the cores were subjected to the electric field. The results of these tests showed negligible increase of about 3% in hydraulic permeability following pressure injection, as opposed to the 28% to 57% increase with the electric field. Hence the increase in the hydraulic permeability of the cores is deemed to be more likely due to the applied electric gradient than pressure disturbance for these low permeability cores.

Oil impregnated sandstone cores

Sandstone core specimens retrieved from a deep oil formation in Pennsylvania were used in the experiments to assess oil recovery, permeability change, and effect of the magnitude of current density under the applied electric field. Unlike the Kentucky cores discussed above, the Pennsylvania cores had very low initial oil content. In order to better control the oil and water saturation, these cores were impregnated with Pennsylvania oil and surrogate formation water prior to testing. First, they were dried and vacuumed. Then, the oil and water were injected into the cores using a high pressure injection pump (Quizix Pump) to attain the desired initial oil-water saturations. The physical properties of the four Pennsylvania cores and the surrogate formation fluids (Pennsylvania oil and surrogate formation water) used in the experiments are given in Tables 2.4 and 2.5, respectively. Once saturated, the cores were tested for electrically enhanced mass transport under a constant applied voltage gradient of 4 V/cm and current density of 1 Amp/m^2 for 130 hours.

Table 2.4. Physical properties of the oil impregnated sand stone cores (Pennsylvania field)

Core	Porosity (%)	Bulk density (gr/cm^{3})	Horizontal Permeability (mD)	Oil saturation (%)	Water saturation (%)
PA1	14.5	2.49	3.6	42	58
PA2	12.8	2.43	2.3	48	52
PA3	14.4	2.47	8.3	53	47
PA4	11.5	2.45	0.5	40	60

Table 2.5. Physical properties of the formation oil and water (Pennsylvania field)

fluid	**Properties**
Injected oil (PA field oil)	API 47; Dynamic viscosity = 38.7 cP Specific gravity =0.79 at 20°C
Electrolyte solution (Surrogate formation water)	Salinity= 33,000 ppm Major elements: Na, Cl, Mg, S, K, Ca, Br Electrical conductivity = 45,000 µS pH = 7.50

Table 2.6 presents the oil recovery results for the Pennsylvania core specimens, PA1, PA2, PA3 and PA4. Once again, most of the oil was produced at the catholyte and the oil recovered at the anolyte was negligible. The total oil recovered was in the range of 0.5 to 6% by mass of the initial oil content of the cores. Similar to the Kentucky cores, the highest oil recovery corresponded to core PA3 which had the highest initial oil content and highest hydraulic permeability.

Table 2.6. Oil recovery results of the oil impregnated sand stone cores (Pennsylvania field)

Core	Recovered oil at the anode side (ml)	Recovered oil at the cathode side (ml)	Total recovered oil (%)
PA1	0.0056	0.0457	1.1
PA2	0.014	0.23	3.8
PA3	0.020	0.377	6.3
PA4	0.0024	0.0198	0.6

Overall, compared to the Kentucky cores, less oil was recovered from the Pennsylvania cores. Although both Kentucky and Pennsylvania cores where sandstone, the possible differences in their pore structure and distribution would have contributed to the difference in the oil recovery. Furthermore, while the surrogate formation water was same in both cases, the formation oil viscosities were different (API 22 for Kentucky vs. API 47 for Pennsylvania cores). A higher voltage gradient was necessary for Kentucky cores (12 V/cm for Kentucky vs. 4 V/cm for Pennsylvania cores) to achieve the desired current density of 1 Amp/m^2. The higher electrical field intensity might have contributed to the higher oil recovery in Kentucky cores. The higher intensity field is prone to generate heat and lower the viscosity of the residing oil, hence its flow ability. Indeed, although the temperature was not measured for the cores, the Kentucky cores felt warmer to the touch than the Pennsylvania cores during the EK tests.

To investigate the effect of applied current density on oil recovery, additional tests were conducted on PA1 and PA4 cores under increased current density of 4 A/m^2. Although this level of current density is hardly feasible in field applications, the 75 hours of elevated current density resulted in additional 2.6% and 1.5% of the original oil mass extracted from PA1 and PA4, respectively. As expected, the higher current density resulted in higher oil recovery. A similar

behavior was observed in the field experiments. Higher current density results in higher EO flow of the formation water which in turn increases the viscous drag at the oil interface. Higher current density promotes the rate of electrode reactions that affect the reduction of interfacial tension between the pore fluids, also resulting in more oil production [96, and 105].

Figure 2.6 shows the change in the hydraulic permeability of the Pennsylvania cores specimens (pre- and post EK tests) and the equivalent EO permeability. Once again the equivalent EO permeability is at least one order of magnitude higher than the hydraulic permeability for all the cores. Also, the change in the hydraulic permeability of the cores after the EK tests is significant, at about 50% on the average. The electrically enhanced increase in the permeability was validated on core PA3 by multiple permeability measurements at different pressure injections which showed about 2% increase in the post test permeability. This was significantly smaller than the 38% increase after electrical field application for the same core.

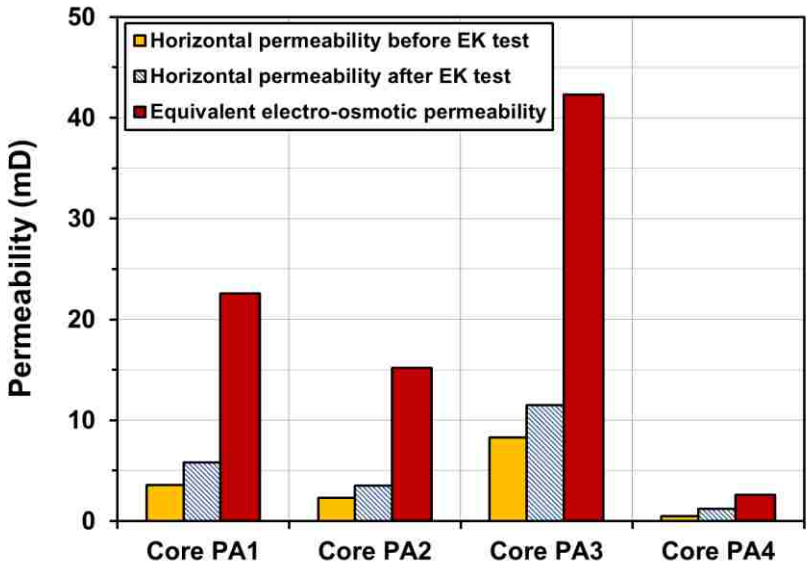

Figure 2.6. Changes in the permeability of the oil impregnated cores (Pennsylvania field)

2.6.2 Field experiment

An application in the Pennsylvania field was monitored over time to investigate the effectiveness of electrically enhanced oil recovery accompanied by water flooding (i.e., water pressure). The cumulative oil and water production was monitored at one of the production wells for about 180 days. During this time, some amount of paraffin was observed to produce in the well also. The oil, water, and paraffin production over time are plotted in Figure 2.7. The oil production is about 5% of the water production and the paraffin production is about 4% of oil production by volume.

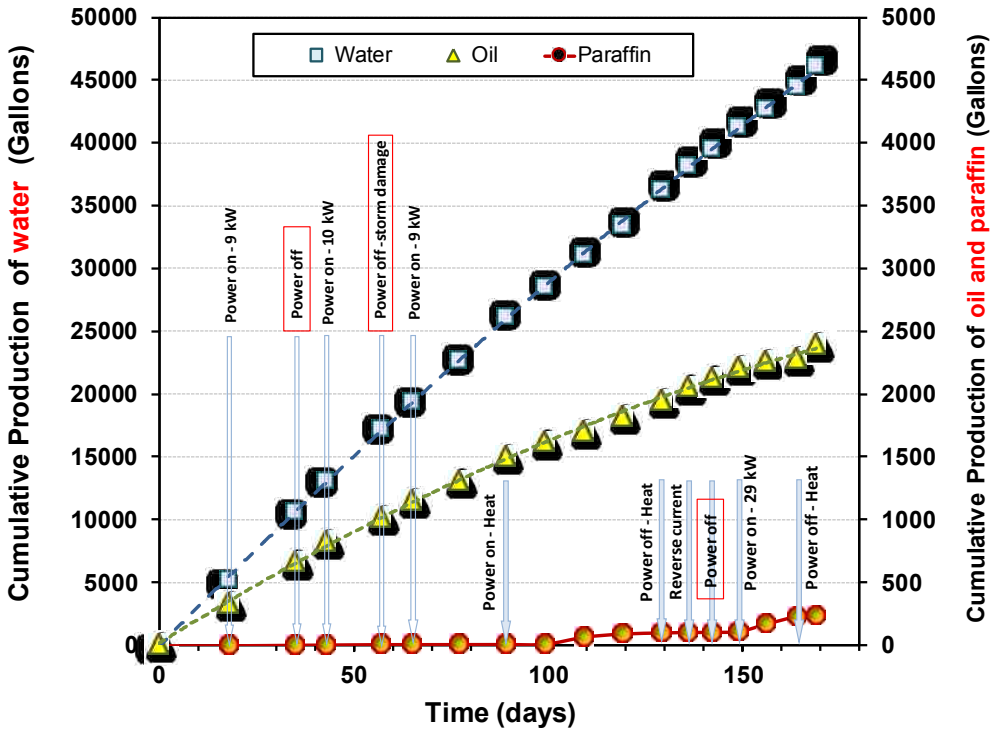

Figure 2.7. Water, oil, and paraffin production (Pennsylvania field)

The oil production appears to decrease with time, and there is no immediate break in oil production when the power is terminated, reversed or re-applied. This is potentially due to the build-up of seepage and suction pressures with electro-osmosis which would require time to dissipate in low permeability formations before the flow regime change or subside [79].

Figure 2.8 shows the oil and paraffin production over time. As observed, the paraffin production increased with power and elevated temperature. When the power was turned off the paraffin production ceased. It is plausible that as pH, ionic concentration and dissolved minerals (e.g. calcite) increase at the production well (cathode), it would create the ideal conditions for excess oil to transform to paraffin. A similar phenomenon was observed in lab experiments on core rock samples with Pennsylvania oil where white colored *foam* like material was formed in the catholyte, identified as paraffin.

Examining the daily production data, it was determined that when the applied current was reversed, the production of paraffin decreased. This is attributable to the counter current flow resulting in decreased oil production and lowering of the pH at the well. Lower pH and less oil available at the location could potentially reverse the paraffin production. The increase in paraffin production corresponded to the periods of elevated temperature due to sustained power over long term (~ at 100 days), or when the maximum power of 29 kW was applied (~ at 150 days). As observed from Figure 2.8, at times of increased paraffin production, the oil production decreased or completely ceased. Among some of the plausible reasons for this exchange are: the easier transport of existing paraffin in the pore space at elevated temperatures, and the increased availability of oil and mineral components to form paraffin under the driving forces of elevated temperature and power. This field experiment is continuing to better investigate the effect of applied DC current to the oil and paraffin production in long term and better evaluate the implications of the results reported above.

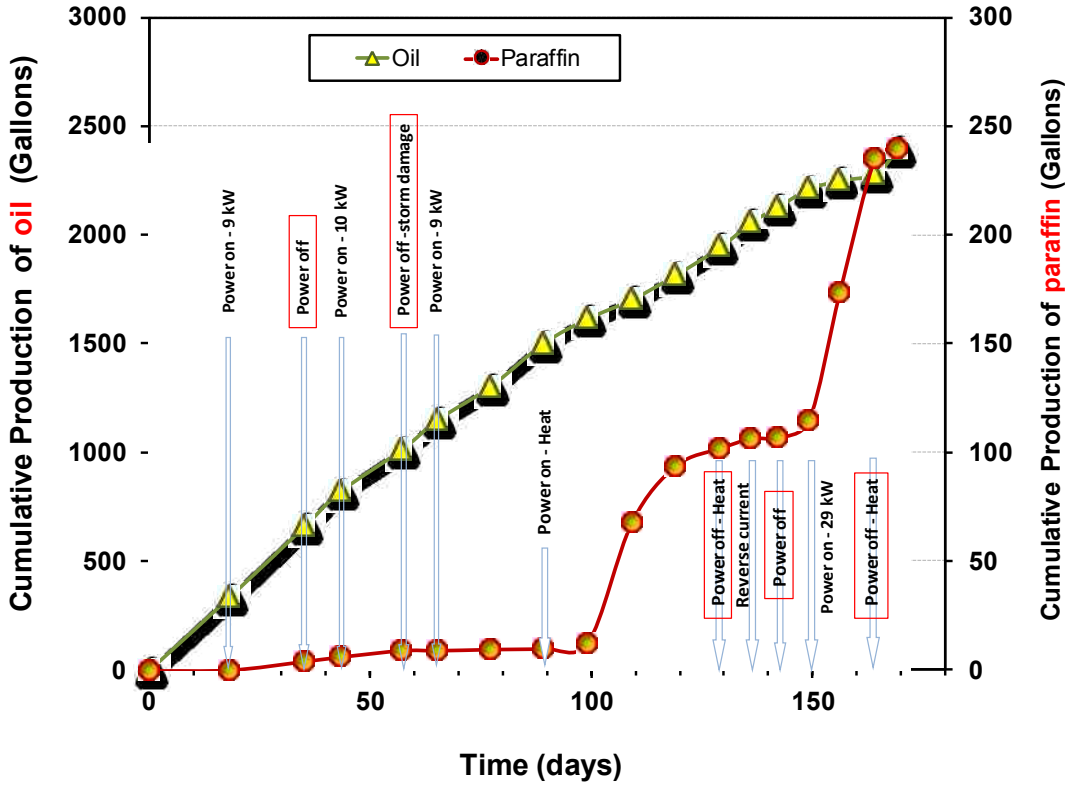

Figure 2.8. Oil and paraffin production (Pennsylvania field)

2.6.3 Electrochemical transformation of oil

The electrochemical reactions result in reduction of the interfacial tension between the formation water and crude oil, as well as reduction in the viscosity of the crude oil. It is postulated that both phenomena eventually lead to increased oil mobility and serve to enhance the oil recovery under applied DC current.

The primary mechanism of interfacial tension reduction under applied electric field is reported as the reaction of electrolysis products of brine/formation water (hydroxyl ions, OH^-) on the acid impurities of oil (carboxylic acids) [39]. This results in formation and accumulation of low solubility surface active carboxylates analogous to that of directly adding a surfactant to

reduce the interfacial tension [96]. The amount of interfacial tension reduction is reported to be proportional to the applied potential [105].

Interactions between the pore fluids and the solids which are normally affected by the ambient pH and redox will be enhanced upon application of DC electric field. These electrochemically enhanced reactions help oil transformation by cracking heavy molecular structure of crude oil into its lighter components with lower viscosity [110]. As a result the functional group fractions of the crude oil including the Saturates, Aromatics, Resins, and Asphaltenes (SARA) will be affected. As the asphaltene and resin content of the formation oil decrease and the aromatic content increases, it is expected that the viscosity of the formation oil decrease. The less viscous the crude oil, the higher is its mobility in the formation. Decrease in the oil viscosity under increased electric field intensity has been reported in the literature [96, 105, and110].

2.6.3.1 Floor Scale Test Set-up

A series of synthetic cores were tested, including three test cells run at low current density of 0.1A/m^2 and three at high current density of 1.0A/m^2 and three control cells at no current. The cells were 100 cm in length and 16.2 cm in diameter as shown in Figure 2.9. Titanium electrodes, and ion exchange resin packs were used at the two ends of each cell. The cells were designed in a manner that minimized transport of pH fronts into the cells and the cells were hydraulically balanced to reduce flow in the cells. Liquid and solid samples were retrieved through the ports placed on the cell walls. The cells were placed in a dark room to minimize biological reactions. Three control formations exactly with identical composition to those of the test cells were prepared. No current was applied to the control cell. Measurements and sampling were conducted on the control cells at less frequent intervals than the test cells.

Figure 2.9. Floor scale surrogate core test set-up

Three different crude oils representing a wide range of dynamic viscosity were used as the formation oil. The same brine solution was used in all cells as the surrogate formation water. The physical properties of the crude oils and the brine solution are presented in Table 2.7. The six test cells were divided to three pairs, each one of the pairs which had the same formation oil but tested under a different current density.

The surrogate formation cores were prepared to simulate the formation characteristic of an oil field located in California. The massed sand at 52% (mean particle size 0.23 mm), silt at 40%, (mean particle size 0.025 mm) and Georgia Kaolinite clay at 8% (mean particle size 0.0011mm), constituting the dry composition of the cores were first dried in the oven at temperature set to 60°C for 24 hours. This allowed accurate determination of the added water to the formation mixture as well as facilitate the mixing of solid particles with heavy crude oils and

formation water. The soils were transferred to the cleaned container of a small concrete mixer and mixed with the pre-massed brine solution first and then the formation oil (based on the target water and oil saturations) to make a homogeneous mixture. The formation mixture was then transferred to the cleaned cell sealed at one end and packed in 2 inch lifts with consistent compaction energy applied to each lift to produce a uniform core. Once the formation mixture was packed, the cell was sealed and massed.

The initial porosity, water and oil saturation of the formation was determined using samples of the mixture and mass-volume of the core in the sealed cell. The sealed cores were left sitting horizontally for 24hrs for the internal fluids to uniformly distribute and equilibrate. A sample of the packed core formation was tested for hydraulic permeability. The representative synthetic core permeability was measured as 510mD. Table 2.8 presents the physical properties of each oil type core specimen.

Table 2.7. Physical properties of the formation oils and water

fluid	Properties
PA field oil	API 47; Dynamic viscosity = 38.7 cP Specific gravity =0.79 at 20°C
CA field oil	API 17.4; Dynamic viscosity = 2782 cP Specific gravity =0.95 at 20°C
Canadian field oil	API 13; Dynamic viscosity = 52000 cP Specific gravity =0.98 at 20°C
Electrolyte solution (Surrogate formation water)	Salinity= 33,000 ppm Major elements: Na, Cl, Mg, S, K, Ca, Br Electrical conductivity = 45,000 µS pH = 7.50

Table 2.8. Physical properties of the synthetic cores

Formation oil type	Porosity (%)	Water saturation (%)	Oil saturation (%)
PA field oil	30.3	43.1	41.5
CA field oil	28.5	46.0	46.1
Canadian field oil	30.5	43.1	43.2

In order to isolate the electrochemical reactions postulated to take place in the bulk of the formation from the electrolysis products of water at the electrodes, pH control systems were designed and installed adjacent to the working electrodes. A 12mm thick layer of Weak Base Anion (WBA) ion exchange resin pack that removes strong acids was placed between the titanium mesh anodes and the core face. Similarly, a 12mm thick layer of Weak Acid Cation (WAC) that removes strong bases was placed between the titanium mesh cathodes and the core face. The electrolyte reservoirs were connected to the anode and cathode caps via tubular connections to simply keep the electrodes and the exchange resins wet for good current conduction.

2.6.3.2 Measurements

Voltage, Current and ORP Measurements

The voltage and current were measured continuously using a data acquisition system at eight different intervals along each cell. At the electrodes, the voltage drop measurements were made across the cathode and anode interfaces to the first port, 5cm into the core from the edge on both sides. Internally, the voltage drop was measured at 10 cm intervals between the consecutive ports. The current was measured continuously across the top and the bottom working electrodes

separately (see Figure 2.9 for placement of the electrodes) to discern current behavior variation between the top and bottom side of the cylindrical core because of gravity segregation or fluid separation. The oxidation reduction potentials (ORP) were measured periodically at the eight probe locations. These measurements were conducted by removing a place holder at the designated port and inserting the ORP probe to the middle of the core. The ORP was measured against an Ag/AgCl reference electrode.

Gravimetric, FTIR and pH Measurements

Based on the observed changes in the ORP over time, formation samples were taken for gravimetric (oil-water content) and pH determinations, and Fourier Transfer Infrared (FTIR) analysis. These samples were taken from the opposite side of the ORP probe locations, where the sampler was inserted to near centerline of the cell. About 3 grams of formation was sampled using vacuum extraction at each sampling. In order to avoid disturbing frequently the integrity and homogeneity of the formation soil, some sample extractions were skipped at intermediate locations and times during the test.

The gravimetric analysis was conducted according to ASTM method D 2974 (ASTM 2000). The FTIR analysis of the oils was conducted on centrifuge extracted samples using HERMLE Labnet Compact Centrifuge Z 206A. The extracted oil was collected in the bottom compartment of 2mL plastic filtration micro-centrifuge tubes. The FTIR spectra were conducted on Thermo Scientific Nicolet iS10 FT-IR Spectrometer equipped with zinc selenite ATR sampling accessory using 128 scans at data point spacing of 0.482 cm^{-1} and range of 650-4000 cm^{-1}.

Viscosity and SARA Analysis

These analyses were conducted on core samples collected at the three locations (anode, cathode and central regions) of the 1 Amp/m^2 test cell cores and also the corresponding control cores at the termination of the tests (107 days). These analyses were conducted by a certified laboratory.

2.6.3.3. RESULTS

Voltage Gradient and Current Density

Typical variations of voltage gradient between adjacent sections in the cell and the current density at the top and bottom half, and the entire cell at 0.1 and 1 A/m^2 are given for the CA oil in Figures 2.10 and 2.11, respectively. As observed in both Figures 2.10 and 2.11, the measured current density at the top and at the bottom halves of the cells ran close, which indicates uniform current density distribution in the formation. Also, the measured current density in the entire cell remained fairly constant around 0.80 and 0.06 A/m^2 for the high and low current density cells, respectively. The current loss from that of the applied (1.0 A/m^2 and 0.1A/m^2) was due to the low conductivity exchange resins placed in front of the electrodes and potentially due to consumed current in electrochemical transformations. The gradual decrease in current density is attributed to the void formation from sampling and potential gas accumulation in those voids throughout the core.

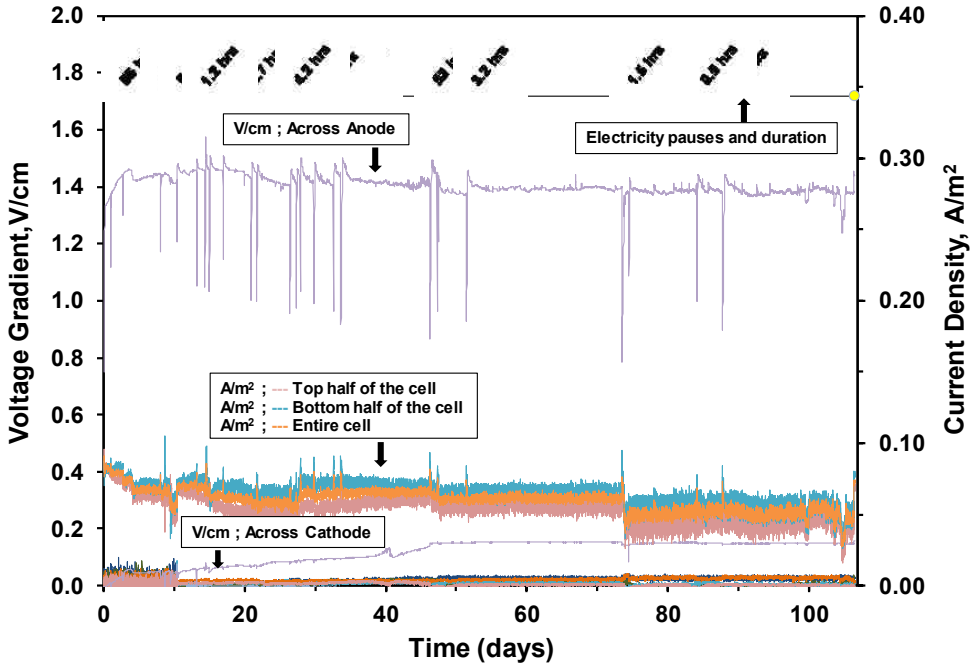

Figure 2.10. Variation of voltage gradient and current density for CA oil cell@ 0.1 A/m^2

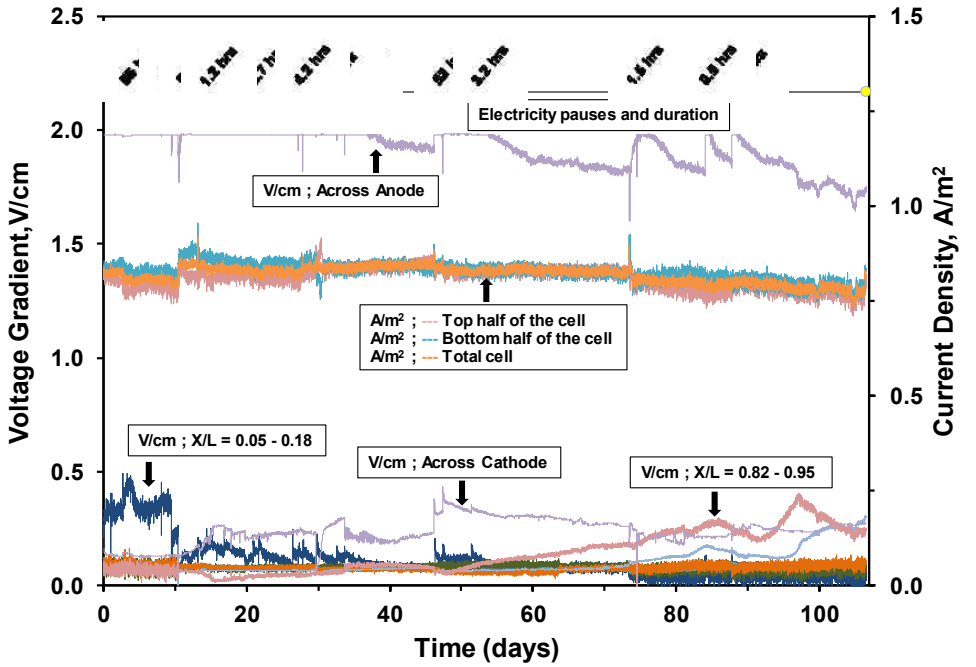

Figure 2.11. Variation of voltage gradient and current density for CA oil cell @ 1 A/m^2

The maximum voltage drop was observed across the anode and the core edge as shown in the spatial and temporal variations of voltage gradients in the California oil cells in Figures 2.12 and 2.13. The large voltage drop across the anode interface is attributed to discontinuity of conduction due to a gap formed between the resin pack and the formation soil. A similar voltage drop with lower intensity is observed across the cathode. In general the internal voltage gradients measured between the ports are rather low.

For the regions close to anode, the voltage gradient is significant at the beginning of the test and it gradually diminishes over time. In contrast, the voltage gradient at the region close to cathode is negligible initially and gradually increases over time. This can be explained by the "electro-osmotic pumping" effect. As the fluids are displaced the pH changes and the oxidation reduction reactions set in, the alterations in the conductivity of the formation results in changes in voltage gradient in different sections of the core. The varying voltage gradients develop alternating zones of fast and slow mass transport hence alternating zones of pressure gradients [79]. The net effect is the transient EO pumping of the transported mass from high pressure to low pressure zones, as the local gradients (electrical followed by the pressure) keep alternating. It is noteworthy that measurements of other parameters such as pH and ORP that can relate to electrochemical activity showed relatively larger changes at regions of large voltage gradients compared to those at other regions of the cell.

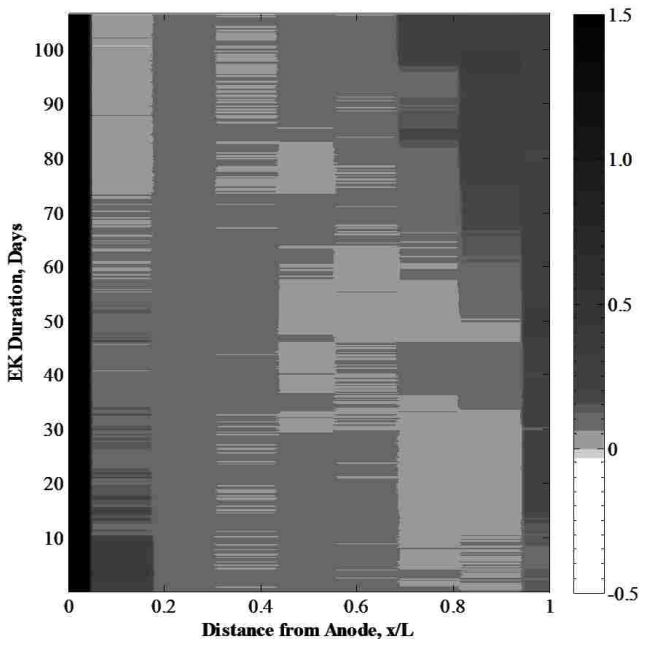

Figure 2.12. The voltage gradient evolution of CA oil cell @ 1A/m^2

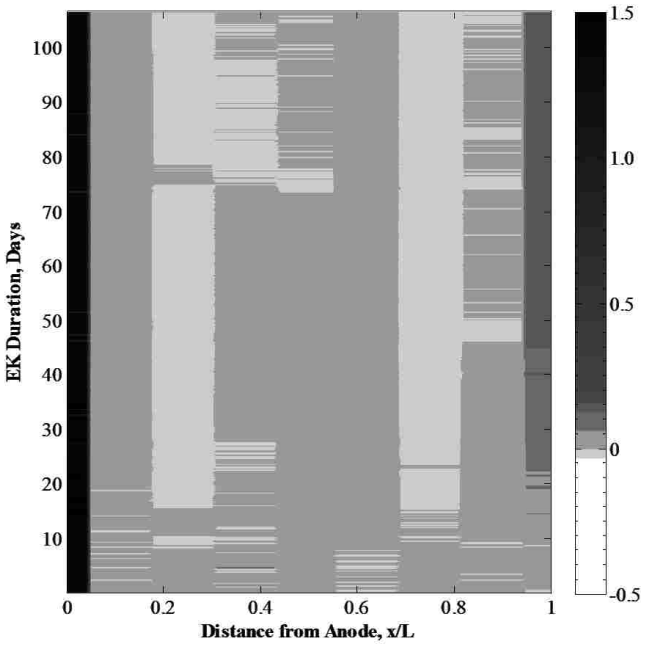

Figure 2.13. The voltage gradient evolution of CA oil cell @ 0.1A/m^2

Gravimetric Results

The changes in water and oil contents over time were measured gravimetrically along the length of each formation cell. The measured changes in water and oil content of the low current density cells (0.1 A/m^2) were negligible. The time variation of water and oil content distributions along the three oil cells for high current density (1 A/m^2) are given in Figure 2.14, 2.15, and 2.16 respectively. In the PA oil cell, the overall water content increased and the overall oil content decreased. A decrease in the overall oil content was expected since oil was observed to seep into the anode and the cathode reservoirs. Water content was higher at the edges suggesting water diffusion from both reservoirs.

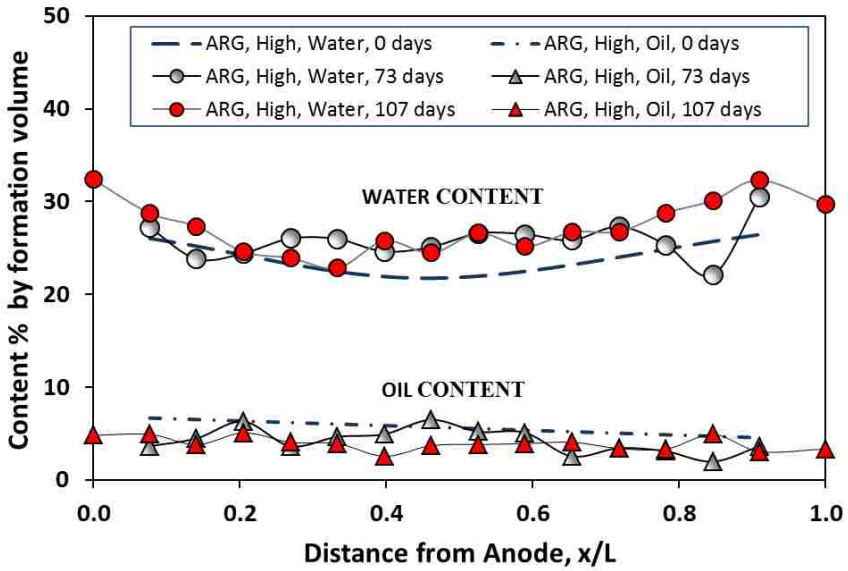

Figure 2.14. Oil-water content measured in PA oil cell @ 1 A/m^2

For the CA oil cell, the water and oil contents are given in separate frames in Figure 4b for clarity. The water content increased slightly near the cathode electrode, typical for electrically induced flow of water. Meanwhile, oil content increased progressively toward the cathode, particularly in section from x/L=0.7 to 1.0 during the initial 45 days. At 73 days, oil content

peaked at x/L=0.8 but decreased significantly near the cathode due to an earlier transport of oil into the cathode reservoir. By 107 days, the oil peak had developed a tail of increased oil content spanning approximately from the middle of the formation, but decreasing sharply at the cathode end, possibly due to the seepage into the cathode chamber. By that time about 10 ml of oil had migrated into the cathode reservoir.

As observed in Figure 2.15, the oil peaks and the water dips mirror image each other, indicating water displacement of oil at the cathode end. The water front that had progressed from x/L=0.3 in 73 days to x/L=0.5 in107 days is the electroosmotic advection that transport oil the oil toward the cathode. Hence it is concluded that some electrically induced water flow and oil flow might have taken place in the California oil cells subject to high current density. The sharp accumulation of oil between x/L=0.7 and 0.8 suggest formation of an oil bank in that region.

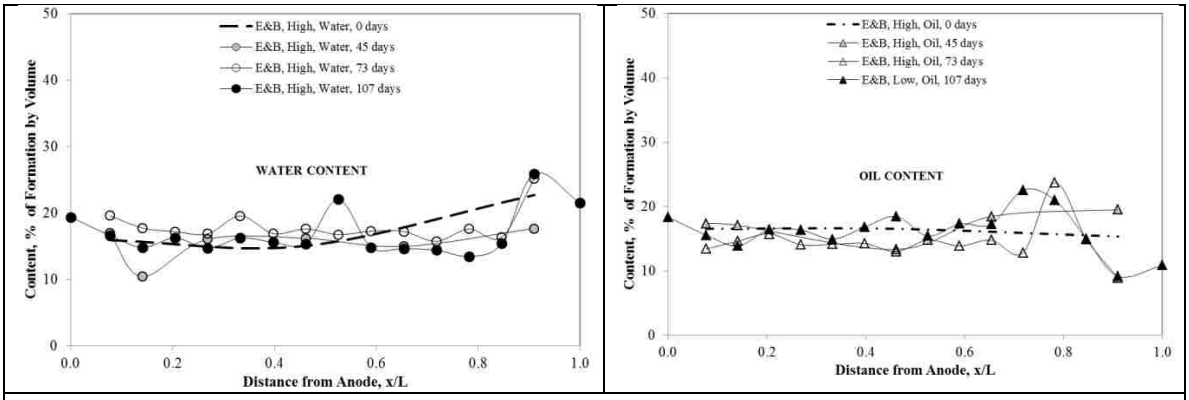

Figure 2.15. Oil-water content measured in CA oil cell @ 1 A/m^2

In the Canadian oil cell, the variability of water and oil distributions along the length of the formation as well as the overall water content increase as shown in Figure 2.16. The pattern of water distribution suggests transport of water through the formation toward the cathode as

characteristic of electroosmotic flow. Although the oil content remained fairly constant at around its initial distribution for the duration, an alternating pattern of oil accumulation that tends to smooth to a more uniform distribution over time was observed. The water content increase at the cathode side of the cell without a significant change in the oil content suggests electroosmotic flow in the cell.

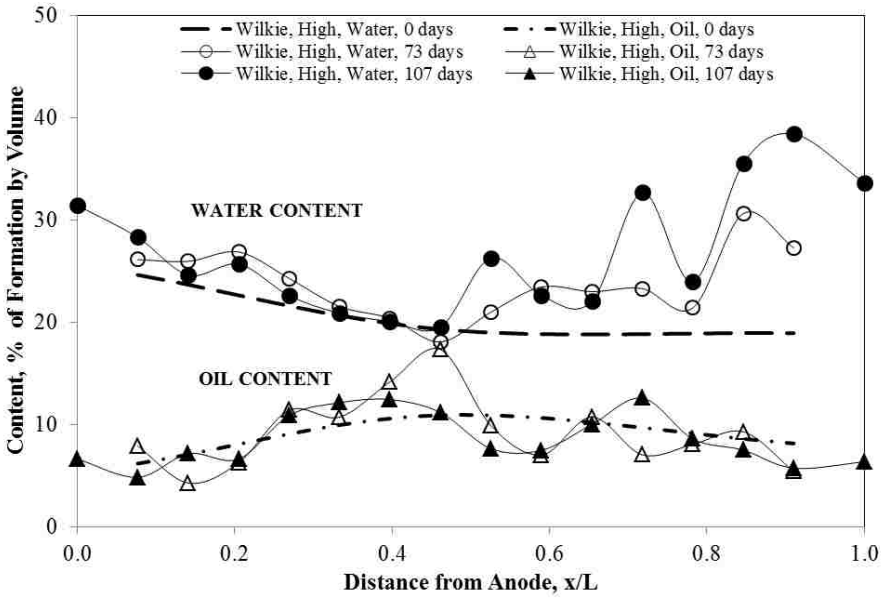

Figure 2.16. Oil-water content measured in Canadian oil cell @ 1 A/m^2

The changes in water and oil contents along each formation demonstrate some internal displacement of water and oil. The diffusion of water into the formation from the reservoirs appears to have displaced oil out of the formation over time. Regardless, the distribution of oil remained fairly constant along the length of the formation for all cells as expected.

Although the tests were not designed to monitor and measure oil production at the anode and cathode water reservoirs, oil flow was observed in cells. In the PA oil cells, oil was visually

observed to seep into the anode and cathode reservoirs. This was attributed to low viscosity of the PA oil, and higher tendency to diffuse out as well as be transported. In CA oil cell at 1.0 A/m^2, oil transport into the cathode side water reservoir was observed to occur at around 45 days. No visual oil transport was observed to either of the water reservoirs in the Canadian oil cells which were attributed to the high viscosity of the Canadian oil.

ORP and pH Results

The evolution of ORP distribution and pH at high current density application (1 A/m^2) for PA, CA, and Canadian oil cores are shown in Figures 2.17, 2.18, and 2.19 respectively. A constant pH of about 6 was maintained within all formation cells for about 30 days of continuous current application, after which the ion-exchange resins were depleted and had to be replaced. A sharp change in the pH of the formation close to the anode and particularly the cathode occurred shortly before the time of the replacement but did not propagate deeper into the formation for the next two months of continuous current application. Hence the pH of the central sections of the cores remained at a constant value at around 6.

As expected, the regions close to anode (x/L= 0 to 0.3) developed oxidative state. At high current density, the ORP measurements near anode region shifted up after about 60 days and prevailed over time. In the middle regions (x/L = 0.3 to 0.65) the ORP did not change appreciably, but displayed a slow transition towards reductive state in time. Near the cathode region all cores displayed reductive states. The shift happened early on in PA and CA oil cells even when neutral pH was maintained in this region. The changes in ORP were larger in magnitude at high current density (1 A/m^2) cores than the low ones (0.1 A/m^2). The larger spatial variability in ORP in high current cores is indicative of the redox reactions driven by the intensity of the applied current.

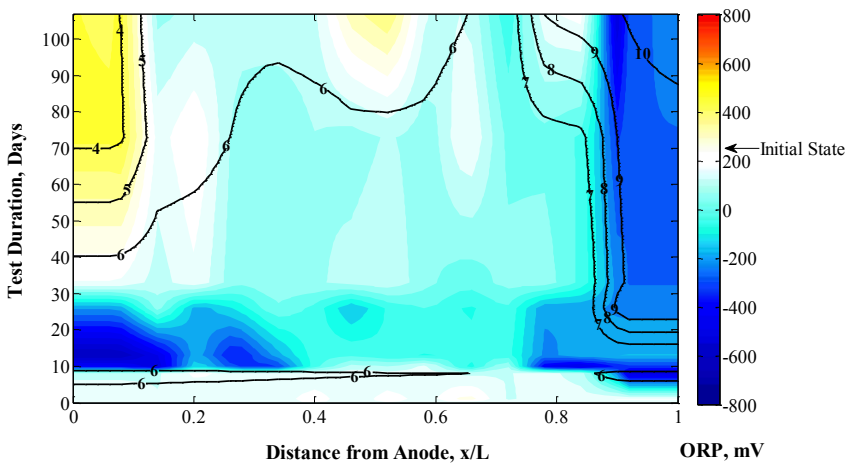

Figure 2.17. Time evolution of ORP measurements and pH contours for PA oil cell at 1 A/m^2

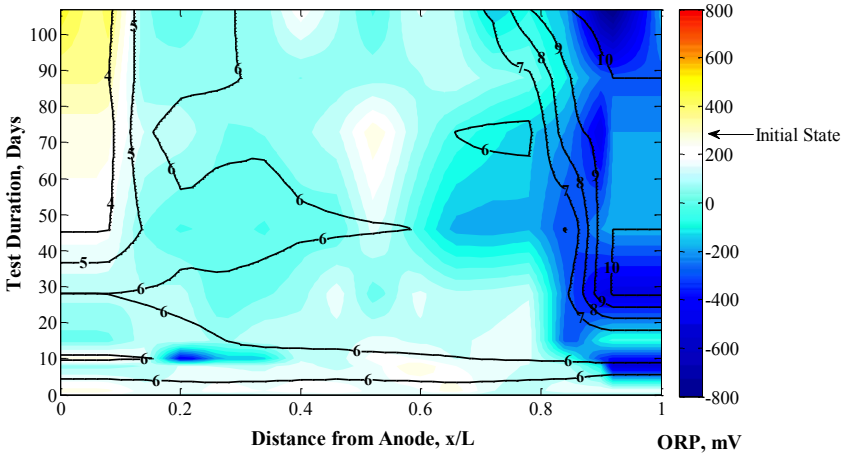

Figure 2.18. Time evolution of ORP measurements and pH contours for CA oil cell at 1 A/m^2

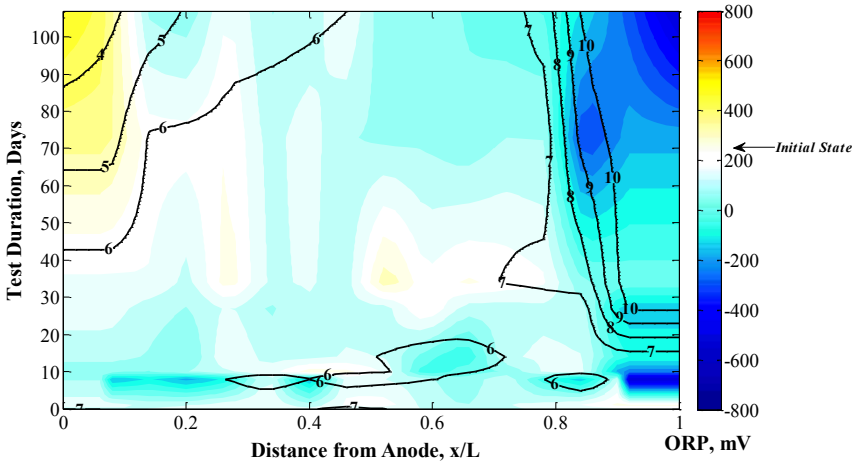

Figure 2.19. Time evolution of ORP measurements and pH contours for Canad. oil cell at 1 A/m^2

FTIR Analysis

Complete FTIR analysis was conducted only on the 1Amp/m^2 run core samples since the low current density cores showed very little or no change in their FTIR spectra and ORP distribution over time. The normalized ORP and the average normalized FTIR absorbance for asphaltenes (S,O,H; C-N, C-O, C=O, OH functional groups) are plotted for all three oils in Figure 2.20. This data was obtained at the center of each core, where pH remained constant at around 6. As observed, those samples for which ORP increased above the initial, the asphaltene content increased as well, while the asphaltene content decreased when the ORP decreased below the initial value. Hence, for neutral pH conditions, a reductive environment promotes a drop in asphaltene content while an oxidative environment tends to increase it.

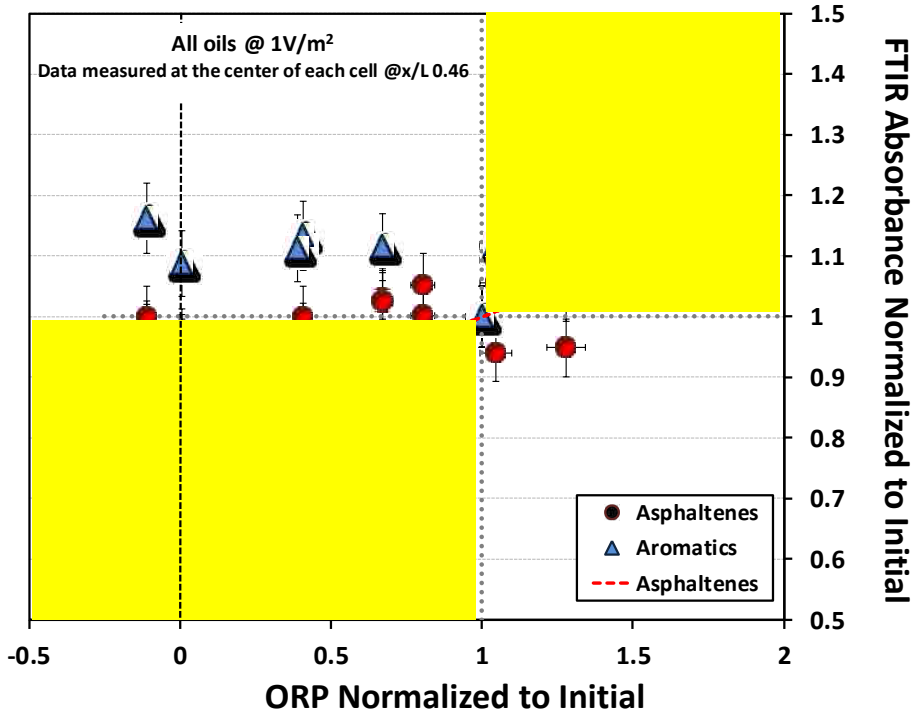

Figure 2.20. ORP and FTIR absorbance for asphaltenes for all three oil samples at the center of each core

The FTIR absorbance values for asphaltenes and aromatics normalized to their initial values measured at all three locations (anode region, central region and cathode region) of the cores for all crude oil samples tested at 1 A/m^2 are correlated to the normalized ORP measured at the same location in Figure 2.21. There are three discernible regions on this graph. The first area is the cathode region in which ORP is negative and the FTIR absorbance of asphaltenes has reduced compared to its initial state. The second area is the central area where the ORP is positive and the FTIR absorbance appears to be constant compared to the initial state, yet it is clearly a transition zone. The third area is the anode region where ORP is positive and well above the initial and the FTIR absorbance are all above the initial values. The aromatic contents are almost all above the original for all ORP distribution, showing no discernible relation between the two parameters, hence independent of the state of ORP.

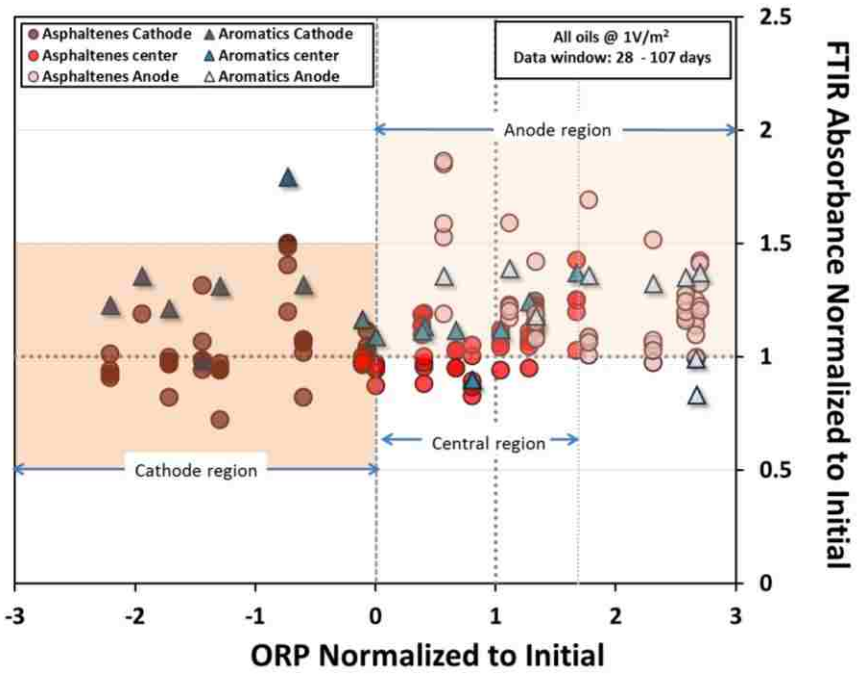

Figure 2.21. The Normalized ORP versus normalized FTIR absorbance for asphaltenes and aromatics for all oil samples tested at 1A/m^2

Viscosity and SARA Analysis

At the completion of the core runs in 107 days, the systems were turned off, cells dismantled and representative specimens from the anode, center, and cathode regions of the cores of 1 Amp/m^2 were collected. Samples were collected, along with corresponding ones from control cores at this time as well.

The viscosity of the oils extracted from 107-day formation samples showed a significant drop in all regions compared to their control value for the PA and Canadian oils, as shown in Figures 2.22 and 2.23. For PA oil sample, the viscosity dropped by 35% in the anode region, 23% in the middle region, and about 13% in the cathode section. For the Canadian oil sample, the viscosity at the anode region dropped by 69% and by 26% in the cathode region.

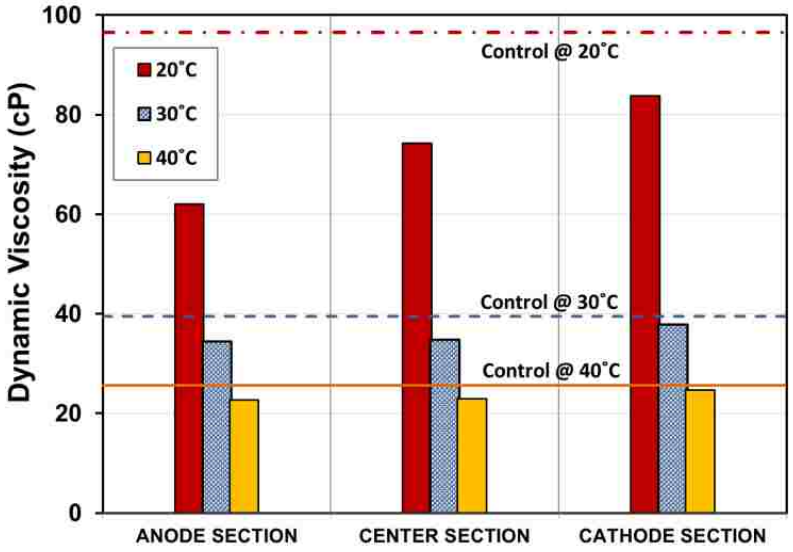

Figure 2.22. The post-test viscosity distribution of **PA** oil cell compared to its control

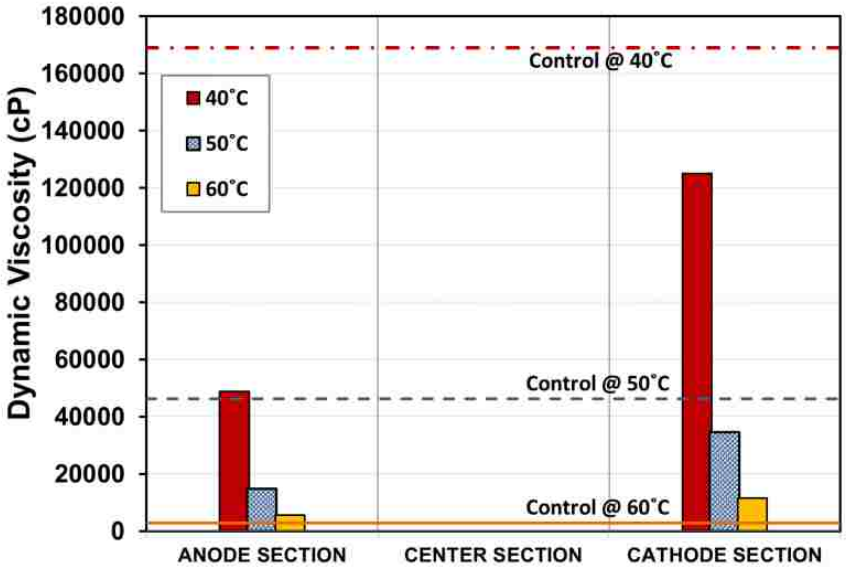

Figure 2.23. The post-test viscosity distribution of **Canadian** oil cell compared to its control

The SARA analysis measures the contents of saturates, asphaltenes, resins and aromatics in crude oil. It is a method for characterization of heavy oils based on fractionation, whereby a heavy oil sample is separated into smaller quantities or fractions, with each fraction having a different composition. The post-test SARA results of the test cores' oils and those of the accompanying control cores oils are given in Figures 2.24, 2.25, and 2.26. As it can be seen in Figure 2.24, the PA oil sample contains mostly saturates. It appears that there are no marked changes in the SARA components of PA oil sample.

The largest changes in the SARA analysis occur in Canadian oil sample, presented in Figure 2.26. There is significant increase in the saturate content of the oil and a significant decrease in the asphaltene content of the oil both at the anode and cathode regions. The aromatic and the resin contents do not show as large a change from the control. In concert with the

viscosity analysis, the CA oil sample SARA analysis show a decrease in saturates and aromatics while a substantial increase of asphaltenes in the anode region.

The findings of viscosity and SARA for the PA and Canadian oil cores comply well with the FTIR analysis conducted. In all of these tests the largest changes were observed with Canadian oil samples, and the smallest ones with PA oil samples. Important to note is that the data presented show clearly that electrically enhanced oil transformations take place in the test cores that result in substantial changes in oil viscosity and distribution of the functional groups in crude oil. As the lighter components (aromatics) of the oil increase and the heavier components (asphaltenes) decrease, which can be detected by drop in ORP at neutral or slightly alkaline conditions, the viscosity of the oil decrease as well.

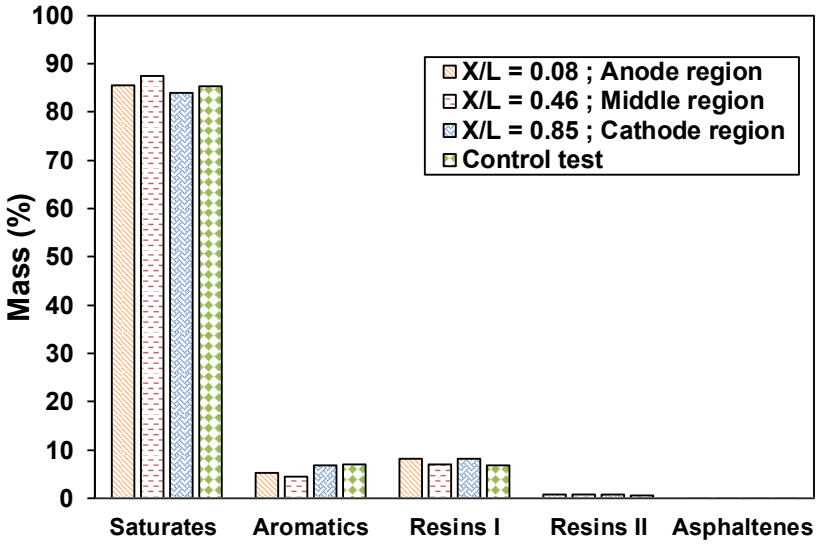

Figure 2.24. The post-test SARA distribution of PA core oil compared to its control

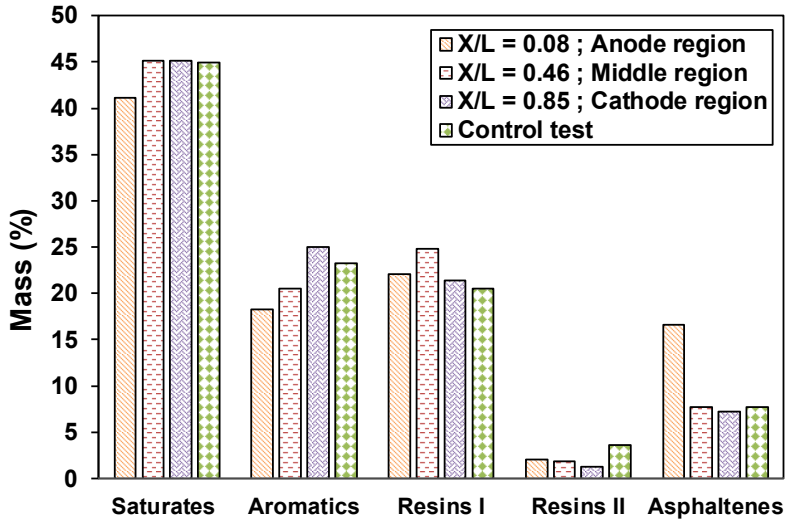

Figure 2.25. The post-test SARA distribution of CA core oil compared to its control

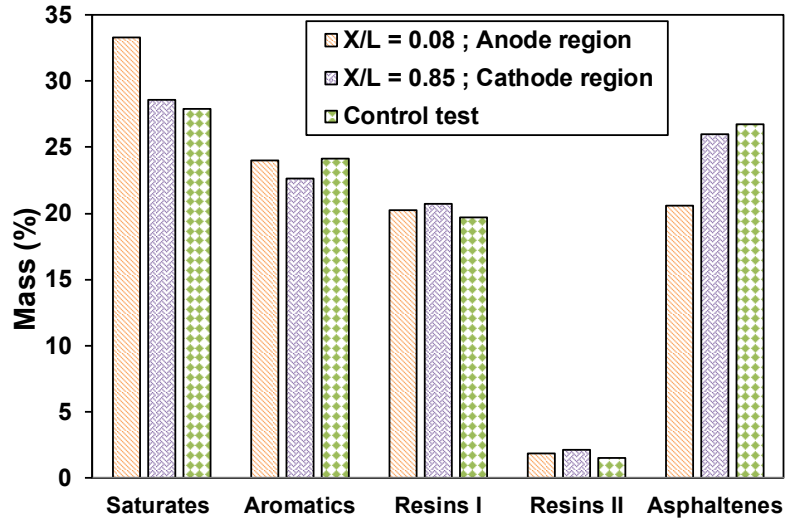

Figure 2.26. The post-test SARA distribution of Canadian core oil compared to its control

The results of these experiments indicated that electrochemical reactions do take place which affect the transformation of heavy crude oil into its different components due to the passage of current through the formation. As the lighter components (aromatics) of the oil increase and the heavier components (asphaltenes) decrease, the viscosity of the oil decrease which in turn increases the mobility of the crude oil. The viscosity analysis on the formation oil retrieved from formation sample taken at the end of the experiments showed a significant drop in the viscosity of the formation oil, specifically for heavy crude oil.

Chapter 3

Set of governing equations

3.1. Incompressible single phase flow under applied pressure gradient

The basic equation describing the flow of a fluid through a porous medium is the continuity equation which states that mass is conserved and expressed as:

$$\frac{\partial}{\partial t}(\varphi\rho) + \nabla[\rho v] = q \tag{3.1}$$

Where, φ is the porosity, ρ is fluid density, v is the fluid velocity, and q is the sources or sinks, that is, outflow and inflow per volume at designated well locations. For low flow velocities v, flow through porous media is modeled through empirical Darcy's law in which the fluid velocity, v is related to pressure p and gravity forces through the following gradient law:

$$v = \frac{-\mathbf{K}}{\mu}(\nabla P_w - \rho_w g \nabla z) \tag{3.2}$$

Where, **K** is the permeability, μ is the viscosity, g is the gravitational constant and z is the spatial coordinate in vertical direction. In most real field geological reservoir models, **K** is an anisotropic diagonal tensor [5, 13, 16, 30, 34, and 46]. In equation 3.2., there are two driving forces in porous media flow: gravity and the pressure gradient. Since gravity forces are approximately constant inside a reservoir domain Ω, pressure gradient is considered as the main driving force and can be considered as the main unknown parameter. To solve for the pressure, Darcy's law (Eq. 3.2) with the continuity equation (Eq. 3.1) are combined. Assuming that the

porosity φ is constant in time and the fluid is incompressible, the temporal derivative term in Eq. 3.1 vanishes and the following equation for the water pressure is obtained:

$$\nabla . v_w = -\left[\frac{\mathbf{K}}{\mu_w}(\nabla P_w - \rho_w g \nabla z)\right] = \frac{q_w}{\rho_w} \tag{3.3}$$

To complete the single phase flow model, boundary conditions needed to be specified. In petroleum and reservoir engineering, the common practice is to use no-flow boundary conditions [5, 13, 16, 30, 34, and 46]. Hence, on the reservoir boundary $\partial\Omega$ we impose $v_w = 0$, where n is the normal vector pointing out of the boundary $\partial\Omega$. This gives an isolated flow system where no water can enter or exit the reservoir.

3.2. Two phase immiscible flow under applied hydraulic gradient

Assuming Darcy's law holds for flow of both phases and considering the mass conservation in the system, the simplified two phase flow equations are [6, and 6]:

$$\frac{\partial}{\partial t}(\Phi S_w \rho_w) = -\nabla[\rho_w v_w] + q_w \tag{3.4}$$

$$v_w = \frac{-k_{rw}\boldsymbol{k}}{\mu_w}(\nabla P_w - \rho_w g \nabla z) \tag{3.5}$$

$$\frac{\partial}{\partial t}[\Phi S_o \rho_o] = -\nabla[\rho_o v_o] + q_o \tag{3.6}$$

$$v_o = \frac{-k_{ro}\boldsymbol{k}}{\mu_o}(\nabla P_o - \rho_o g \nabla z) \tag{3.7}$$

$$S_w + S_o = 1 \tag{3.8}$$

$$P_C = P_o - P_w \tag{3.9}$$

Table 3.1 summarizes all the parameters used in the simplified two phase flow equations.

Table 3.1. Parameter's description used in the equations 3.4 to 3.9

Parameter	Definition	Unit (metric)
Φ	Porosity of the media	-
S_w	Water saturation	-
ρ_w	Mass density of water	Kg/m^3
v_w	Velocity of water phase	m/day
q_w	Source/sink term in water phase	m^3/day
$\boldsymbol{k}$	Intrinsic permeability of the medium	m^2
k_{rw}	Relative permeability of water phase	-
μ_w	Dynamic viscosity of the water	Pa.sec
P_w	Hydraulic pressure in water phase	kPa
S_o	Oil saturation	-
ρ_o	Mass density of oil	Kg/m^3
v_o	Velocity of oil phase	m/day
q_o	Source/sink term in oil phase	m^3/day
k_{ro}	Relative permeability of oil phase	-
μ_o	Dynamic viscosity of the oil	Pa.sec
P_o	Hydraulic pressure in oil phase	kPa
g	Gravitational constant	m/sec^2
z	Elevation	m
P_C	Capillary pressure	kPa

Capillary pressure used in the equations is due to the curvature and surface tension of the interface between the oil and water phases. The flow equations are obviously nonlinear.

Nonlinearity is a characteristic feature of multiphase porous-media flows, since the permeability of the medium to one fluid varies with the saturation of any other fluid [5, 13, 16, 30, 34, and 46].

It is important to note that the simplified two phase flow equations are valid under the following assumptions

1) The two fluids are immiscible and incompressible and there is no exchange of chemical species among the fluid phases
2) The rock matrix is incompressible
3) The total flow rate of oil and water (as displacing fluid) remains constant
4) The gradient in phase pressure of the individual phases is a driving force of that specific phase
5) The effective permeability for the individual phases is a function of saturation of the phases involved

These set of equations supplied with proper initial and boundary conditions and are solved using different solution techniques. One important phenomenon in two phase flow is the contribution of viscous coupling through momentum transfer between the fluids. The contribution of viscous coupling is ignored in this simple representation of two phase flow. The contribution of viscous coupling in two phase flow is discussed in the following section.

3.3. Contribution of viscous coupling

As discussed in section 3.2, Darcy's Law for single phase flow has been directly extended to two phase flow using effective permeability coefficient (k_α):

$$v_\alpha = \frac{-1}{\mu_\alpha} k_\alpha (\nabla P_\alpha - \rho_\alpha g \nabla z) \tag{3.10}$$

α = *w,* for wetting phase; or *n,* for non-wetting phase

Where, u_α is the velocity, μ_α is dynamic viscosity, k_α is effective permeability, ∇P_α is hydraulic gradient (pressure gradient) and ρ_α is density of phase α. In reservoir simulation, the relative permeability term, $k_{r\alpha}$ is used widely, where:

$$k_\alpha = \boldsymbol{K}.k_{r\alpha} \tag{3.11}$$

Where, $\boldsymbol{K}$ is absolute permeability, and $k_{r\alpha}$ is relative permeability with respect to phase α. Relative permeability coefficients are typically determined as a function of the wetting phase saturation using standard experimental procedures [21, 31, 34, and 37].

The validity of the key assumption, that Darcy Law holds for two phase flow equations has been disputed since it implies that the flow of two fluids are essentially uncoupled and each flow has its own channel with pressure and elevation gradients acting as the driving forces. Viscous coupling between the two immiscible fluids due to momentum transfer across the fluid-fluid interface is omitted [12, 21, 33, and 72]. The generalized immiscible two phase flow model states that the flow of each fluid phase is a linear function of the gradients of both phases [12, 21, 33, and 72]. Therefore, fluid flow of each phase depends not only on the gradient of that particular phase but also on the corresponding gradient of the other phase. In oil recovery applications, depending on the characteristics of the formation rock, water and the residing oil, viscous drag could have significant contribution to the quantity of oil produced. Indeed, actual production rates of heavy oil up to 100 times higher than those computed by Darcy approach which omits the viscous coupling has been reported in literature [12].

Four generalized relative permeability coefficients are used in pressure driven flow. These include two diagonal ($k_{r,ww}\ and\ k_{r,nn}$), and the two off-diagonal ($k_{r,wn}\ and\ k_{r,nw}$) coefficients that capture the contribution of the viscous drag through momentum transfer [12, 21, 33, and 72], given in the following equation:

$$\begin{bmatrix} v_w \\ v_o \end{bmatrix} = -\boldsymbol{K} \begin{bmatrix} \frac{k_{r,ww}}{\mu_w} & \frac{k_{r,wn}}{\mu_n} \\ \frac{k_{r,nw}}{\mu_w} & \frac{k_{r,nn}}{\mu_n} \end{bmatrix} \begin{bmatrix} \nabla P_w \\ \nabla P_n \end{bmatrix} \tag{3.12}$$

Where, K is absolute permeability of the medium; v_w and v_n are the flow velocities; μ_w and μ_n are the dynamic viscosities; and ∇P_w and ∇P_n are the pressure gradients in the wetting and non-wetting phases, respectively.

The two diagonal coefficients can be determined as a function of the wetting phase saturation using standard test methods of steady state or un-steady state flow in rock cores. This requires injection of water and oil simultaneously at constant rates into the core. Once steady state flow is reached, the volumetric flow rate is measured. Given that the absolute permeability, pressure gradients, and dynamic viscosity of the fluids are known, the diagonal relative permeability coefficients can be determined at specific saturation levels. Experimental evaluation of the off-diagonal coefficients ($k_{r,wn}\ and\ k_{r,nw}$) is more challenging and only few studies have reported these coefficients from steady state experiments [19, 23, 36, 61, and 72]. These tests require that upon achieving steady state, the gradient in one phase is set to zero (the injection of that phase is cut off) while the gradient in the other phase is maintained. Then the volumetric flow rate of the cut-off phase is measured to compute the off-diagonal coefficients. These coefficients are reported to range between 0 to 24% depending on the fluids and porous medium condition. Figure 3.1 is an example of the experimentally evaluated off-diagonal coefficients [72].

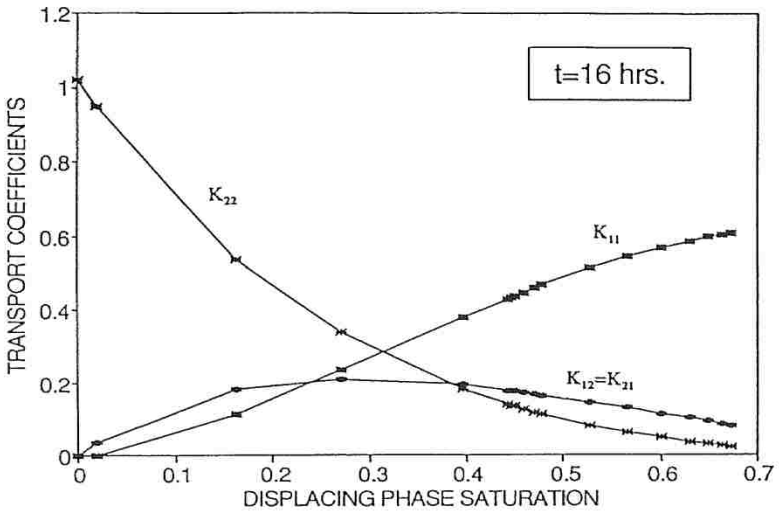

Figure 3.1. Experimentally evaluated transport coefficients [72]

Because of the difficulties associated with the experimental process, various numerical methods, including Lattice Boltzman Method (LBM) have been employed to evaluate the off-diagonal coefficients [19, 72, and 77]. Figure 3.2 shows the analytically evaluated off diagonal coefficients in a sand stone rock [77]

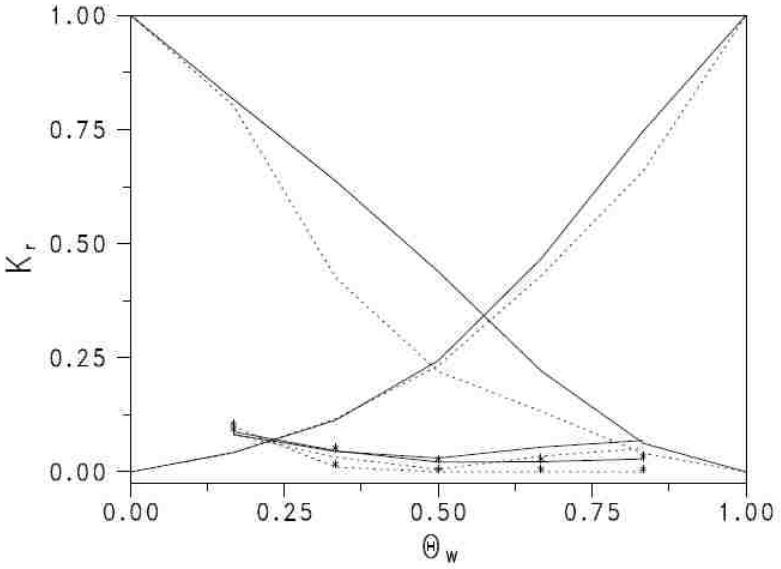

Figure 3.2. Analytically evaluated transport coefficients [77]

3.4. Two phase immiscible flow under applied hydraulic and electrical gradient

In the case of applied electric field to the formation in electrically enhanced oil recovery application, the contribution of applied electric gradient in generating flow in both phases should be considered. Electro-Osmotic (EO) velocity of a fluid in surface charged porous medium is given by Helmholtz-Smoluchowski equation as [102]:

$$v_e = \frac{-\varepsilon\xi}{\mu}\nabla E \tag{3.13}$$

Where, ε is the permittivity of the medium, ξ is zeta potential, μ is dynamic viscosity of the pore fluid, and ∇E is the applied electric gradient. The electro-osmotic (EO) permeability (k_e) of the medium is then defined as:

$$\boldsymbol{k_e} = \frac{-\varepsilon\xi}{\mu} \tag{3.14}$$

It should be noted that the *absolute EO permeability coefficient*, as it is referred to in here, is the EO permeability when only a single fluid (i.e., water) is present in the pores. From this point on, $\boldsymbol{k_e}$ is regarded as the absolute EO permeability coefficient for *water* only.

The coupled flow under applied electric gradient can be represented through use of four relative permeability coefficients similar to the coupled flow under hydraulic gradient (as given in equation 3.12):

$$\begin{bmatrix} v_w \\ v_o \end{bmatrix} = -\boldsymbol{k_e}\begin{bmatrix} (k_{er,ww}) & (k_{er,wo}) \\ (k_{er,ow}) & (k_{er,oo}) \end{bmatrix}\begin{bmatrix} \nabla E_w \\ \nabla E_o \end{bmatrix} \tag{3.15}$$

Where, the viscous coupling is considered through the off-diagonal coefficients for the water and the oil phases, $k_{er,wo}$ and $k_{er,ow}$, respectively. Equation 3.15 is analogous to the basic equation used in pressure driven two-phase flow given in Equation 3.12, where $\boldsymbol{k_e}$ replaces the $\boldsymbol{K}$ and electric gradient is the driving force. Electro-osmotic (EO) velocity given by Helmholtz-Smoluchowski (Eq. 3.13) is a well-accepted theory to describe the electroosmotic flow of water in surface charged geological media.

Equation 3.15 is an extension of the Helmholtz-Smoluchowski equation for immiscible two phase flow. The contributions of different physical and chemical parameters to the oil and water production are lumped into the generalized relative EO permeability coefficients introduced in Equation 3.15. Analogous to the Darcy Law for immiscible two phase flow, the generalized off-diagonal relative EO permeability coefficients are used to capture the contribution of the viscous coupling. Experimental and analytical evaluation of these coefficients is discussed in detail in chapter 4.

Upon addition of electrical gradients to the applied hydraulic and elevation gradients, the resulting fluid flow expressions for each phase can be expressed as:

$$\begin{bmatrix} v_w \\ v_o \end{bmatrix} = -\boldsymbol{k}\begin{bmatrix} \frac{k_{r,ww}}{\mu_w} & \frac{k_{r,wo}}{\mu_o} \\ \frac{k_{r,ow}}{\mu_w} & \frac{k_{r,oo}}{\mu_o} \end{bmatrix}\begin{bmatrix} \nabla P_w - \rho_w g \nabla z \\ \nabla P_o - \rho_o g \nabla z \end{bmatrix} - \boldsymbol{k_e}\begin{bmatrix} (k_{er,ww}) & (k_{er,wo}) \\ (k_{er,ow}) & (k_{er,oo}) \end{bmatrix}\begin{bmatrix} \nabla E_w \\ \nabla E_o \end{bmatrix} \tag{3.12}$$

In most of the reservoirs for electrically assisted oil transport, the oil phase is non-polar and the applied electric gradient does not create any flow in the oil phase. Hence, $k_{er,wo}$ and $k_{er,oo}$ coefficients are set to zero (see further details in chapter 4). Furthermore, when an electric

field is applied to the porous medium, because of the random distribution of fluids within the pores, it is an accepted assumption that the applied electric field will be the same in both phases ($\nabla E_w = \nabla E_o$) [45, 80]. Based on these two conditions, Equation 3.12 reduces to:

$$\begin{bmatrix} v_w \\ v_o \end{bmatrix} = -\boldsymbol{k} \begin{bmatrix} \frac{k_{r,ww}}{\mu_w} & \frac{k_{r,wo}}{\mu_o} \\ \frac{k_{r,ow}}{\mu_w} & \frac{k_{r,oo}}{\mu_o} \end{bmatrix} \begin{bmatrix} \nabla P_w - \rho_w g \nabla z \\ \nabla P_0 - \rho_o g \nabla z \end{bmatrix} - \boldsymbol{k_e} \begin{bmatrix} k_{er,ww} \\ k_{er,ow} \end{bmatrix} \begin{bmatrix} \nabla E_w \\ \nabla E_w \end{bmatrix} \tag{3.13}$$

Now, the system of equations to be solved under applied initial and boundary conditions is:

$$\frac{\partial}{\partial t}(\Phi S_w \rho_w) = -\nabla[\rho_w v_w] + q_w \tag{3.14}$$

$$v_w = -\boldsymbol{k}\frac{k_{r,ww}}{\mu_w}(\nabla P_w - \rho_w g \nabla z) - \boldsymbol{k}\frac{k_{r,wo}}{\mu_o}(\nabla P_o - \rho_o g \nabla z) - \boldsymbol{k_e} k_{er,ww}(\nabla E_w) \tag{3.15}$$

$$\frac{\partial}{\partial t}[\Phi S_o \rho_o] = -\nabla.[\rho_o v_o] + q_o \tag{3.16}$$

$$v_o = -\boldsymbol{k}\frac{k_{r,ow}}{\mu_w}(\nabla P_w - \rho_w g \nabla z) - \boldsymbol{k}\frac{k_{r,oo}}{\mu_o}(\nabla P_o - \rho_o g \nabla z) - \boldsymbol{k_e} k_{er,ow}(\nabla E_w) \tag{3.17}$$

$$S_w + S_o = 1 \tag{3.18}$$

$$P_C = P_o - P_w \tag{3.19}$$

There are several alternatives in formulation of the partial differential equations in the above system including (i) formulation in phase pressures, (ii) formulation in phase pressure and

saturation, and (iii) formulation in global pressure [13, 15, 16, 26, 30, 31, and 66]. When formulated in phase pressures, simultaneous solution techniques can be used to solve the system of equations. When, formulated in phase pressure and saturation, Implicit Pressure Explicit Saturation (IMPES) technique can be used to solve the system of equations. Finally, to reduce the coupling in the system, equations can be formulated in global pressure [13, 15, 16, 26, 30, 31, and 66].

3.5. Formulation in phase pressure (oil pressure) and saturation (water saturation)

Capillary pressure is a function of water saturation and the direction of saturation change (drainage or imbibition). Different empirical correlations between saturation and capillary pressure have been developed including the Brooks and Corey [21] correlation expressed as:

$$P_C = P_d S_w^{(-1/\lambda)} \tag{3.20}$$

Where, P_C is capillary pressure, P_d is entry capillary pressure, and λ is related to the pore size distribution of the porous medium (in the range of 0.2 to 3.0).

Relative permeability coefficients are function of wetting phase saturation (usually water saturation). These coefficients must be determined experimentally or using empirical correlations for specific porous medium of interest. However, there are several analytical expressions between relative permeability coefficients and wetting phase saturation including the Brooks and Corey [23] correlation expressed as:

$$k_{r,ww} = S_w^{\frac{2+3\lambda}{\lambda}} \tag{3.21}$$

$$k_{r,oo} = {S_o}^2[1 - (1 - S_o)^{\frac{2+\lambda}{\lambda}}] \quad (3.22)$$

There is no analytical expression yet developed for correlating diagonal and off-diagonal relative permeability coefficients ($k_{r,ow}$) to the wetting phase saturation. This coefficient needs to be experimentally determined as a function of wetting phase saturation for the porous medium of interest (see chapter 4, section 4.4).

Assuming that the capillary pressure has a unique inverse function as:

$$\mathrm{S_w} = {P_C}^{-1} \quad (3.23)$$

Equations 3.14 to 3.17 can be combined as the following:

$$\frac{\partial}{\partial t}(\Phi S_w \rho_w) = \nabla\left[\rho_w\left(\boldsymbol{k}\frac{k_{r,ww}}{\mu_w}(\nabla P_o - \frac{dP_c}{dS_w}\nabla S_w) + \boldsymbol{k}\frac{k_{r,wo}}{\mu_o}\nabla P_0\right) + \boldsymbol{k_e} k_{er,ww}\nabla E_w\right] + q_w \quad (3.24)$$

$$\frac{\partial}{\partial t}(\Phi(1 - S_w)\rho_O) = \nabla\left[\rho_O\left(\boldsymbol{k}\frac{k_{r,ow}}{\mu_w}(\nabla P_o) + \boldsymbol{k}\frac{k_{r,oo}}{\mu_o}\nabla P_0\right) + \boldsymbol{k_e} k_{er,ow}\nabla E_o\right] + q_o \quad (3.25)$$

To solve the system of equations, appropriate initial and boundary conditions are needed to be specified in the space domain Ω (ϵR^3) and time interval *T(0, T)*. For initial conditions, usually the main unknown (phase pressures) are specified over the entire domain at t = 0. For boundary conditions the following cases are possible [13, 15, 16, 26, 30, 31, and 66]:

a) When the phase pressure is specified as a function of position and time (Dirichlet)

b) When the pressure gradient is known (Neumann)

c) When the phase pressure and pressure gradient in an impervious boundary are specified (Mixed)

In reservoir simulation, usually the now flow boundary condition is used [13, 15, 16, 26, 30, 31, and 66].

3.6. Solution schemes

There are varieties of solution schemes for the set of equations used in reservoir simulation [13, 15, 26, 30, and 66]. Among these schemes, IMPES (Implicit pressure, explicit saturation), simultaneous solution, sequential, and adaptive implicit methods are widely used in petroleum industry. The simultaneous solution method solves the coupled non-linear equations simultaneously and implicitly. The advantage of this method is its stability and can take very large time steps while stability is maintained. The sequential methods solve the set of equations in an implicit fashion without developing a full coupling between the equations [13, 15, 26, 30, and 66]. Compared to IMPES and simultaneous solution schemes, the sequential schemes are less stable but more computationally efficient. The adaptive implicit scheme seek an efficient middle ground between the IMPES and sequential solution schemes in the sense that at a given time step, the expensive simultaneous solution scheme is assigned to the blocks that require it, and the IMPES scheme is implemented on the remaining blocks [13, 15, 26, 30, and 66]. In this study the IMPES technique is used and is described in the following section.

3.7. IMPES technique

This technique is widely used in petroleum industry and was developed by Sheldon and coworkers [101] and Stone and Grader [104]. The method separates the computation of pressure from saturation. The coupled system is split into a pressure equation and a saturation equation and

the pressure and saturation equations are solved using implicit and explicit time approximation approaches.

In the following section the flow of two phases, one water phase *w* and one oil phase *o* are considered and the pressure and saturation equations are derived.

3.7.1. The Saturation Equation for Incompressible Immiscible Flow

As discussed before, continuity equations for the two phases have the following form:

$$\frac{\partial}{\partial t}(\varphi S_\alpha \rho_\alpha) + \nabla.[\rho_\alpha v_\alpha] = q_\alpha \tag{3.26}$$

Defining the water and oil phase mobility (functions of water saturation) as the following:

$$\lambda_w(s_w) = \left(\frac{k_{r,w}}{\mu_w}\right) \tag{3.27}$$

$$\lambda_o(s_w) = \left(\frac{k_{r,o}}{\mu_o}\right) \tag{3.28}$$

The total mobility:

$$\lambda = \lambda_w + \lambda_o \tag{3.29}$$

The fractional flow for water and oil phases (function of water saturation) is defined as [13, 26, and 30]:

$$f_w = \frac{\lambda_w}{\lambda} \; ; \; f_o = \frac{\lambda_o}{\lambda} \tag{3.30}$$

The total velocity and total flow are defined as:

$$v = v_w + v_o \quad ; \quad q = q_w + q_o \tag{3.31}$$

Multiplying Darcy's law for each phase with the mobility of the other phase and ignoring the contribution of viscous coupling under applied pressure gradient:

$$\lambda_o v_w = -\mathbf{K}\lambda_w\lambda_o(\nabla P_w - \rho_w g\nabla z) \tag{3.32}$$

$$\lambda_w v_o = -\mathbf{K}\lambda_w\lambda_o(\nabla P_o - \rho_o g\nabla z) \tag{3.33}$$

Subtracting equation 3.32 from equation 3.33 gives:

$$\lambda_w v_o - \lambda_o v_w = -\mathbf{K}\lambda_w\lambda_o(\nabla P_c + (\rho_o - \rho_w)g\nabla z) \tag{3.34}$$

To find an expression that only contains the total velocity and the saturation of the wetting phase, we use the fact that $v_o = v - v_w$ to get:

$$\lambda_w v - (\lambda_w + \lambda_o)v_w = -\mathbf{K}\lambda_w\lambda_o(\nabla P_c + (\rho_o - \rho_w)g\nabla z) \tag{3.35}$$

Considering $s = s_w$ and using the fractional flow of water as $f(s) = \frac{\lambda_w}{\lambda_w+\lambda_o}$ we have:

$$v_w = f(s)v - \mathbf{K}\lambda_o f(s)(\nabla P_c + (\rho_o - \rho_w)g\nabla z) \tag{3.36}$$

Inserting this equation into continuity equation for the wetting phase:

$$\varphi\frac{\partial S}{\partial t} + \nabla.[f(s)v - \mathbf{K}\lambda_o f(s)(\nabla P_c + (\rho_o - \rho_w)g\nabla z)] = \frac{q_w}{\rho_w} \tag{3.37}$$

This is the saturation equation. Similarly, the saturation equation for the incompressible and immiscible two phase flow under applied pressure and electric gradients can be derived as:

$$\varphi \frac{\partial S}{\partial t} + \nabla.\left[f(s)v - \mathbf{K}\lambda_o f(s)(\nabla P_c + (\rho_o - \rho_w)g\nabla z) - \boldsymbol{k_e}\nabla E_w(f(s)k_{er,ow} + (f(s)-1)k_{er,ww})\right] = \frac{q_w}{\rho_w} \quad (3.38)$$

3.7.2. Pressure Equation for Incompressible Immiscible Flow

Summing the Darcy's law over the two phases we get the following equation:

$$v = v_w + v_o = -\mathbf{K}\lambda_w(\nabla P_w - \rho_w g\nabla z) - \mathbf{K}\lambda_o(\nabla P_o - \rho_o g\nabla z) \quad (3.39)$$

Taking divergence on both sides and considering the fact that $\nabla.[v] = q$ we have:

$$\nabla.[v] = -\nabla\{\mathbf{K}\lambda_w(\nabla P_w - \rho_w g\nabla z) + \mathbf{K}\lambda_o(\nabla P_o - \rho_o g\nabla z)\} = q \quad (3.40)$$

This is the pressure equation. Similarly, the pressure equation for the incompressible and immiscible two phase flow under applied pressure and electric gradients can be derived as:

$$\nabla.[v] = -\nabla\left\{\mathbf{K}\lambda_w(\nabla P_w - \rho_w g\nabla z) + \mathbf{K}\lambda_o(\nabla P_o - \rho_o g\nabla z) + \boldsymbol{k_e}\nabla E_w(k_{er,ww} + k_{er,ow})\right\} = q \quad (3.41)$$

Designing numerical methods for the pressure equation that correctly account for flow dynamics and properly balance the spatial and temporal derivatives is a very difficult task due to the many prominent scales that occur in porous media permeability [15, 26, 30, and 66]. There are two unknown phase pressures, P_w and P_o in the pressure equation. By introducing the

capillary pressure, $P_{cow} = P_o - P_w$ which is assumed to be a function of water saturation, one of these pressures can be eliminated. However, this leads to coupling between the pressure equation and the saturation equation. To avoid this coupling, instead of using the phase pressures, P_w and P_o , a global pressure P can be introduced. The global pressure is defined to contain saturation-dependent pressure terms, to give a better decoupling of the pressure and saturation equations [15, 26, 30, and 66]. The global pressure is defined as $P = P_o - P_c$, where the saturation-dependent complementary pressure P_c is defined by [18, 28] :

$$P_c(S_w) = \int_1^{S_w} f_w(\beta) \frac{\partial P_{cow}}{\partial S_w}(\beta) d\beta \tag{3.42}$$

Where, the fractional-flow function $f_w = \frac{\lambda_w}{\lambda}$ measures the water fraction of the total flow. Since $\nabla P_c = f_w \nabla P_{cow}$, the total velocity can be expressed as a function of the global pressure:

$$v = v_w + v_o = -\mathbf{K}(\lambda_w + \lambda_o)\nabla P + \mathbf{K}(\lambda_w \rho_w + \lambda_o \rho_o) g \nabla z + \boldsymbol{k_e} \nabla E_w (k_{er,ww} + k_{er,ow}) \tag{3.43}$$

Using the total mobility and global pressure, the following pressure equation can be obtained:

$$-\nabla . \{ \mathbf{K}\lambda \nabla P - \mathbf{K}(\lambda_w \rho_w + \lambda_o \rho_o) g \nabla z + \boldsymbol{k_e} \nabla E_w (k_{er,ww} + k_{er,ow}) \ \} = q \tag{3.44}$$

To make the pressure equation complete, appropriate boundary conditions need to be prescribed (e.g. imposing no-flow boundary conditions).

3.8. Other approaches for incorporating viscous coupling

Another approach of incorporating viscous coupling is based on the application of rational thermodynamics. A theory of two-phase flow is developed in which interfacial areas are introduced as separate thermodynamic entities possessing mass, momentum, and energy and their macro-scale effects are explicitly included [48, 60, and 82]. In this theory, the momentum balance equations were derived not only for phases but also for the interfaces. The following extended form of Darcy's law is developed [48]:

$$u_\alpha = -\frac{k_\alpha}{\mu_\alpha}\left(\nabla P_\alpha - \rho_\alpha g - \psi_{\alpha a}\nabla a_{nw} - \psi_{\alpha S}\nabla S_w\right) \tag{3.43}$$

Where, $\psi_{\alpha a}$ and $\psi_{\alpha S}$ are material properties, a_{nw} is the specific area of fluid-fluid interfaces (amount of interfacial area per unit volume of the porous media). The average velocity of fluid-fluid interfaces are given as:

$$u_{nw} = -k_{nw}\left[(\nabla a_{nw}\sigma_{nw}) + \psi_{nw}\nabla S_w\right] \tag{3.44}$$

Where, k_{nw} is the permeability of interface, ψ_{nw} is a material property, σ_{nw} is the macroscale interfacial tension. Equations 3.43 and 3.44 must be supplemented with the following equations of balance of volume for phase saturation and specific interfacial area (assuming incompressible phases and constant mass density for interface):

$$n\frac{\partial}{\partial t}(S_\alpha) + \nabla[u_\alpha] = q_\alpha \tag{3.45}$$

$$\frac{\partial}{\partial t}(a_{nw}) + \nabla[a_{nw}\, u_{nw}] = E_{nw} \tag{3.46}$$

Where, E_{nw} is the net rate of production of interfaces (proposed to be function of saturation and its time rate of change). If a porous medium is fully saturated by a given phase, there are no fluid-fluid interfaces (a_{nw} = 0). As the porous medium is invaded by another phase (due to either imbibition or drainage), interfaces are created ($E_{nw} > 0$) [82]. As the invasion process continues, the saturation of the invading phase at some point reaches a maximum value. At this point, generation of interfacial area stops ($E_{nw} = 0$), and beyond this point destruction of interfacial area starts ($E_{nw} < 0$).

The potential significance of terms appearing in the set of equations, are investigated through Dynamic Pore Network Modeling [60]. Based on this analysis, it was found that including interfacial area and saturation gradient ($\nabla a_{nw}\ and\ \nabla S_w$) can implicitly account for the moving boundary between the two fluids during drainage.

A series of simplifying assumptions are made [82] to reduce the set of equations to the following system:

$$n\frac{\partial}{\partial t}(S_w) + \nabla[u_w] = q_w \qquad \text{with} \qquad u_w = -\frac{k_{rw}\underline{\underline{K}}}{\mu_w}(\nabla P_w - \rho_w g) \tag{3.47}$$

$$n\frac{\partial}{\partial t}(S_o) + \nabla[u_o] = q_o \qquad \text{with} \qquad u_o = -\frac{k_{ro}\underline{\underline{K}}}{\mu_o}(\nabla P_o - \rho_o g) \tag{3.48}$$

$$\frac{\partial}{\partial t}(a_{nw}) + \nabla[a_{nw}\, u_{nw}] = E_{nw} \qquad \text{with} \qquad E_{nw} = -\underline{K}_{nw}\nabla(a_{nw}) \tag{3.49}$$

$$S_w + S_o = 1 \tag{3.50}$$

$$P_C = P_o - P_w \tag{3.51}$$

$$P_C = P_C(S_w, a_{nw}) \tag{3.52}$$

The constitutive relationships used in this theory are:

a) *Relative permeabilities*

$$k_{r\alpha} = S_{\alpha e}^{\,2} \qquad S_{\alpha e} = \frac{S_\alpha - S_{\alpha r}}{1 - S_{wr} - S_{nr}} \tag{3.53}$$

Where, $S_{\alpha r}$ is the residual saturation of phase α.

b) *Specific interfacial area (a_{nw})*

$$a_{nw}(S_w, P_C) = (a_{00} + a_{10} S_w + a_{01} P_C + a_{20} S_w^{\,2} + a_{11} S_w P_C + a_{02} P_c^{\,2}) \tag{3.54}$$

c) *Production/destruction rate of specific interfacial area (E_{nw})*

$$E_{nw}(S_w, P_C) = e_{nw}(S_w, P_C) \frac{\partial}{\partial t}(S_w) \tag{3.55}$$

In general, constitutive relationships (mainly capillary pressure and relative permeability curves) could be found using pore network modeling or Latice Boltzman Method (LBM) simulation. In pore network models, under static condition, there is no pressure gradient and thus no flow over the network. Under steady state condition, the saturation values do not change with time and the interfaces are at rest too, but there is a pressure gradient over the domain, and thus the fluids flow. Under transient conditions, the fluid-fluid interfaces move with time and the saturation changes. Dynamic pore network models can simulate the distribution of fluids and their

local pressure values under static, steady state, and transient conditions in an idealized porous medium [60, and 82].

The Latice Boltzman method involves solving the microscopic Boltzman equation which can be viewed as a discrete approximation of the incompressible Navier-Stoke equations based on Kinetic theory. In this method, fluid flow is represented by the distribution functions of fluid particles moving on a regular lattice [3, 71, and 90]. One of the main shortcomings of this method is the high computational cost compared to the pore network modeling.

In this study, the IMPES method is used to solve the system of governing equations. The details of the numerical modeling and simulations are provided in chapters 5 and 6 respectively.

3.9. Up-scaling issue

Intrinsic heterogeneities (porosity, permeability, water saturation) influence the multi-phase flow behavior in natural porous medium. Typically, the scale of these heterogeneities cannot be resolved and the up-scaling techniques are required [31, 34, and 46]. Different forces are likely to dominate on different scales. While on smaller scales capillary effects are more pronounced, the gravity effects and the viscous effects become more important at larger scales. In the simulation of multi-phase flow on larger scales (reservoir simulation), it is necessary to parameterize the effects of small-scale heterogeneities on the large-scale flow behavior [16, 30, and 34].

A variety of techniques have been developed and applied to transfer the information from the process scale to the simulation scale. These techniques are commonly referred to as up-scaling [16, 30, and 34]. The choice of the appropriate up-scaling method depends on the averaging scale, since the relative importance of capillary and gravity forces change with scale

core scale and higher [30, and 34]. In reservoir simulation, reservoir heterogeneity imposes a large range of scale and their interaction with various transport mechanisms control the overall performance of subsurface flow and transport processes. Modeling these processes at large scale requires proper scale up of both heterogeneity and the underlying transport mechanisms. The results from a fine scale numerical flow simulation reflecting the full physics of transport processes over a small volume of the reservoir, can be integrated with the volume averaging technique to provide effective description of transport at coarse scale [30, and 34].

Chapter 4

Evaluation of Transport Coefficients

4.1. Importance of transport coefficients

Evaluation of relative permeability coefficients is one of the key steps in reliable simulation of two phase flow in porous media. An extensive body of work exists on evaluation of these coefficients for two phase flow under pressure gradients. Oil transport under an applied electrical gradient in porous media is also governed by the principles of two phase flow, but is less understood. In this chapter, relative permeability coefficients under applied electric field are evaluated for a specific case of two phase fluid flow in water-wet porous media, where the second fluid phase is oil. It is postulated that the viscous drag on the oil phase, exerted by the electro-osmotic flow of the water phase is responsible for the transport of oil in the absence of a pressure gradient. Reliable prediction of the flow patterns necessitates accurate representation and determination of the relative permeability coefficients under the electrical gradient.

Mathematical models for petroleum reservoir simulation are valuable in predicting the oil production and visualizing reservoir flow patterns. Accurate determinations of the constitutive relations (e.g., capillary pressure and relative permeability curves) that influence these flow patterns are critical to these predictions. As discussed in chapter 3 (section 3.3), the literature is rich on experimental [15, 19, 23, 35, 61, and 72], and analytical [19, 71, and 77] methods of evaluation of relative permeability coefficients under applied pressure gradient. These studies examine the relative permeability coefficients as a function of the wetting phase saturation in two phase (e.g., water and oil) flow using standard test conditions. Figure 4.1 shows the

experimentally evaluated two diagonal coefficients for a rock sample (Core C in Table 4.1) under applied pressure gradient.

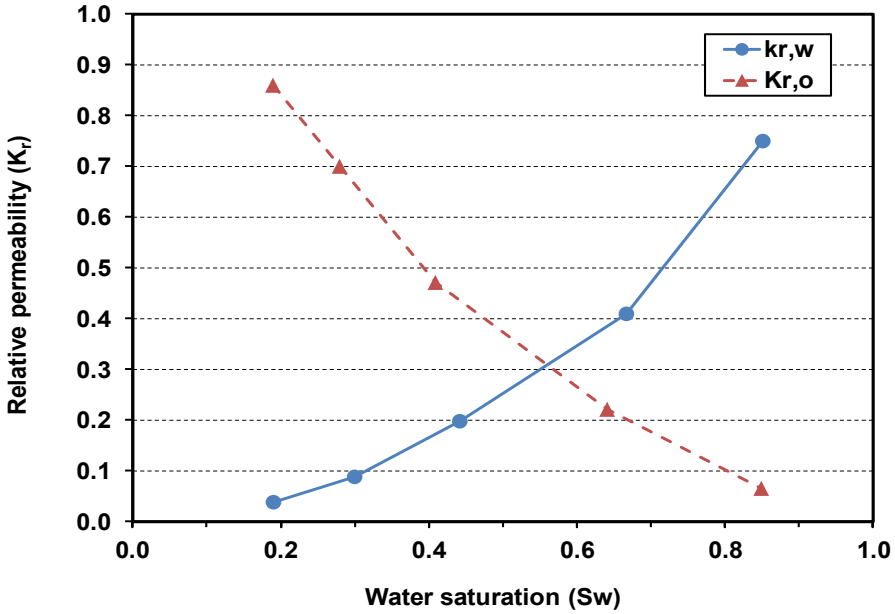

Figure 4.1. Experimentally evaluated diagonal relative permeability coefficients

The EO transport of non-conductive liquids (e.g., oil) using conductive liquids (e.g., water) in capillaries, otherwise known as *EO viscous pumps* has been investigated for MEMS devices and microfluidic fabrication technologies [39, 40, 41, and 74]. EO pumps are fabricated mostly of porous glass or fused silica with deprotonated silanol groups on the surface and are based on the EO flow of electrolyte to generate both flow and pressure differentials under a DC electric field [20, and 95]. The performance of EO pumps has been reported to depend on the porosity, tortuosity, and pore size of the matrix, pH and ionic concentration of the electrolyte [20, and 95]. The basic premise of EO pumps is that the electroosmotic flow of the conducting fluid

exerts a drag force on the non-conducting fluid to generate two phase flow, which is similar to the postulated behavior of electrically enhanced oil recovery.

In electrically enhanced oil recovery applications, a similar viscous drag phenomenon leads to oil transport under an applied electric field [4, 9, 10, 28, 41, 42, 47, 110, and 111]. In chapter 3, the EO relative permeability coefficients were introduced (see section 3.3). In order to evaluate the relative permeability coefficients as a function of water saturation, the porous medium is assumed to be water wet. So, here on after, the wetting phase refers to water (i.e., formation water) and the non-wetting phase refers to oil. Furthermore, when an electric field is applied to the porous medium, because of the random distribution of fluids within the pores, it is an accepted assumption that the applied electric field will be the same in both phases ($\nabla E_w = \nabla E_o$) [44, and 80]. In the following sections, the contribution of each of the four relative permeability coefficients to the flow and the experimental and analytical approaches used to evaluate them are discussed separately.

4.2. Diagonal relative permeability coefficient for water phase, $k_{er,ww}$

The first diagonal relative permeability coefficient ($k_{er,ww}$) was evaluated experimentally for four sand stone rock core specimens as a function of water saturation. Table 4.1 presents the properties of the rock cores and the flooding fluids used in the experiment. The cores were 36 mm in diameter and 82 mm in length. Initially, each core was dried and air vacuumed. Then, an electrolyte solution (simulating the formation water of same salinity) and oil were injected simultaneously at constant injection rate using a high pressure injection pump (Quizix Pump). The core saturation was determined once a steady state flow condition was reached. Then, the core was transferred to the electrokinetic (EK) test cell (Same cell as in Figure 2.4). In the EK cell the glass frits separated the core compartment from the formation water in the electrode

reservoirs, and the electric field was applied using titanium mesh electrodes placed at the two end caps of the core.

Table 4.1. Properties of the sandstone core and fluids used for evaluation of relative electro-osmotic permeability coefficients

Material	Properties
Sandstone core A	Porosity:14.5% , permeability: 3.6 mD , bulk wet density: 2.49 g/cm^3
Sandstone core B	Porosity:14.4% , permeability: 8.3 mD , bulk wet density: 2.43 g/cm^3
Sandstone core C	Porosity:12.8% , permeability: 2.3 mD , bulk wet density: 2.47 g/cm^3
Sandstone core D	Porosity:11.5% , permeability: 0.5 mD , bulk wet density: 2.45 g/cm^3
Crude Oil	API 25; dynamic viscosity = 0.0387 pas-sec; Specific gravity =0.79 at 20°C
Electrolyte solution	NaCl; Salinity= 30,000 ppm; Electrical conductivity = 45,000 µS

The typical current densities used in field applications of electrically enhanced oil recovery have been reported to be in the range of 1.0-1.5 Amp/m^2 [110, and 111]. To achieve a current density of 1 Amp/m^2 in laboratory, constant voltage gradient of 4V/cm was applied to each core. The volume production of each liquid was monitored at the cathode reservoir over time for 36 hours. Knowing the measured volume of the produced water, the applied electric gradient and the absolute EO permeability of the core (k_e), the $k_{er,ww}$ coefficient could be computed at the specific initial water saturation of the core. At the end of each experiment, the core was dried and air vacuumed and the procedure was repeated to establish the next water saturation level and to find the corresponding $k_{er,ww}$ coefficient. Figure 4.2 shows the measured $k_{er,ww}$ coefficient variation at four different water saturations of the four rock cores designated A, B, C, and D. As

observed, the $k_{er,ww}$ coefficients increased with water saturation, owing to higher water production by the EO flow.

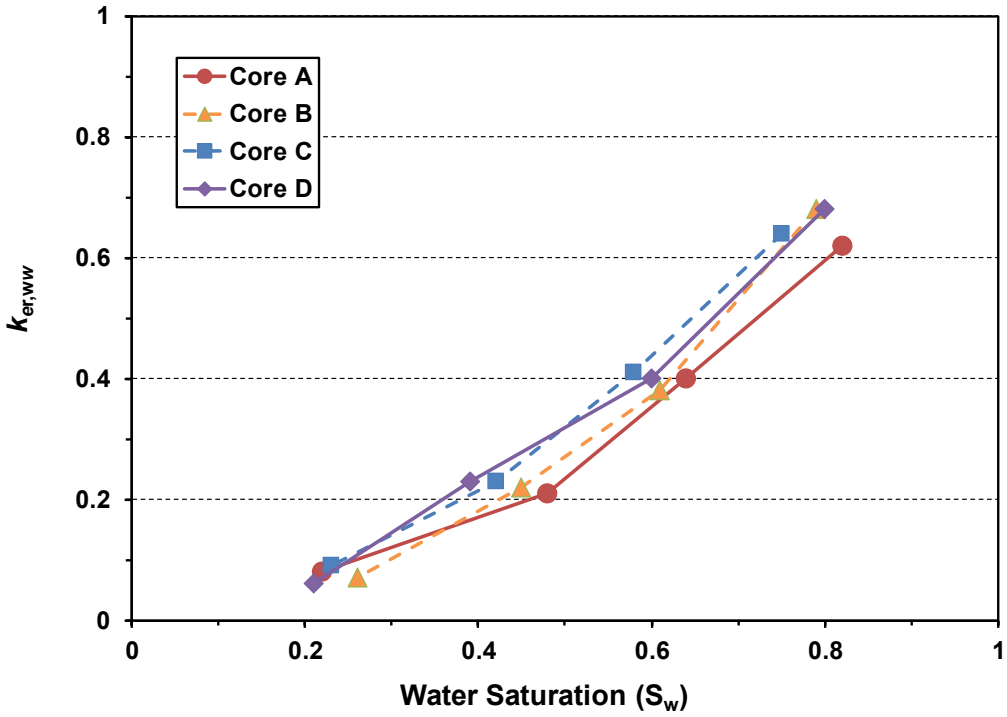

Figure 4.2. Evaluated $k_{er,ww}$ coefficient for the core samples

4.3. Diagonal relative permeability coefficient for oil phase, $k_{er,oo}$

Most crude oils are mixtures of non-polar compounds. Hence unlike water, which is polar and may contain dissolved charged particles, direct application of electric field do not create a notable electroosmotic body force, as it does in the formation water necessary to generate flow. Furthermore, to better understand the effect of applied electric field on the oil phase in two phase immiscible flow, one can compare the absolute EO permeability of the porous medium computed with either oil or water properties, using Helmholtz-Smoluchowski equation. The computed ratio

of k_e (cm^2/V.sec) of a given formation with oil to that with water is significantly low, ranging between10^{-7} to 10^{-3}. This stems from the large differences between the dynamic viscosity and the permittivity of the two liquids. The dynamic viscosity of most crude oils is in the range of 0.038-0.339 Pas.sec (for heavy crude oils the range is 1-5 Pas.sec), while for water it is around 0.001Pas.sec. The range of relative permittivity of most oils is 2.5-5, while for water it is 80. In conclusion, $k_{er,oo}$ was set equal to zero assuming negligible effect of the applied electric gradient on the oil phase body force.

4.4. Off-diagonal relative permeability coefficients for oil-water coupling, $k_{er,wo}$ and $k_{er,ow}$

Evaluation of the off-diagonal relative permeability coefficients is one of the major challenges when using two phase flow principles with coupling between the phases. Experimental procedures similar to those employed in evaluation of the off-diagonal relative permeability coefficients under pressure gradient cannot be used for electrical gradient case. It is difficult to find experimentally the flow of one phase generated due to the applied electric gradient in the other phase simply because in practice the electric gradient cannot be applied solely to one phase. To simplify the evaluation, it is assumed in here that the EO body force occur in the water phase only since the applied electric field cannot create appreciable EO body force in the oil phase, as discussed above. This implies that even though the electric field is applied to the entire medium simultaneously (both the water and the oil phases), the coupling coefficient, $k_{er,ow}$, can be evaluated experimentally by measuring the quantity of oil produced.

The volume of oil production at cathode was monitored for 36 hours during the EK tests of the rock cores designated A, B, C, and D. Once again, knowing the measured volume of the produced oil, the applied electric gradient and the absolute EO permeability of the core, the

$k_{er,ow}$ coefficient could be computed at the specific water saturation of the core. Figure 4.3 shows the distribution of the evaluated coefficients for the core specimens in two different scales for clarity.

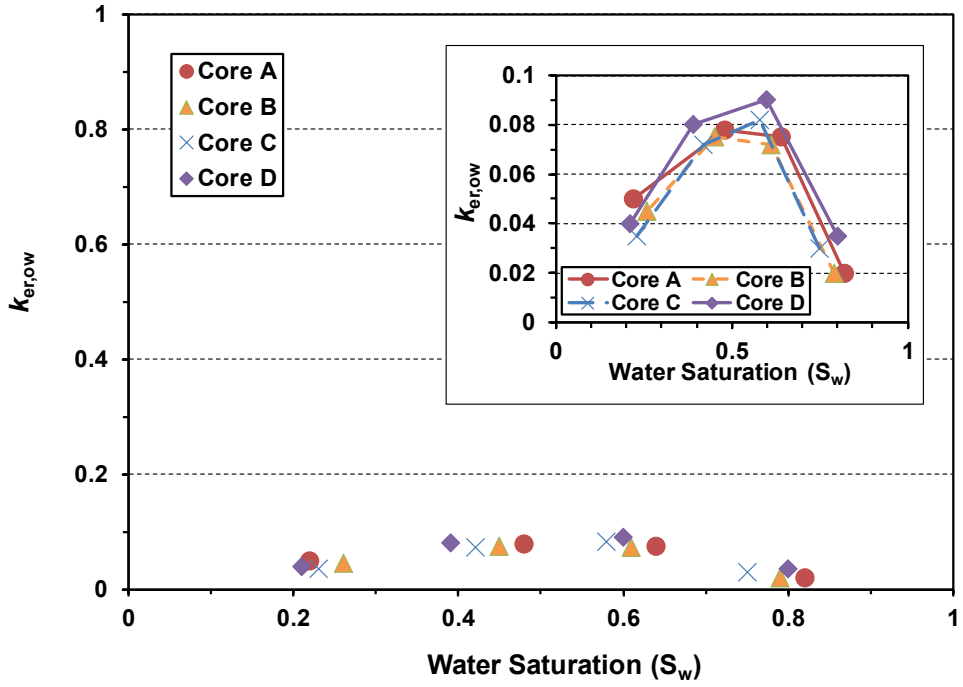

Figure 4.3. Experimentally evaluated $k_{er,ow}$ coefficient for the core samples

As observed from Figure 4.3, the coupling coefficient $k_{er,ow}$ varies from 0.02 to 0.08, on the dimensionless scale of 0 to 1. This is attributed to the viscous drag effect of water on the oil phase which results in the oil production. At low water saturations, the dragging capacity of the water is low owing to less water available in the pore space. As the water saturation increases the mass that creates the momentum to drag more oil increases. However, after a critical level of water saturation, the produced oil decreases despite the increase in the dragging capacity of the water, because less oil is available in the in the pore space. Relying on the contribution of the

relative permeability coefficients of the four rock cores tested, the oil recovery was determined to be in the range of 1 to 10% of the total liquid production, which can constitute a significant oil production in large scale residual oil recovery operations [4, 47, 1110, and 111].

The $k_{er,wo}$ coefficient, reflecting the contribution of oil to water production, was set to zero since EO body force in the oil phase was assumed to be insignificant, hence no viscous drag by oil exists at the interface to cause water flow.

Alternatively, the relative coefficient can be evaluated analytically. In the following section, we discuss the analytical evaluation of the off-diagonal coupling coefficients.

4.5. Analytical evaluation of coupling coefficients

The analytical representation of coupling coefficients is based on the principles of *EO viscous pumps* which use conductive liquids (e.g., water) to pump non-conductive liquids (e.g., oil) in micro-channels [39, 40, and 106]. A simple micro-channel (capillary), similar to EO viscous pump, is considered to evaluate the $k_{er,ow}$ coefficient. Figure 4.4 shows a schematic of the micro-channel filled with the two immiscible fluids. In this depiction, the inner layer is oil (crude oil, assumed to possess no electrical conductivity) and the outer layer, near the channel wall is water (the formation water, with electrical conductivity).

Under an applied electric gradient, the water with EO mobility will be driven by electro-osmosis, and the oil with no or negligible EO mobility will be dragged by the interfacial viscous force between the water and oil [39, 40, and 106]. To evaluate the $k_{er,ow}$ coefficient, the electric field is applied only to the water phase through the two end electrodes. The velocity and volume

of flow of each phase can then be calculated and used for evaluation of the $k_{er,ow}$ coefficient as a function of water saturation, or the volume fraction of water in the capillary.

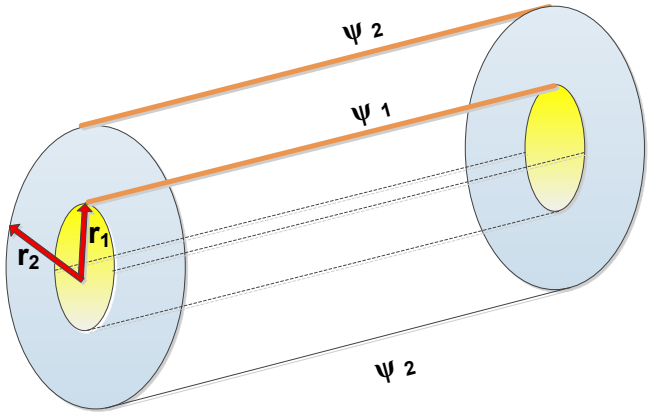

Figure 4.4. Schematic of the capillary used in the analysis

Several simplifying assumptions are needed for this analytical treatise. These assumptions are that, i) the two fluids are simple Newtonian fluids, ii) the fluid properties are constant and independent of local electric field, ion concentration, and temperature, and iii) two phase flow is steady and fully developed with no slip-boundary conditions both at the interface and at the wall. Accordingly, the continuity equations (velocity and momentum) for each phase are expressed as:

$$\begin{cases} \nabla v_\alpha = 0 \\ \rho_\alpha \left(\frac{\partial v_\alpha}{\partial t} + v_\alpha \nabla v_\alpha \right) = -\nabla P_\alpha + \nabla(\mu_\alpha \nabla v_\alpha) + (\rho_e)_\alpha \nabla E \end{cases} \tag{4.1}$$

Where,v_α, ρ_α , and $(\rho_e)_\alpha$ are the velocity, mass density, and the electric charge density of phase α, respectively. For small Reynolds number (typical for the range of EO velocities in geological media) the inertial force is zero. Therefore, the continuity equations can be simplified as:

$$\begin{cases} \nabla u v_\alpha = 0 \\ -\nabla P_\alpha + \nabla(\mu_\alpha \nabla v_\alpha) + (\rho_e)_\alpha \nabla E = 0 \end{cases} \tag{4.2}$$

The effect of the electric gradient on the flow can be evaluated by setting to zero the pressure gradients in both phases. Hence, when the electric gradient is applied to the water phase only, equation 4.2 reduces to:

$$\begin{cases} \mu_w \nabla^2 v_w = -(\rho_e)_w \nabla E \\ \mu_o \nabla^2 v_o = 0 \end{cases} \tag{4.3}$$

The charge distribution of each phase is required to calculate the phase velocities. The Poisson equation describes the electric potential distribution in cylindrical coordinates:

$$\frac{1}{r}\frac{\partial}{\partial r}\left(r\frac{\partial \psi}{\partial r}\right) + \frac{\partial^2 \psi}{\partial z^2} = \frac{-\rho_e}{\varepsilon} \tag{4.4}$$

Where, ψ is the surface potential and ε is the permittivity of the fluid. Equation 4.4 can be further simplified based on the assumption of thermodynamic equilibrium and the Debye-Huckel approximation for a low surface potential [74], as:

$$\frac{1}{r}\frac{d}{dr}\left(r\frac{\partial\psi}{\partial r}\right) = k^2\,\psi \tag{4.5}$$

Where, k is the reciprocal of EDL (Electric Double Layer) thickness (Debye length) defined as [55]:

$$k = \left(\frac{2ne^2{z_0}^2}{\varepsilon K_B T}\right)^{1/2} \tag{4.6}$$

Where, e is the elementary charge; n is the ionic concentration in equilibrium solution, K_B is the Boltzman constant; T is absolute temperature.

The boundary conditions imposed on the channel wall and at the oil-water interface are:

$$\begin{cases} \psi(r_1) = \psi_1 \\ \psi(r_2) = \psi_2 \\ \frac{d\psi}{dr} = 0 \quad at\ r = 0 \end{cases} \tag{4.7}$$

Where, ψ_2 is the surface potential on the channel wall, ψ_1 is the potential at the interface between the two fluids, $r_1$is the radius of inner layer (oil layer), and r_2 is the radius of the entire channel. The electric potential distribution in the channel is found by solving equation 4.5 under boundary conditions specified in equation 4.7 as:

$$\begin{cases} \psi(r) = \psi_1\ \frac{I_0(k_1 r)}{I_0(k_1 r_1)} \qquad for\ \ 0 \le r \le\ r_1 \\ \\ \psi(r) = \psi_2\ \frac{I_0(k_2 r)}{I_0(k_2 r_2)} + \psi_1\ \frac{I_0(k_2(r-2r_1)}{I_0(k_2 r_1)} \qquad for\ \ r_1 \le r \le r_2 \end{cases} \tag{4.8}$$

Figure 4.5 shows the charge distribution in the capillary for the case when $\Psi_1 = \Psi_2 = -25$ mV and the water saturation is $S_w = 0.8$

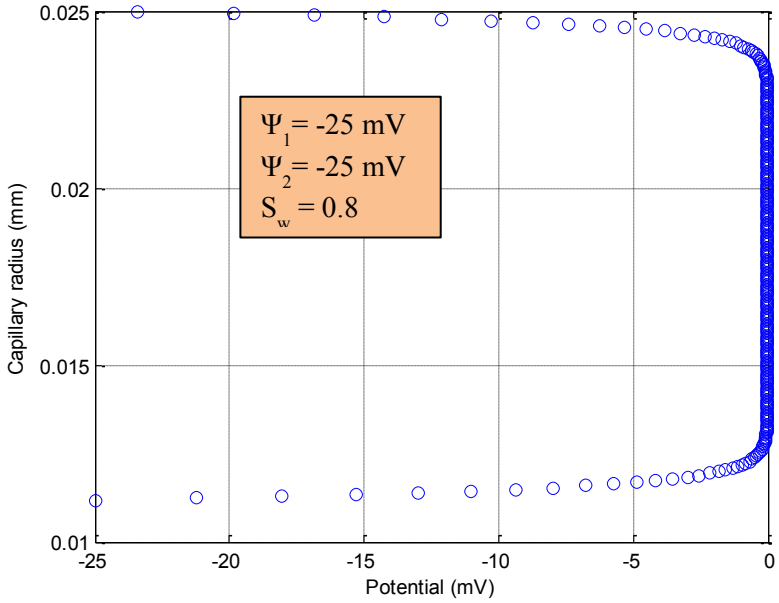

Figure 4.5. Charge distribution in the capillary

The charge density distribution can then be written as:

$$\begin{cases} \rho_e(r) = -\varepsilon_o k^2 \psi_1 \frac{I_0(k_1 r)}{I_0(k_1 r_1)} & for\ 0 \le r \le r_1 \\ \rho_e(r) = -\varepsilon_w k^2 \psi_2 \frac{I_0(k_2 r)}{I_0(k_2 r_2)} + \psi_1 \frac{I_0(k_2(r-2r_1))}{I_0(k_2 r_1)} & for\ r_1 \le r \le r_2 \end{cases} \quad (4.9)$$

Where, I_0 is zero order modified Bessel function of the first kind; $k_1$and k_2 are the reciprocal of EDL thickness of the inner and outer layers, respectively; and $\varepsilon_o$and ε_w are the permittivity of the inner and outer layers, respectively.

Figure 4.6 shows the micro-scale representation of the interfacial forces in the capillary. At the oil-water interface the continuity of velocity and hydrodynamic shear stress can be expressed as [40]:

$$\begin{cases} v_w = v_o \\ \tau_o = \tau_w - \rho_e(r_1)\nabla E \end{cases} \tag{4.10}$$

Where the shear stress at each phase is:

$$\tau_w = \mu_w \frac{\partial v_w}{\partial j} \quad and \quad \tau_o = \mu_o \frac{\partial v_o}{\partial j} \tag{4.11}$$

Where, j is the normal direction to the interface between the two fluids.

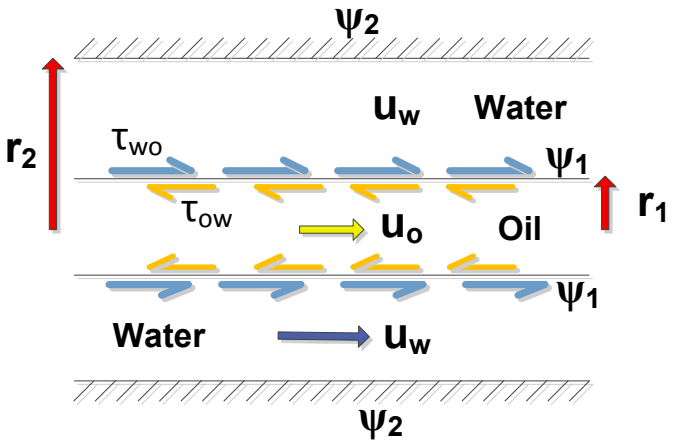

Figure 4.6 Micro-scale representation of the interfacial forces

The velocity of each phase is found by solving equation 4.3 using the charge density from equation 4.9, and the continuity conditions given in equation 4.10:

$$v_o = \frac{\epsilon_w \psi_2 k^2 \nabla E}{\mu_o} \left[\psi_2 \frac{I_0(kr_1) - I_0(kr_2)}{k^2 I_0(kr_2)} + \frac{\psi_1}{I_0(kr_1)} \int_{r_2}^{r_1} f(r)dr - \left[\frac{\psi_1}{I_0(kr_1)} f(r_1) + 2\psi_2 \frac{r_1 I_1(kr_1)}{k I_0(kr_2)} + \psi_1 \frac{r_1 I_1(kr_1)}{k I_0(kr_1)} \ln\left(\frac{r_1}{r_2}\right)\right]\right] \quad (4.12)$$

$$v_w = \frac{\epsilon_w \psi_2 k^2 \nabla E}{\mu_w} \left[\psi_2 \frac{I_0(kr) - I_0(kr_2)}{k^2 I_0(kr_2)} + \frac{\psi_1}{I_0(kr_1)} \int_{r_2}^{r} f(r)dr - \left[\frac{\psi_1}{I_0(kr_1)} f(r_1) + 2\psi_2 \frac{r_1 I_1(kr_1)}{k I_0(kr_2)} + \psi_1 \frac{r_1 I_1(kr_1)}{k I_0(kr_1)} \ln\left(\frac{r}{r_2}\right)\right]\right] \quad (4.13)$$

Where, I_1 is first order modified Bessel function of the first kind, and $f(r)$ is given as:

$$f(r) = 1/2(r - 2r_1)^2 \bar{}_0F_1\left[2, \frac{1}{4}k^2(r - 2r_1)^2\right] + 2r_1(r - 2r_1) \bar{}_pF_q\left[\frac{1}{2}; 1, \frac{3}{2}; \frac{1}{4}k^2(r - 2r_1)^2\right] \quad (4.14)$$

Where, $\bar{}_0F_1$ is the Hypergeometric ${}_0F_1$ regularized function, and $\bar{}_pF_q$ is the Hypergeometric PFQ function (the generalized Hypergeometric function).

Finally, the flow rate of each phase can be found as:

$$\begin{cases} q_o = \int_0^{r_1} 2\pi v_o dr \\ q_w = \int_{r_1}^{r_2} 2\pi v_w dr \\ q = q_o + q_w \end{cases} \quad (4.15)$$

In order to quantify $k_{er,ow}$ as a function of water saturation, first the oil velocity and oil flow were obtained solving equations 4.12, 4.13, and 4.15 by *Mathematica 8*, and *Maple 15*,

respectively. Then, the $k_{er,ow}$ coefficient was found for the corresponding q_o for the particular water saturation using:

$$k_{er,ow} = \frac{q_o}{k_e \nabla E \, A_o} \tag{4.16}$$

Where, A_o is the cross-sectional area of the oil phase.

Figure 4.7 shows the velocity profiles at the wall-liquid interface for a capillary with the radius of 0.1 mm and Sw = 0.2 for three different cases where the interface potential varies from zero to -50 mV. As observed in Figure 4.7, as the interfacial potential increases, the velocity of water in the capillary increases.

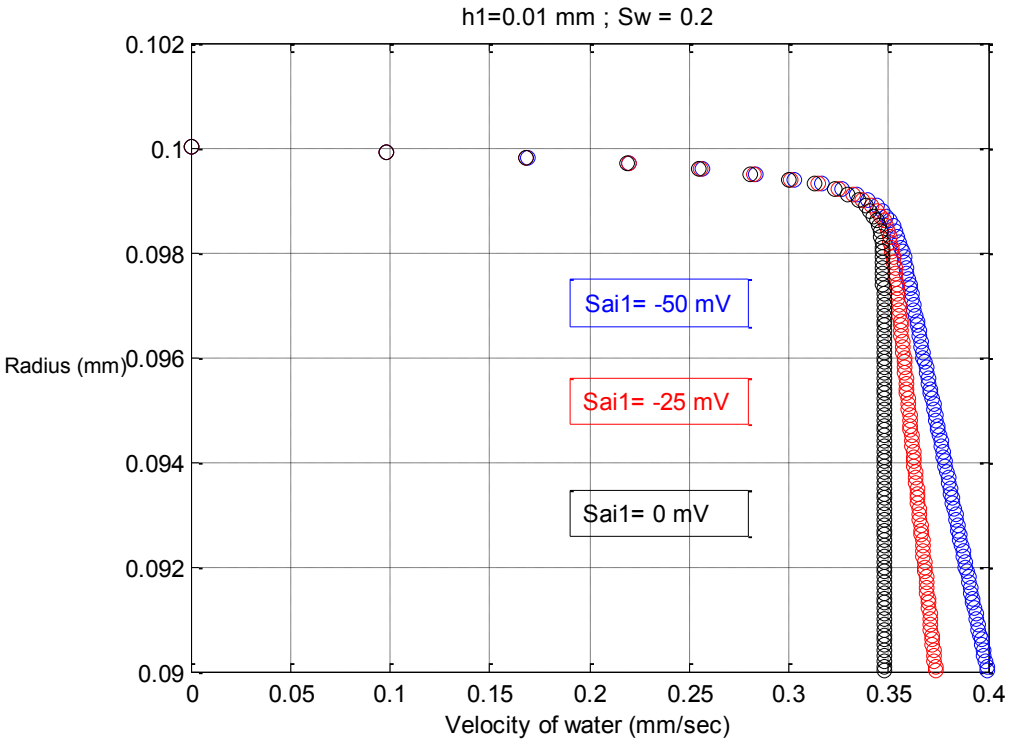

Figure 4.7. Velocity profile across the capillary

Properties of the two fluids used in the analytical evaluation of $k_{er,ow}$ coefficient are listed in Table 4.2. From equations 4.13 and 4.14, it can be discerned that the parameters affecting the fluid flow are: potential at the interface (ψ_1), potential at the wall surface (ψ_2), reciprocal of EDL thickness for the formation water (k_2), oil/water saturation (determined by the ratio of r_1 , r_2), and the radius of the capillary (r_2). Normally, as the potential at the wall and the interface increases, the electro-osmotic effect becomes noticeable which results in larger flow rates.

Table 4.2. Properties of the two fluids used in the parametric study

Parameter	unit	value
Oil		
Dynamic viscosity of oil (μ_o)	pas-sec	38.7 x 10^{-3}
Vacuum permittivity (ε)	Faraday/m	8.854 x 10^{-12}
Permittivity of oil (ε_o)	F/m	~3ε
Formation water		
Element charge (e)	C	1.6 x 10^{-19}
Boltzman constant (K_B)	J/K˚	1.38 x 10^{-23}
Dynamic viscosity of water (μ_w)	pas-sec	10^{-3}
Permittivity (ε_w)	F/m	~87ε
Working temperature (T)	K˚	293
Ionic concentration (n)	M	1 x 10^{-6}

The capillary size, surface potential and water and oil saturation are important input parameters for the analytical solution of the coupling coefficient. The pore throat size of common reservoir rocks varies within the range of 1 to 30μm [62, 80, and 94]. The pore throat size distribution of a core sample can be obtained using image analysis techniques [45]. Although the bundle of capillary tube modeling approach does not represent the realistic flow behavior of the porous medium, it is reasonable to apply this model for the problem at hand with the assumptions

that, i) each capillary may have a different radius (r_c), ii) all capillaries have the same orientation, and iii) there is no intersection between the capillaries. For the evaluation of $k_{er,ow}$ coefficient in this study, a constant nominal capillary radius of 10μm was adapted to represent the mean diameter of the pore throat size of the cores tested.

The zeta potential of common water wet reservoir rock minerals (quartz, kaolinite, and calcite) in contact with connate water varies within the range of -50 to +50 mV [73, and 76]. In this analysis, the representative channel wall surface potential was set to -25 mV. The interface between water and non-polar oil could possess substantial negative charge even in the absence of chemicals that reduce surface tension [49]. Hydroxyl ions, released by the dissociation-association equilibrium of the water molecules adsorb at the oil-water interface and create a negatively charged layer whose magnitude strongly depend on pH [49, and 76]. The magnitude of this interface charge depends largely on the ionic composition of the aqueous phase, while the nature of the oil phase is of secondary importance. Typical range of the interface potential is $-20^{+/-}$ 5 mV [49]. In this analysis, the oil-water interfacial potential was set at 0 mV and -15 mV, for two separate solution schemes.

Water and oil saturations were found based on their respective volume fractions in the capillary. The volume fractions of these components were varied by changing the values of r_1 and r_2. Figure 4.8 shows the velocity profile for half of the capillary for the case when the charge density at the oil-water interface is set to zero (ψ_1=0 mV). As observed in Figure 4.8, the oil velocity profile is constant which results in plug flow and the water velocity increases within EDL length and remains constant across the capillary. The velocity profile for when the interface possess charge (ψ_1=-15 mV) is shown in Figure 4.9. In this case, the water velocity increases

across the capillary which results in higher water flow. The oil flow remains as plug flow, but at increased quantity as expected.

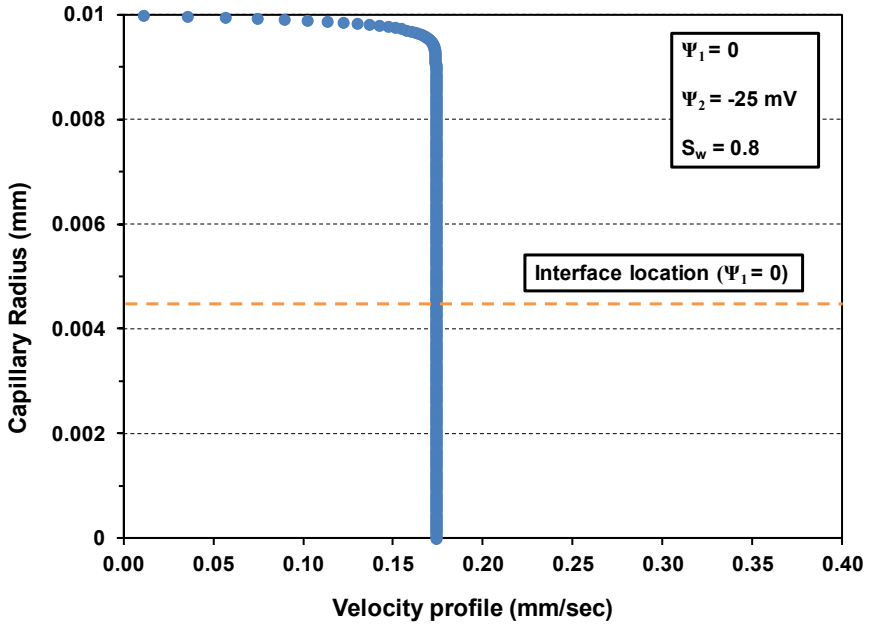

Figure 4.8. Velocity profile across the capillary (zero interface potential)

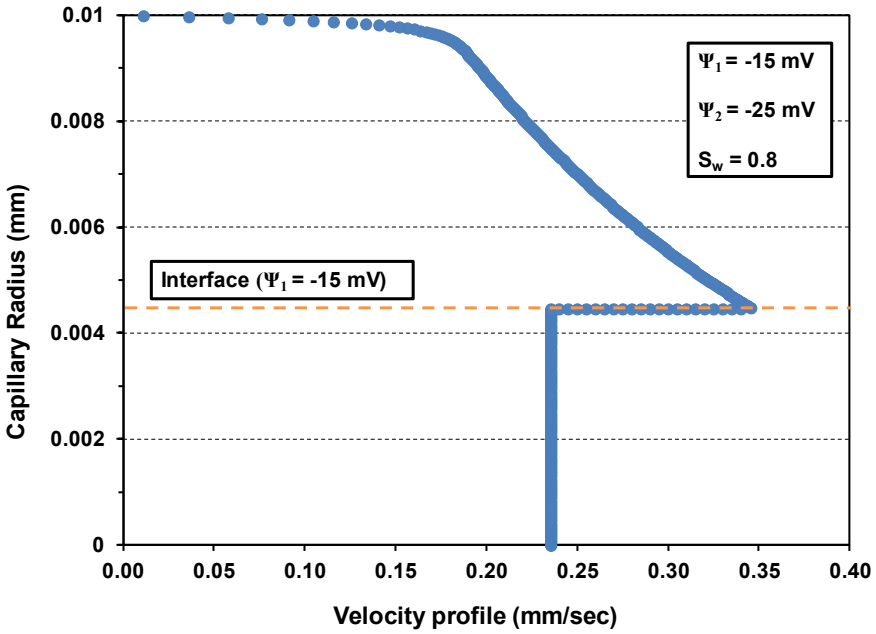

Figure 4.9. Velocity profile across the capillary (with interface potential)

Figure 4.10 shows the analytically evaluated $k_{er,ow}$ coefficient as a function of water saturation. As also observed in the case of experimentally evaluated $k_{er,ow}$ coefficient (see Figure 4.3), the coefficient increases with increasing in water saturation initially, to slightly over 0.1 at 50% water saturation. The coefficient decreases beyond the 50% saturation, because of less oil available in the capillary to be produced. The behavior and the magnitudes of the experimentally and the analytically determined coefficient of oil-water coupling are very similar over the range of water saturation they were evaluated, as shown in Figure 4.3 and Figure 4.10, respectively.

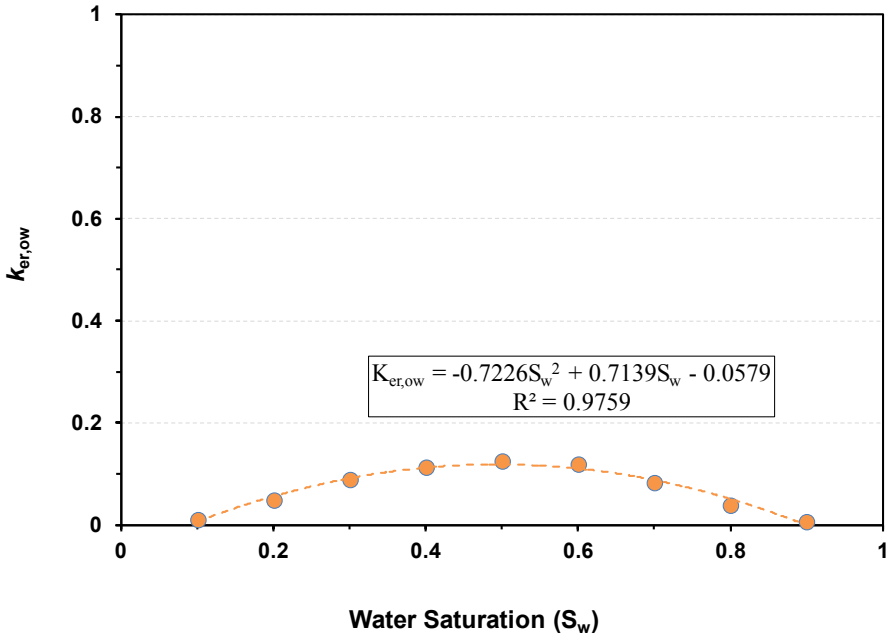

Figure 4.10. Analytically evaluated $k_{er,ow}$ coefficient as a function of water saturation

In a general case, the magnitude of the dynamic viscosity of oil and the hydrodynamic drag at the oil-water interface are expected to change over the duration of the oil recovery, hence

the actual coefficient would be expected to deviate from the predicted ones over time. Also, it should be noted that the complex geometry of the pore structure of reservoir rock can't be modeled accurately through bundle of capillary representation. But, the close agreement of the experimental and analytical approaches presented here for evaluation of $k_{er,ow}$ coefficient provides evidence for a useful initial estimate of the coefficient.

4.6. Scaling Issues in evaluation EO transport coefficients for reservoir simulation

The introduced experimental and analytical evaluation of the generalized EO permeability coefficients aim to provide a base to development of the constitutive relationships in the electrically enhanced oil recovery (EEOR) reservoir simulation. It should be noted that reservoirs are strongly heterogeneous and anisotropic. The up-scaling issues in EEOR reservoir simulation remain the same as other conventional methods (e.g. vertical averaging of the petro-physical properties).

The viable current densities used in practical applications of EEOR are in the range of 1-1.5 Amp/m^2. The current density used in the experiments in this study was 1 Amp/m^2. The properties of the brine solution used in the laboratory experiments were adjusted to be as close as possible to the formation water in actual reservoirs. Also, the formation rock and formation oil used in the experiments were actually taken from an oil field in Pennsylvania to represent the real formation characteristics. Despite these preliminary precautions, obviously, there are still some scaling issues between the laboratory experiments and reservoir scale. Two of the major differences are provided in the following section.

The applied DC current in the laboratory scale over the course of the experiment is fairly uniform and conveniently manageable. The distribution of electric field strength is uniform and

temporal and spatial fluctuations in electric field intensity are not a concern. However, in the reservoir scale, the current density is not uniform in the formation and temporal and spatial fluctuations of electric field intensity affects the oil production which in turn makes the laboratory developed relative permeability coefficients not accurately representing the entire reservoir and for the duration of production.

The temperature within the formation in the laboratory scale is fairly constant and the thermal effects are negligible. However, in the reservoir scale, the thermal effects could be significant, specifically in the regions close to injection and production wells where the electrodes are inserted. This effect is particularly important if the applied power to the reservoir lasts for a long time which could generate significant heat due to formation resistivity in the regions close to injection and production well. This thermal effect is not accounted for in the laboratory experiments reported in this study.

Chapter 5

Numerical Implementation

Commonly used numerical methods for solving two phase flow partial problems include i) *finite difference method*, in which functions are represented by their values at certain grid points and derivatives are approximated through differences in these values, ii) *method of lines,* where all but one variable is discretized and the result is a system of ODEs in the remaining continuous variable, iii) *finite element method*, where functions are represented in terms of basic functions and the PDE is solved in its integral form, and iv) *finite volume method*, which divides space into regions or volumes and computes the change within each volume by considering the flux (flow rate) across the surfaces of the volume [5, 13, 16, 26, 28, 46, and 66].

When applied to reservoir simulation, finite difference method (FDM) can be very easy to implement and in its basic form is restricted to handle only rectangular shapes. The method introduces considerable geometrical error and grid orientation effects. Finite element method (FEM), on the other hand can handle complicated geometries, and reduces the grid orientation effects. The quality of a FEM approximation is often higher than in the corresponding FDM approach. However, it is not easy to implement and is slower than FDM [13, 26, 28, 46, and 66].

In finite volume method (FVM), physical quantities are calculated at control volumes and the method is conservative (i.e. the flux entering a given volume is identical to that leaving the adjacent volume). The method can easily be formulated to allow for unstructured meshes. FVM is in between FDM and FEM, faster and easier to implement than FEM; and more accurate and versatile than FDM [15, 26, and 28].

The finite volume method is used in this study for numerical simulation of flow. In this chapter, numerical modeling of single and two phase flow using finite volume method are discussed.

5.1. Finite Volume Method (FVM)

The finite volume method is a discretization method which is well suited for the numerical simulation of various types (e.g. elliptic, parabolic or hyperbolic) of conservation laws [15, 26, 28, and 66]. The method has been extensively used in several engineering fields, such as fluid mechanics, heat and mass transfer or petroleum engineering. Some of the important features of the finite volume method are similar to those of the finite element method [15, 26, 28, and 66]. The method may be used on arbitrary geometries, using structured or unstructured meshes [37, and 66]. An additional feature of the method is the local conservation of the numerical fluxes.

Local conservation of the numerical fluxes makes the finite volume method an attractive choice when modeling problems for which the flux is of importance, such as in fluid mechanics. The finite volume method is locally conservative because it is based on a balance approach [6, 11, 28, 66, and 70]. In fact, a local balance is written on each discretization cell which is often called control volume. By the divergence formula, an integral formulation of the fluxes over the boundary of the control volume is then obtained. The fluxes on the boundary are discretized with respect to the discrete unknowns.

In classical finite-difference methods, partial differential equations (PDEs) are approximated by replacing the partial derivatives with appropriate divided differences between point-values on a discrete set of points in the domain [6, 11, 26, 28, 36, 66, and 70]. Finite-volume methods are derived from conservation of physical quantities over cell volumes. Thus, in

a finite-volume method the unknown functions are represented in terms of average values over a set of finite-volumes, over which the integrated PDE model is required to hold [6, 11, 26, 28, 36, 66, and 70].

A finite-volume method can be viewed as a conservative finite-difference scheme that treats the grid cells as control volumes. One of the simplest schemes of finite volume method is a cell-centered finite-volume method, which is also referred to as the two-point flux-approximation scheme [6, 11, 26, 28, 36, 66, and 70]. This method is widely used in the petroleum industry which is also used in this study.

5.2 FVM method for single phase flow

The following elliptic equation for single phase flow of water was derived in chapter 3 (Eq. 3.3):

$$\nabla . v_w = -\nabla . \left[\frac{\mathbf{K}}{\mu_w}(\nabla P_w - \rho_w g \nabla z)\right] = \frac{q_w}{\rho_w} \tag{5.1}$$

To derive a set of finite-volume mass-balance equations for Equation 5.1, denote by Ω_i (a grid cell in Ω), consider the following integral over Ω_i:

$$\int_{\Omega_i}(\frac{q_w}{\rho_w} - \nabla . v_w)dx = 0 \tag{5.2}$$

Invoking the divergence theorem and assuming that v_w is sufficiently smooth, Equation 5.2 transforms into the following mass-balance equation [6, 11, 26, 28, and 66]:

$$\int_{\partial\Omega_i} v_w.n.dv = \int_{\Omega_i} \frac{q_w}{\rho_w} dx \tag{5.3}$$

Where, n is the outward-pointing unit normal on $\partial\Omega_i$. Corresponding finite-volume methods are now obtained by approximating the pressure P_w with a cell-wise constant function $P_w = \{P_{w,i}\}$, and estimating $v_w.n$ across cell interfaces ($\gamma_{ij} = \partial\Omega_i \cap \partial\Omega_j$)from a set of neighboring cell pressures [11, 26, and 66]. To formulate the two-point flux-approximation (TPFA) finite volume scheme that is frequently used in reservoir simulation, it is convenient to reformulate Equation 5.1 slightly to the following form [11, 26, and 66]:

$$-\nabla.\lambda\nabla u = f \tag{5.4}$$

Where, $\lambda = \frac{\mathbf{K}}{\mu_w}$, u is the flow potential (e.g. $u_w = P_w + \rho_w g z$), and $f = \frac{q_w}{\rho_w}$. Now, the model can be expressed as:

$$-\nabla.\lambda\nabla u_w = \frac{q_w}{\rho_w} \tag{5.5}$$

Equation 5.4 can be solved for u. The TPFA scheme uses two points, the cell-averages u_i and u_j, to approximate the flux as:

$$v_{ij} = -\int_{\Omega_{ij}} \lambda\nabla u\,.n.dv \tag{5.6}$$

A regular hexahedral grid with gridlines aligned with the principal coordinate axes is considered in this study. Also, it is assumed that γ_{ij} is an interface between adjacent cells in the

x–coordinate direction so that $n_{ij} = (1,\ 0,\ 0)^T$. The gradient ∇u on γ_{ij} in the TPFA method can now be replaced with the following expression:

$$\delta u_{ij} = \frac{2(u_j - u_i)}{\Delta x_i + \Delta x_j} \tag{5.7}$$

Where, Δx_i and Δx_j denote the respective cell dimensions in the x-coordinate direction. Substituting Equation 7 in 6, the following expression for v_{ij} is obtained:

$$u_{ij} = \delta u_{ij} \int_{\gamma_{ij}} \lambda dv = \frac{2(u_j - u_i)}{\Delta x_i + \Delta x_j} \int_{\gamma_{ij}} \lambda dv \tag{5.8}$$

In most reservoir simulation models, the permeability **K** is cell-wise constant, and is not well-defined at the interfaces [6, 11, 13, 26, 46, and 66]. Therefore λ needs to be approximated on γ_{ij}. In the TPFA method, to approximate λ on γ_{ij} , a distance-weighted harmonic average of the respective directional cell permeability ($\lambda_{i,ij} = n_{ij}.\lambda_i n_{ij}$ *and* $\lambda_{j,ij} = n_{ij}.\lambda_j n_{ij}$) can be used [26, and 66]. The n_{ij} directional permeability (λ_{ij}) on γ_{ij} is computed as follows:

$$\lambda_{ij} = \left(\Delta x_i + \Delta x_j\right) * \left(\frac{\Delta x_i}{\lambda_{i,ij}} + \frac{\Delta x_j}{\lambda_{j,ij}}\right)^{-1} \tag{5.9}$$

For orthogonal grids with gridlines aligned with the coordinate axes, the flux v_{ij} in the TPFA method can be approximated as:

$$v_{ij} = -|\gamma_{ij}|\lambda_{ij}\delta u_{ij} = 2|\gamma_{ij}|\left(\frac{\Delta x_i}{\lambda_{i,ij}} + \frac{\Delta x_j}{\lambda_{j,ij}}\right)^{-1}(u_i - u_j) \tag{5.10}$$

By summing over all interfaces to adjacent cells, an approximation to $\int_{\partial\Omega_i} v_w.n.dv$ can be found and the associated TPFA method is obtained by requiring the mass balance equation (Eq. 5.3) to be satisfied for each grid cell $\Omega_i \in \Omega$. In the reservoir simulation literature, the flux v_{ij} is usually expressed in a more compact form and terms that do not involve the cell potentials (u_i) are usually gathered into an interface transmissibility t_{ij} [13, 26, 66, and 70]. In the TPFA method, the transmissibility is defined as [11, 13, 26, and 66]:

$$t_{ij} = 2|\gamma_{ij}|\left(\frac{\Delta x_i}{\lambda_{i,ij}} + \frac{\Delta x_j}{\lambda_{j,ij}}\right)^{-1} \tag{5.11}$$

Inserting the expression for t_{ij} into Equation 5.10, the TPFA scheme for equation 5.4, seeks a cell-wise constant function $u = \{u_i\}$ that satisfies the following system of equations:

$$\sum_j t_{ij}\,(u_i - u_j) = \int_{\Omega_i} \frac{q_w}{\rho_w} dx \tag{5.12}$$

This system is symmetric and can be made positive definite with preserving the symmetry by forcing $u_1 = 0$ [11]. This can be achieved by adding a positive constant to the first diagonal of the matrix $\mathbf{A} = [a_{ik}]$, where:

$$a_{ik} = \begin{cases} \sum_j t_{ij} & if\ k = i \\ -t_{ik} & if\ k \neq i \end{cases} \tag{5.13}$$

The matrix **A** is sparse and consists of a tridiagonal part corresponding to the *x*-derivative, and two off-diagonal bands corresponding to the *y*-derivatives. A simple code can be developed and used to solve equation 5.12 using TPFA scheme.

5.3 FVM for two phase flow

The pressure and saturation equations for the case of applied pressure gradient were derived in chapter 3 and are expressed respectively as:

$$-\nabla.\{\mathbf{K}\lambda\nabla P - \mathbf{K}(\lambda_w\rho_w + \lambda_o\rho_o)g\nabla z\} = q \tag{5.14}$$

$$\varphi\frac{\partial S}{\partial t} + \nabla.[f(S)v - \mathbf{K}\lambda_o f(S)(\nabla P_c + (\rho_o - \rho_w)g\nabla z)] = \frac{q_w}{\rho_w} \tag{5.15}$$

These equations form a model consists of pressure equation (Eq. 5.14) and saturation equation (Eq. 5.15). The equations are nonlinearly coupled. The coupling is primarily through the saturation-dependent mobility λ_α in the pressure equation and through the pressure-dependent velocities v_α in the saturation equation. However, the equations are also coupled through other terms that depend on pressure or saturation (e.g. viscosities and capillary and complementary pressures).

As discussed in chapter 3, in a sequential approach, each equation is solved separately and different methods can be used to discretize the two fundamentally different equations. The IMPES (implicit pressure, explicit saturation) method is a popular method in the petroleum industry [6, 11, 13, 26, and 66].

For the global pressure and total velocity formulation of incompressible and immiscible two-phase flow, a sequential splitting method in the following steps can be used [6, 11, 13, 26, 46, and 66]. First, the saturation distribution from the previous time step (or initial data) is used to

compute the saturation-dependent coefficients in pressure equation, before the equation is solved for global pressure and total velocity. Then, the total velocity v is kept constant as a parameter in saturation equation, while the saturation is advanced in time. Next, the new saturation values are used to update the saturation-dependent coefficients in pressure equation, and the pressure equation is solved again, and so on.

Different numerical schemes can be developed for pressure and saturation equations without being concerned about the nonlinear coupling between the two equations. The advantage of a sequential method is its efficiency and potential spatial accuracy and its disadvantage is the splitting errors introduced by decoupling the equations [6, 11, 13, 26, 46, and 66]. In some cases (gas-dominated reservoirs), splitting errors may lead to unphysical flow predictions, unless very small splitting steps are used [13, 26, 46, and 66]. To avoid this, an extra loop for each time step can be used and iterated a few times until convergence is achieved between solving the pressure and saturation, before moving on the next time step. The corresponding method is called sequential implicit method [6, 11, 13, 26, 46, and 66]. In the following section, the sequential splitting method is used for simulation of simple two-phase model.

5.4. Discretizing the Pressure Equation

To discretize the pressure equation with a finite-volume method, terms corresponding to gravity are moved to the right-hand side and the single-phase formulation (5.14) is expressed as:

$$-\int_{\partial\Omega_i} \mathbf{K}\lambda(S^k{}_w)\nabla P^{k+1} dv = \int_{\Omega_i} q\, dx - \int_{\partial\Omega_i} \mathbf{K}\{\lambda_w(S^k{}_w)\rho_w + \lambda_o(S^k{}_w)\rho_o\} g\nabla z.n.\, dv \qquad (5.16)$$

Where, the superscript k represents the time step. The integrals over the cell boundaries can be computed with a TPFA scheme, as presented for the single-phase flow in sections 5.2. For the case of two phase flow, the pressure equation may be discretized with the same method used to discretize the single-phase pressure equation (sections 5.2). The main difference between the two cases is that for two-phase flow, the pressure is a dynamic function of saturation, and must therefore be solved repeatedly throughout the simulation.

5.5. Discretizing the Saturation Equation

In reservoir simulations, algorithms for solving the pressure equation usually accounts for the majority of the computational time [6, 11, 13, 26, 46, and 66]. Most commercial reservoir simulators use an implicit or semi-implicit time discretization to evolve saturation profiles in time, while a conservative finite volume method is used to resolve the spatial derivatives. Considering a cell Ω_i with edges γ_{ij} and associated normal vectors n_{ij} pointing out of Ω_i, using the θ-rule for temporal discretization (i.e. θ=0, explicit scheme; θ=1, fully implicit scheme; and θ=1/2, Crank-Nicholson scheme), a finite-volume scheme takes the following general form [13, 26, and 28]:

$$\frac{\varphi_i}{\Delta t}\left({S_i}^{k+1} - {S_i}^{k}\right) + \frac{1}{|\Omega_i|}\sum_{j\neq i}[\theta\, F_{ij}(S)^{\,k+1} + (1-\theta)F_{ij}(S)^{\,k}] = \frac{q_i({S_i}^{k})}{\rho} \tag{5.17}$$

Where, φ_i is the porosity in Ω_i, q_i denotes the source term, Δt is the time step, and ${S_i}^{k}$ is the cell-average of the water saturation at time $t = t_k$,

$${S_i}^{k} = \frac{1}{|\Omega_i|}\int_{\Omega_i} S(x, t_k)dx \tag{5.18}$$

F_{ij} is a numerical approximation of the flux over edge γ_{ij} expressed as:

$$F_{ij}(S) \simeq \int_{\gamma_{ij}} f(S)_{ij}[v_{ij} + d_{ij}(S) + g_{ij}(S)].n_{ij}dv \tag{5.19}$$

Where, $f(S)_{ij}$ represents the fractional-flow function associated with γ_{ij} , v_{ij} is the Darcy flux, d_{ij} the diffusive flux, and g_{ij} the gravitational flux across the edge.

Different finite-volume schemes can be defined and used for the edge integrals in equation 5.19. For a first-order scheme, it is common to use upstream weighting for the fractional flow such as [6, 11, 13, 26, 46, and 66]:

$$f(S)_{ij} = \begin{cases} f(S)_i & if\ v.n_{ij} \geq 0 \\ f(S)_j & if\ v.n_{ij} < 0 \end{cases} \tag{5.20}$$

If θ is set to zero in the temporal discretization, the resulting scheme is a first-order explicit scheme which could be an accurate scheme with stability restrictions imposed on the time step [6, 11, 13, 26, 46, and 66]. To avoid the time-step restriction, one can use implicit schemes for which $\theta > 0$. For instance, $\theta = 1$ gives a fully implicit scheme. However, this introduces other difficulties such as excessive numerical diffusion for large time steps and also the need for a fast solver for the corresponding nonlinear system of equations [6, 11, 13, 26, 46, and 66]. In this study a first order explicit scheme is used.

5.6. Implicit and explicit solver

In this section sequential IMPES formulation of an incompressible and immiscible two-phase flow system is discussed. Displacement of oil in a reservoir filled with oil through water

injection is simulated. For simplicity, gravity and capillary forces are neglected. Under these assumptions, equations 5.14 and 5.15 reduce to the following system of equations:

$$-\nabla.\{\mathbf{K}\lambda(s)\nabla P\} = q \tag{5.21}$$

$$\varphi\frac{\partial S}{\partial t} + \nabla.[f(S)v] = \frac{q_w}{\rho_w} \tag{5.22}$$

Since only water is injected and the production would be a mixture of oil and water, the source term for the saturation equation becomes:

$$\frac{q_w}{\rho_w} = \max(q,0) + f(s)\min(q,0) \tag{5.23}$$

Expressions for the saturation dependent quantities need to be supplied to these equations. The following simple analytical expressions will be used [23, and 31]:

$$\lambda_w(s) = \frac{(S^*)^2}{\mu_w} \qquad \lambda_o(s) = \frac{(1-S^*)^2}{\mu_o} \qquad S^* = \frac{S-S_{wc}}{1-S_{or}-S_{wc}} \tag{5.24}$$

Where S_{or} is the irreducible oil saturation (i.e. the lowest oil saturation that can be achieved by displacing oil by water), and S_{wc} is the connate water saturation (i.e. the saturation of water trapped in the pores of the rock during formation of the rock).

The TPFA scheme can be simply programmed to solve equation 5.21. In fact, the only difference between the single phase and two phase flow (Eq. 5.4, and 5.21) is that the input K to be used in the code in two phase flow case (corresponds to $\mathbf{K}\lambda$) depends on saturation. This dependence involves the viscosities μ_w and μ_o, the irreducible oil saturation S_{or}, and the connate water saturation S_{wc}.

For the saturation equation, a finite-volume scheme with the following form can be used:

$$s_i^{n+1} = s_i^n + (\delta_x^t)_i[\max(q_i, 0) - \sum_j f(s^m)_{ij} v_{ij} + f(s_i^m)\min(q_i, 0) \quad (5.25)$$

Where, v_{ij} is the total flux (for oil and water) over the edge ij between two adjacent cells (Ω_i and Ω_j), f_{ij} is the fractional flow function at γ_{ij} which can be evaluated using the upwind discretization in equation 5.20, and $(\delta_x^t)_i$ is defined as:

$$(\delta_x^t)_i = \frac{\Delta t}{\Phi_i |\Omega_i|} \quad (5.26)$$

By specifying the time level m in the evaluation of the fractional flow functions, either an explicit ($m = n$) or a fully implicit ($m = n + 1$) scheme can be obtained.

5.7. Two phase flow under applied pressure and electric gradients

The same TPFV finite volume schemes used to solve the pressure and saturation equations are used in this case, except that the electroosmotic permeability tensor and the off-diagonal EO permeability coefficient are now added to the system. To incorporate the flux resulted from applied electric gradient to the reservoir, at a specific time step; first the saturation distribution in the reservoir is found using the described finite volume scheme. Then, using the Archie's law, the electrical conductivity of cells is approximated at that specific time step.

Archie's law is an empirical law in petrophysic that relates the in-situ resistivity of a reservoir rock to its porosity, water saturation, and resistivity of water through the following expression [18, 38]:

$$S_w = (\frac{R_w}{R_t})^{0.5} \Phi \quad (5.27)$$

Where, S_w is the water saturation, R_w is the resistivity of water, R_t is the true resistivity of rock, and Φ is the porosity. From equation 5.27, the electrical conductivity of the reservoir rock can be found as:

$$\sigma^*{}_t = \frac{{S_w}^2}{R_w} \cdot \frac{1}{\Phi^2} \tag{5.28}$$

Assuming a uniform electric field and current density in the reservoir, the radial distribution of potential (voltage) can be found in the reservoir. Then, the flux resulted from potential (voltage) difference in cells are found using the two TPFA scheme. Finally, the total production due to applied electrical gradient at each time step is added to the production due to the applied pressure gradient at that specific time step and so on. It should be mentioned that realistic representation of the two phase flow under applied pressure and electric gradients necessitates considering the transient behavior of the oil viscosity under applied electric field.

Chapter 6

Numerical simulation

In this chapter, several simulations are run using finite volume scheme discussed in chapter 5 via MATLAB programming. Simulations are made for a two dimensional reservoir with single phase flow, two phase immiscible flow under only applied pressure gradient, and two phase immiscible flow under applied pressure and electric gradients.

6.1. Single phase flow

Figure 6.1 shows the pressure contours for a homogeneous and isotropic reservoir. The computational domain is the unit box, $\Omega = [0\ 1]^2$. The grid contains 64*64 cells. The unit permeability tensor is considered for the entire reservoir [11]. The water is injection at the lower-left corner with unit injection rate and is produced at upper-right corner with unit extraction rate (i.e. source/sink term: q([1 4096]=[1 -1]). The no-flow condition is imposed at all boundaries. As it is observed in Figure 6.1, as the water particles flow in the direction of decreasing pressure gradient, the pressure decays from the injector (lower- left corner) to the producer (upper right corner).

Figure 6.2 shows the pressure contour distribution for the same reservoir with characteristics explained in section 6.1, but with a realistic permeability tensor. The permeability tensor used for this simulation was from actual data for a reservoir rock from SPE 10 model in Society of Petroleum Engineering database [114]. As it can be seen from Figure 6.2, the pressure

contours are different compared to Figure 6.1 and the pressure drop is higher when realistic permeability tensor is used for the reservoir.

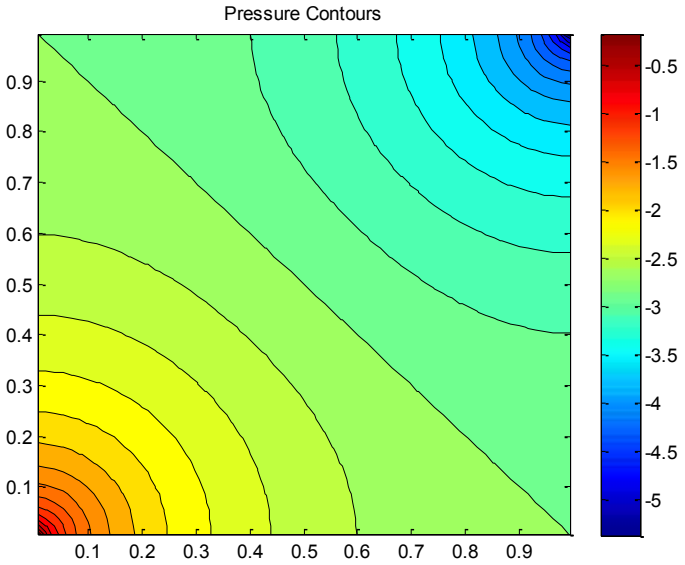

Figure 6.1. Pressure contours for a reservoir with unit permeability tensor

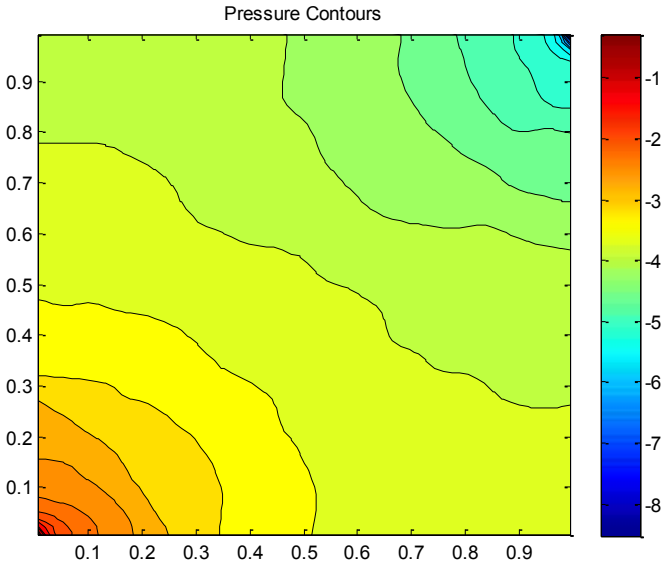

Figure 6.2. Pressure contours for a reservoir with realistic permeability tensor

6.2. Two phase immiscible flow

The fluids (water and oil) used in this simulation are assumed to be immiscible and incompressible. For simplicity, the gravity term and capillary effect are ignored in this simulation. The reservoir is assumed to have unit porosity and unit permeability and the computational domain is within the unit box, $\Omega = [0\ 1]^2$. The grid cells are 64*64. The reservoir is initially assumed to be filled with oil, and ($S_{wc} = S_{or} = 0$). Unit viscosity is considered for both water and oil. The water is injection at lower- left corner with unit injection rate and is produced at upper-right corner with unit extraction rate (i.e. source/sink term: q([1 4096]=[1 -1]). The no-flow condition is imposed at all boundaries. In this non-dimensional model, it takes one time unit to inject one pore volume of water, or in other words the time unit corresponds to the number of injected pore volumes of water [11].

Figures 6.3, 6.4, and 6.5 shows the saturation profile and corresponding pressure contours at three different time levels on a 64 by 64 grid respectively. As observed in these figures, the water breakthrough occurs after 0.7 pore volume of water have been injected. As the water displaces the oil toward the production point over time, the drop in the pressure gradient increases.

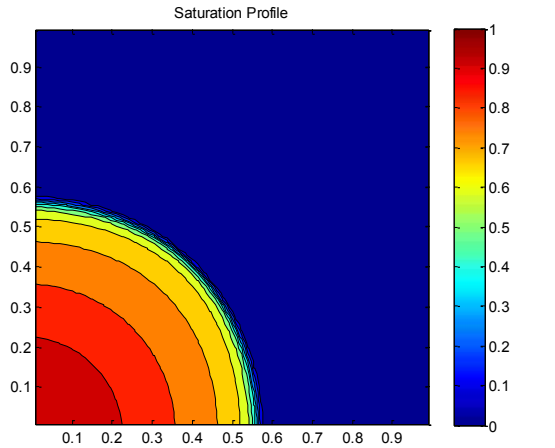

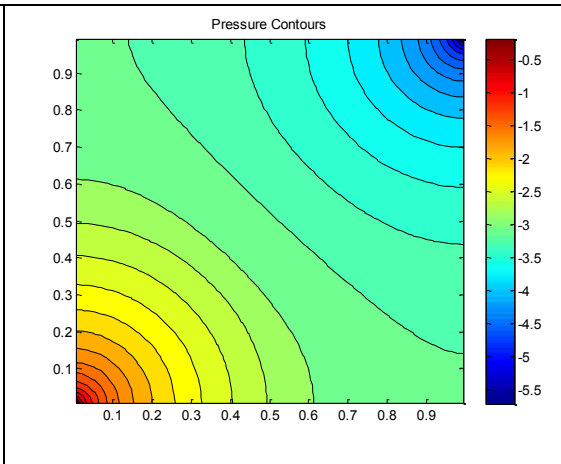

Figure 6.3 Saturation and pressure profiles at t = 0.2

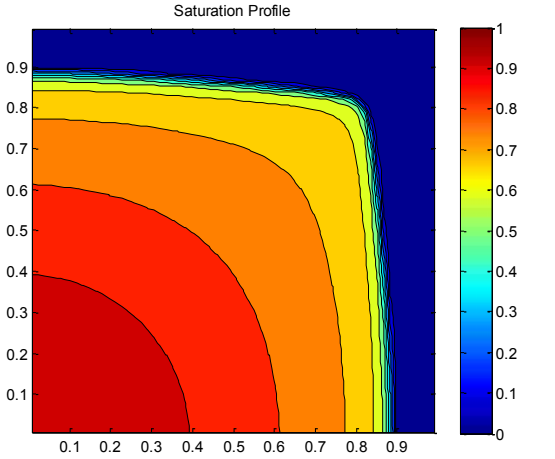

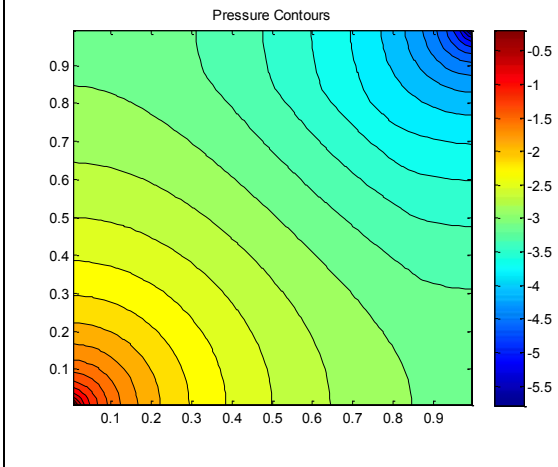

Figure 6.4. Saturation and pressure profiles at t = 0.6

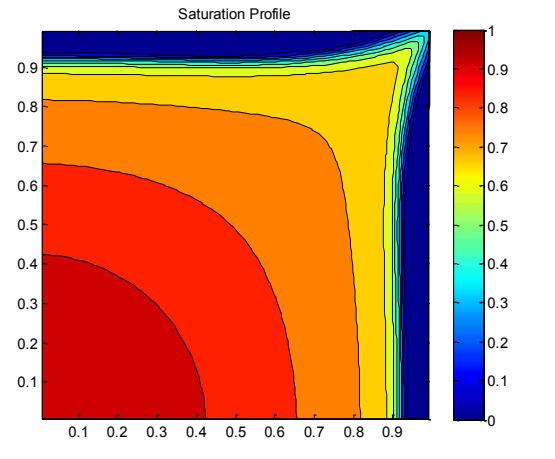

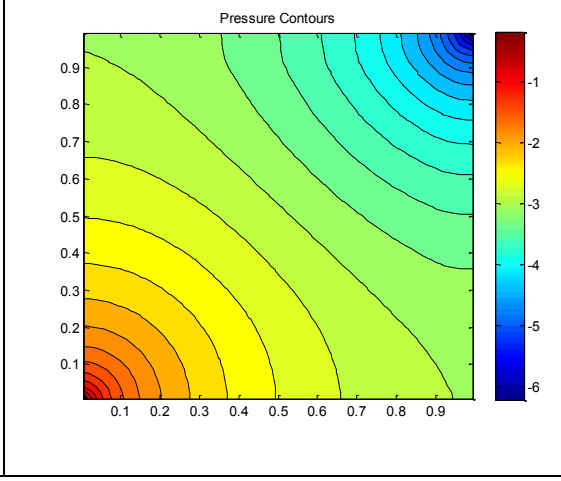

Figure 6.5. Saturation and pressure profiles at t = 0.7

6.3. Effect of viscosity ratio on flow characteristics

To investigate the effect of viscosity ratio ($M = \frac{\mu_o}{\mu_w}$) on the flow characteristics, three different viscosity ratios are used in this simulation. The same reservoir with the same conditions used in section 6.2 is used for this simulation.

Figures 6.6, 6.7, and 6.8, show the saturation profile for three different viscosity ratios of M=1 ; M=10; and M=100 respectively. As it can be seen from these Figures, the viscosity ratio significantly affect the flow. For the case where M=1, most of the oil in the reservoir is displaced after 0.7 pore volume of water have been injected, while very small amount of oil is displaced after the same injection of pore volume for case of M=100. In fact, most of the oil is still in place and extra pore volumes of water need to be injected to displace the oil for high viscosity ratios (M=10, and 100).

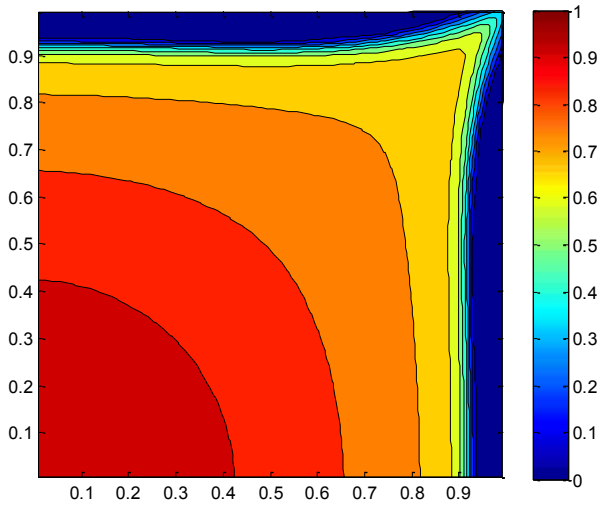

Figure 6.6. Saturation distribution at t = 0.7 for viscosity ratio of M= 1

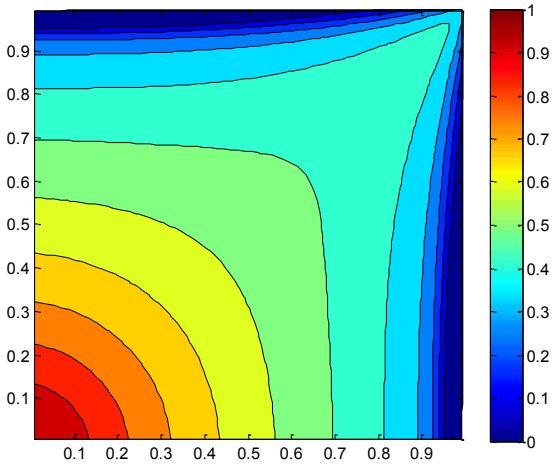

Figure 6.7. Saturation distribution at t = 0.7 for viscosity ratio of M= 10

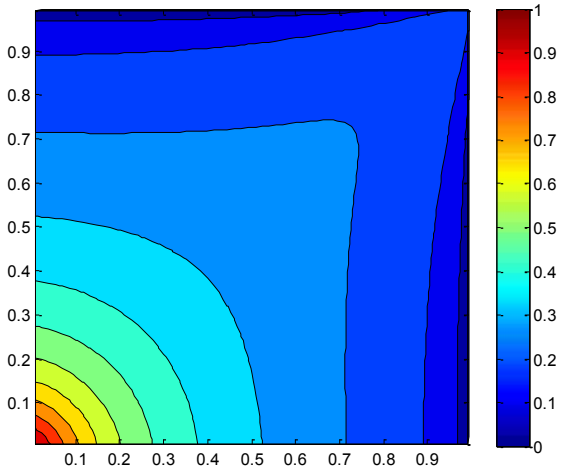

Figure 6.8. Saturation distribution at t = 0.7 for viscosity ratio of M= 100

6.3. Two phase flow under applied pressure and electric gradients

In this section, the SPE 10 model data [114] are used to simulate the two phase flow under applied pressure and electrical gradients. For two dimensional simulations, just one layer of the reservoir is selected. The actual porosity of the reservoir as well as the actual permeability

tensor from the SPE 10 model is used for the reservoir [114]. The tensor of EO permeability is assumed to be constant as $1*10^{-5}$ (cm^2/V.sec) in the entire reservoir. The EO relative permeability coefficients evaluated experimentally for core C in chapter 4 (see Figures 4.2 and 4.3) is used as representative functions of water saturation for the reservoir. The model size is 60 x 220 x 85 cells and the size of each scale cell is 20 ft x 10 ft x 2 ft. The fluids are assumed to be immiscible and incompressible.

Gravity term and capillary effect are ignored in the simulation. The initial saturations of the reservoir is assumed to be S_{wc} = 0.2 and S_{or} = 0.2. The fluid viscosities are $\mu_w = 1\ cp$ and $\mu_o = 38\ cp$. Injection is assumed at lower- left corner and production at upper-right corner and no-flow conditions are assumed at boundaries. Electric field is applied through electrodes (current density: 1 Amp/m^2) assumed to be inserted in the injection and production wells as shown in Figure 6.9.

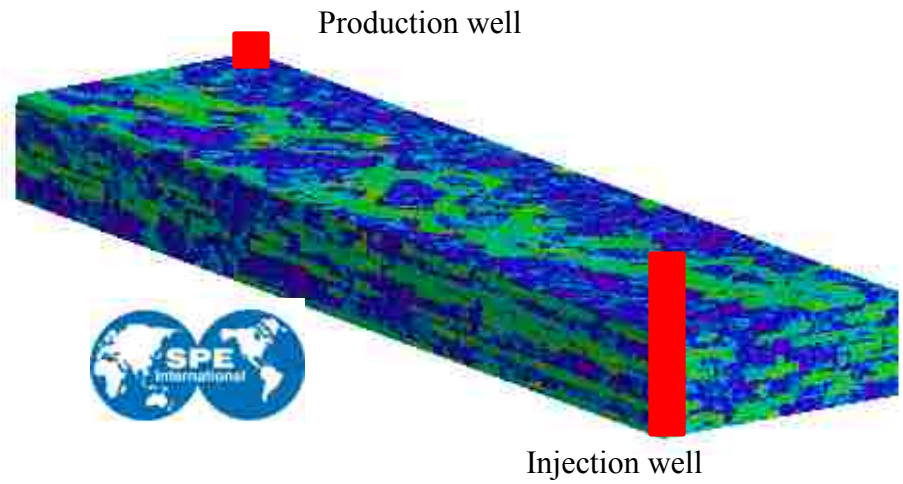

Figure 6.9. Schematic of reservoir and well locations

The saturation, production, and oil recovery profiles at three different times are shown in Figures 6.10, 6.11, and 6.12 respectively. In these Figures, the left hand side graph shows the saturation profile, the middle graph shows the changes in the production profile over time including the fractional flow of water and oil, and the right hand side graph shows the variation of oil recovery (%) with pore volumes of injected water. To investigate the contribution of applied electric field to the oil recovery, two different cases are considered and developed in the oil recovery graph: i) only pressure gradient is applied to the reservoir (blue dots), ii) electric gradient is superimposed on top of pressure gradient (i.e. both pressure and electrical gradients are applied to the reservoir). It should be mentioned that for realistic simulation, the absolute EO permeability tensor as well as the EO relative permeability coefficients as a function of water saturation are necessary for each cell within the reservoir.

As it can be seen from Figure 6.10, after 100 days of water injection, the water is gradually displacing oil toward the production well, but most parts of the reservoir are still filled with oil. The fractional flows of oil and water are 1 and 0 respectively, which means all of the production at this stage is oil and the water has not reached the production well yet. Looking at the oil recovery changes versus water injected pore volumes, only about 5% of the original oil in the reservoir has been extracted. Also, there is no discernible difference in the oil recovery between the two cases after 100 days which is attributed to the fact that most parts of the reservoir are still filled with oil and the water saturation in most parts of the reservoir has not reached the minimum value to activate the electroosmotic flow of water and consequently the EO drag of water on the oil.

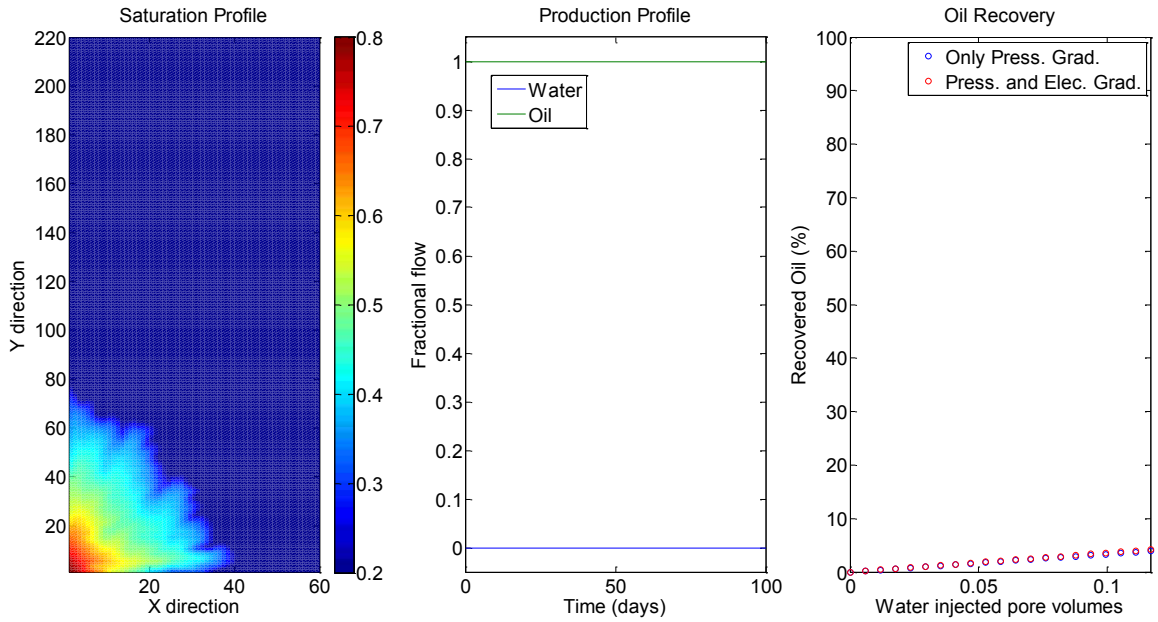

Figure 6.10. Saturation, production, and oil recovery profiles after 100 days

Figure 6.11 shows the saturation, production, and oil recovery profiles after 700 days. After about 650 days, the water has reached the production well as observed in the saturation profile and the fractional flow of water drops while that of oil increases at the same time. At this stage, the water is displacing the oil in most parts of the reservoir and only about 25% of the original oil is recovered. As observed in the oil recovery profile, the contribution of applied electric gradient is about 4% increase in the oil recovery after 700 days.

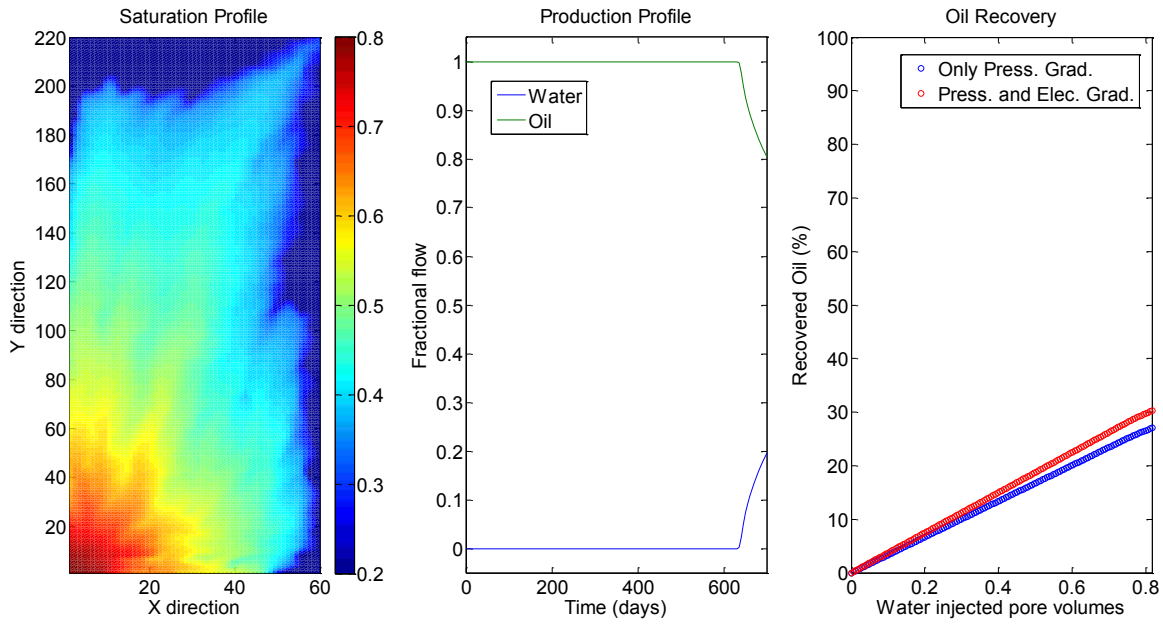

Figure 6.11. Saturation, production, and oil recovery profiles after 700 days

Figure 6.12 shows the saturation, production, and oil recovery profiles after 2500 days. After this long time, the water has filled most parts of the reservoir as observed in the saturation profile. The fractional flow of water is about 0.9 and that of oil is about 0.1 as observed in the production profile which indicates that 90% of production is water and only 10% of the production is oil. About 43% of the original oil in place is recovered at this time and the contribution of applied electric gradient is about 7% increase in the oil recovery as observed in the oil recovery profile.

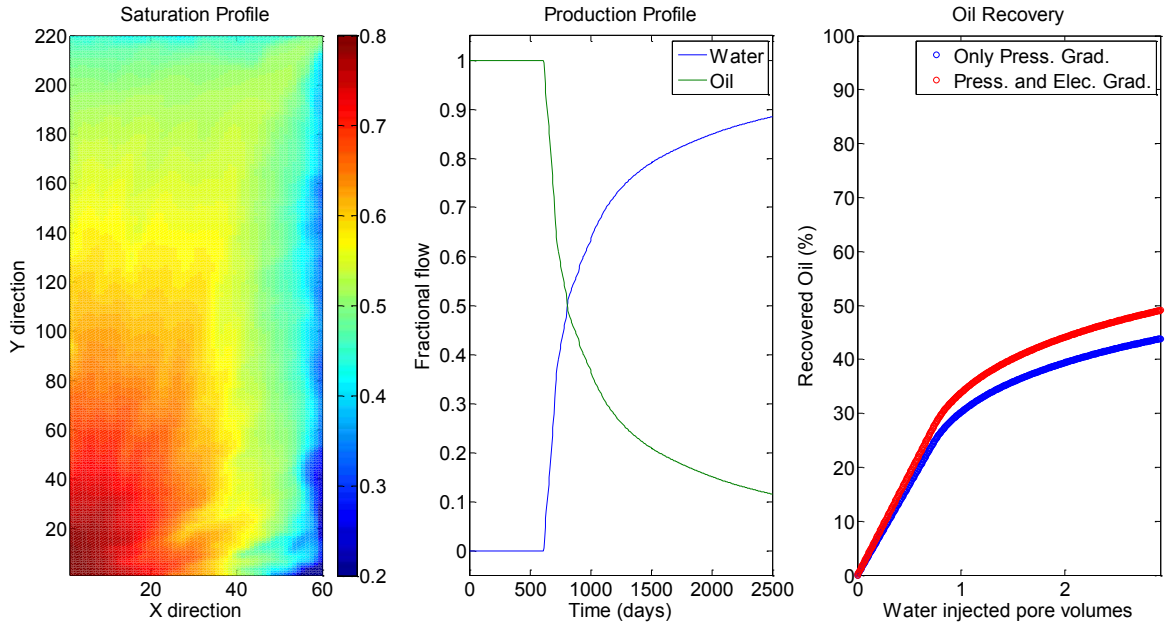

Figure 6.12. Saturation, production, and oil recovery profiles after 2500 days

Chapter 7

Summary and Conclusions

Contributing factors to the electrically assisted oil transport in porous media were found to be (i) viscous drag of oil with electro-osmosis of the water phase, primarily controlled by the oil/water ratio and the hydraulic and electro-osmotic permeability of the formation; (ii) reduction of oil-water interfacial tension due to electrochemical transformation of oil that affect its viscosity, hence increases its mobility, and (iii) increase in the permeability of the formation rock.

A mathematical model that couples the pressure and electric gradient applied to the porous medium and incorporates the viscous drag of water on the oil phase under applied electric gradient was developed. Implicit Pressure Explicit Saturation (IMPES) solution strategy was used to solve the set of governing equations. Relative permeability coefficients under applied electric field were introduced and evaluated as a function of water saturation. The main off-diagonal coefficient that captures the viscous drag of water on the oil phase which also accounts for the oil production under the applied electric field was evaluated both experimentally and analytically and its contribution to the oil production was found to be in the range of 1 to 10%.

Finite Volume Method (FVM) was used to run several simulations based on the IMPES solution strategy. The contribution of applied electric field to the oil recovery from the reservoir (SPE 10th model) was found to be in the range of 4 to 7% based on these simulations. The predictive capabilities of the model can be enhanced by having more realistic information about the reservoir condition (e.g. more accurate constitutive relationships).

Although it was attempted to capture the most important parameters in the development of the mathematical model, to have a model that more realistically represent the electrically assisted oil recovery phenomena, the transient change in the viscosity of formation oil and the non-isothermal effects should also be considered in the model for future researches.

Bibliography

[1] Acar, Y. B. and Alshawabkeh, A. N. (1996), "Electrokinetic Remediation: I. Pilot-scale Tests with Lead-Spiked Kaolinite, " ASCE, Journal of Geotechnical Engineering, Vol. 122, No. 3, pp. 173-185.

[2] Acar Y.B., Alshawabkeh, A.N., and Parker R.A., (1997), "Theoretical and Experimental Modeling of Multi-Species Transport in Soils Under Electric Fields," Technical report, EPA/600/R-97/054

[3] Ahrenholz B., Niessner J., Helmig R., and Krafczyk M., (2011), "Pore-scale determination of parameters for macroscale modeling of evaporation processes in porous media", WATER RESOURCES RESEARCH, VOL. 47, W07543, doi:10.1029/2010WR009519

[4] Al Shalabi, E. W., Haroun, M., Ghosh, B., Pamukcu, S., (2012), "The Application of Direct Current Potential to Enhancing Waterflood Recovery Efficiency", Journal of Petroleum Science and Technology, Taylor & Francis, DOI: 10.1080/10916466.2010.547902, Vol. 30, issue 20, pp. 2160-2168.

[5] Allen, M.B. (1985). "Numerical modeling of multiphase flow in porous media," Journal of advanced water resources, WWRC-85-37, Volume 8.

[6] Allen, M.B., Herrera I., and Pinder, G.F., Numerical modeling in science and engineering, John Wiley & Sons, USA (1988)

[7] Alshawabkeh, A. N. and Acar, Y. B. (1992), "Removal of Contaminants from Soils by Electrokinetics: A Theoretical Treatise, " Journal of Environmental Science and Health, A27 (7): 1835-1861.

[8] Alshawabkeh, A. N. and Acar, Y. B. (1996), "Electrokinetic Remediation: II. Theory, " Journal of Geotechnical Engineering, ASCE, 122(3): 186-196.

[9] Amba S.A., Chilingar G.V., Beeson, C. M., (1964), Use of Direct Electrical Current for Increasing the Flow Rate of Reservoir Fluids during Petroleum Recovery: Journal of Canadian Petroleum Technology, vol. 3, No. 1, pp. 8 - 14.

[10] Amba S.A., Chilingar G.V., Beeson, C. M., (1965), Use of Direct Electrical Current for Increasing the Flow Rate of Oil and Water in a Porous Medium: Journal of Canadian Petroleum Technology, vol. 4, No. 1. pp. 81 - 88.

[11] Aarnes J.E., Gimse T., Lie K., (2007) “Introduction to Multi-phase Flow in Porous Media”, Geometric Modelling, Numerical Simulation, and Optimization, Applied Mathematics at SINTEF, Springer, 2007, pp 265-306

[12] Avraam D. G., and Payatakes A. C., (1995), "Generalized Relative Permeability Coefficients during Steady-State Two-Phase Flow in Porous Media, and Correlation with the Flow Mechanisms". Journal of Transport in Porous Media 20: 135-168

[13] Aziz, K. and Settari, A., Petroleum Reservoir Simulation. Applied Science Publishers Ltd., London UK, (1979)

[14] Bard A.J., Faulkner L.R., (1980). Electrochemical Methods: Fundamentals and Applications. New York: John Wiley & Sons.

[15] Bastian P., (1999). "Numerical Computation of Multiphase Flows in Porous Media". Online text book.

[16] Baviere M., Basic Concepts in Enhanced Oil Recovery Processes, London: Elsevier Applied Science, (2007), ISBN 1-85166-617-6

[17] Bazant, M., Squires, T.M., "Induced-charge electrokinetic phenomena,". Journal of Current Opinion in Colloid & Interface Science 15 (2010) 203–213

[18] Bentsen R.G., (1998). "Effect of momentum transfer between fluid phases on effective mobility", Journal of petroleum science and engineering 21: 27-42.

[19] Bentsen. R.G., and Manai A.A. (1993), "On the use of conventional concurrent and countercurrent effective permeabilities to estimate the four generalized permeability coefficients which arise in coupled two phase flow". Journal of transport in porous media, Vol. 11, pages 243-262, 1993

[20] Brask A., Goranovic B., Bruus H., (2002), "Electroosmotically driven two-liquid viscous pump for no conducting liquids". Journal of Micro Total Analysis Systems, vol. 1, 145– 147.

[21] Brooks, R. and A. Corey (1964). Hydraulic Properties of Porous Media, Hydrology Papers, Volume 3, Colorado State University.

[22] Bruell C.J., Segal B.A., Walsh M.T. (1992), "Electroosmotic removal of gasoline hydrocarbons and TCE from clay," Journal of Environmental Engineering-ASCE 118(1):68-63

[23] Buckley, S. E. and Leverett, M. C., " Mechanisms of fluid displacement in sands, " Transactions, Americam Institute of Mining Mettalurgical and Petroleum Engineering, 1942, 146, 107-116

[24] Cao X. (1997). Numerical Modeling of Electrokinetically Enhanced Transport Mechanism in Soils. MS Thesis, Department of Civil and Environmental Engineering, Lehigh University, Bethlehem, PA.

[25] Carcoana, Aurel (1992). Applied Enhanced Oil Recovery. Prentice Hall

[26] Chen Z., Huan G., Ma Y., (2006). Computational methods for multiphase flows in porous media. Society for industrial and applied mathematics.

[27] Chilingar, G. V., El-Nassir, A., Steven, R.G. (1968), "Effect of Direct Electrical Current on Permeability of Sandstone Core". Journal of Petroleum Technology, Volume 22, Number 7, Pages 830-836

[28] Chilingar, G.V., Sang, C.K., Davis, J.E., Farhangi, H., Adamson, L.G., Sawabini, S. (1968), "Possible use of direct electric current for augmenting reservoir energy during petroleum production". Journal of Petroleum Technology , No. 4, 272-285.

[29] Corey, A. (1994). Mechanics of Immiscible Fluids in Porous Media, 3rd ed., Water Resources Publications, LLC.

[30] Crichlow H., (1977), Modern reservoir engineering- A simulation approach, Prentice Hall Inc., New Jersey

[31] Dake L.P. (1978), Fundamentals of reservoir engineering. Development in Petroleum Science

[32] Dias, M. and Payatakes, C.,"Network models for two-phase flow in porous media Part 1. Immiscible microdisplacement of non-wetting fluids," Journal of fluid mechanics, 1986, vol. 164, pp. 305-336

[33] Dullien F.A., and Dong M., (1996). "Experimental determination of the flow transport coefficients in the coupled equations of two phase flow in porous media", Journal of transport in porous media 25: 97-120

[34] Eichel H., Helmig R., Neueiler I., Cirpka O.A., "Upscaling of Two-Phase Flow Processes in Porous Media", Kluwer Academic Publishers (2004).

[35] Eykholt G.R., and Daniel D.E. (1994), "Impact of System Chemistry on Electroosmosis in Contaminated Soil, " Journal of Geotech. & Geoenviron. Eng. 120(5):797-815.

[36] Eymard R., Gallou T., and Herbin R., "Finite Volume Methods" . (2003). Handbook of Numerical Analysis, vol 7, pp 713-1020

[37] Ezekwe N. (2012), Petroleum Reservoir Engineering Practice

[38] Fleureau J.M., and Dupeyart M., (1988), "Influence of an electric field on the interfacial parameters of a water/oil/rock system: application to oil enhanced recovery". Journal of colloid and interface Science, Vol. 123, No.1, May 1988

[39] Gao Y., Wong T.N., Yang C., and Ooi K.T., (2005), "Two-fluid electroosmotic flow in microchannels". Journal of Colloid and Interface Science 284 (2005) 306–314

[40] Gao Y., Wang C., Wong T.N., Yang C., Nguyen N.T. and Ooi K.T., (2007), "Electro-osmotic control of the interface position of two-liquid flow through a microchannel". Journal of micromechanics and microengineering, 17 - 358–366

[41] Ghazanfari E., Shrestha R., Miroshnik A., Pamukcu S. (2012), "Electrically assisted liquid hydrocarbon transport in porous media". Journal of Electrochimica Acta, Vol. 86, pp. 185–191

[42] Ghazanfari, E., Pamukcu, S., Pervizpour, M., Karpyn, Z., 2012. "Investigation of generalized relative permeability coefficients for electrically assisted oil recovery in oil formations". Journal of Transport in Porous Media, 2012 (Under review)

[43] Ghazanfari, E., Miroshnik A., Shrestha R., Pamukcu S., Wittle J.K., "Investigation of underlying electrochemical processes in electrically enhanced oil recovery". Society of Petroleum Engineers Journal, 2013 (Under review)

[44] Gladkov S.O. (2003). Dielectric Properties of Porous Media. Springer, New York.

[45] Green D. P. (2009), "Extracting pore throat size and relative permeability from MRI based capillary pressure curves". International Symposium of the Society of Core Analysts, , SCA Conference Paper Number 46, 2009.

[46] Green, D.W., and Willhite, G.P., 1998. Enhanced oil recovery. SPE textbook series, Volume 6, Henry L. Doherty Memorial Fund of AIME.

[47] Haroun, M.R., and Chilingar, G.V., Pamukcu, S., Wittle, J. K., Belhaj, H. A., Al Bloushi, M. N., (2009), "Optimizing Electroosmotic Flow Potential for Electrically Enhanced Oil Recovery (EEORTM) in Carbonate Rock Formations of Abu Dhabi Based on Rock Properties and Composition". Society of Petroleum Engineers, IPTC 13812.

[48] Hassanizadeh S.M., and Gray W.G., (1990), “Mechanics and thermodynamics of multiphase flow in porous media including interphase boundaries”. Journal of advanced water resources, Vol. 13, P 169-186

[49] Haydon D. A., and Taylor F. H. (1960), "On Adsorption at the Oil/Water Interface and the Calculation of Electrical Potentials in the Aqueous Surface Phase I. Neutral Molecules and a Simplified Treatment for Ions". Phil. Trans. R. Soc. Lond. A, November 17, 1960 253 1027 255- 275;doi:10.1098/rsta.1960.0024

[50] Helmholtz H (1879). Studien uber electrische grenzschichten. Ann. Phys. Chem. 7(ser.3):337-382.

[51] Ho S.V., Athmer C., Sheridan P.W., Hughes B.M, Orth R., Mckeniz D., Brodsky P.H., Shapiro A., Thornton R., Salvo J., Schultz D., Landis R., Griffith R., Shoemaker S., (1999) "The lasagna technology for in situ-soil remediation. 1. Small field test." Journal of Environmental science and technology, 33 (7):1086-1091

[52] Host-Madsen J., Hogh Jensen K., "Laboratory and numerical investigations of immiscible multiphase flow in soil," Journal of hydrology, Vol. 135, 1992

[53] Hughe, J.M., Peter A.C. Raats, Stephen C. Cowin, "IUTAM symposium on physicochemical and electromechanical interactions in porous media," Springer, Netherland, 2005

[54] Hunter, R. J. (1981). Zeta potential in colloid science. Academic Press, New York, N.Y.

[55] Hunter RJ (2001). Foundations of Colloid Science. Oxford: Oxford University Press.

[56] Jackson M. (2010), Multiphase electrokinetic coupling: insights into the impact of fluid and charge distribution at the pore scale from a bundle of capillary tubes model, Journal of Geophysical Research, Vol. 15.

[57] Ishido T., Mizutani H. (1981), "Experimental and theoretical basis of electrokinetic phenomena in rock-water systems and its applications to geophysics", Journal of Geophysical Research and Solid Earth, Volume 86, Issue B3, pages 1763–1775.

[58] Jacobs, R. A. and Probstein, R. F. (1996), "Two-dimensional modeling of electromigration". AICHE Journal, 42(6): 1685-1696.

[59] Jihong Z., Yu Haiming Y., Wang Yanan W., Zhang Gang Z., Li Xiaobo L., (2009),"Experimental research on further enhanced oil recovery by using high DC electric field", IEEE proceedings.

[60] Joekar-Niasar V., and Hassanizadeh S.M., (2011), "Spesific interfacial area: the missing state variable in two-phase flow equasins". Journal of water resources research, Vol. 47.

[61] Kalaydjian F., (1991), "Commentary on origin and quantification of coupling between relative permeabilities for two phase flow in porous media". Journal of transport in porous media, 6:469-471.

[62] Keighin C.W. (1997) "Physical Properties of Clastic Reservoir Rocks in the Uinta, Wind River, and Anadarko Basins, As Determined by Mercury-Injection Porosimetry". U.S. geological survey bulletin 2146–G

[63] Killough L.E., Gonzalez J.A, (1986), "A fully implicit model for electrically enhanced oil recovery". Proceedings of society of petroleum engineering conference, New Orleans, LA, DOI: 10.2118/15605-MS

[64] Kim H. , and Burgess D.J., (2001), "Prediction of interfacial tension between oil mixtures and water". Journal of Colloid Interface Sci. 241(2):509-13.

[65] Kim S.O., Moon S.H., Kim K.W. (2000), "enhanced electrokinetic soil remediation for removal of organic contaminants". Journal of Environmental Technology, 21(4):417-426

[66] King P.R. (1992), The mathematics of oil recovery. Clarendon press, Oxford

[67] Koplic, J. and Lasseter, T.J., "Two-phase flow in random network models of porous media," Society of petroleum engineering journal, 1985

[68] Korolev VA, Romanyukha OV, Abyzova A.M., (2008), "Electrokinetic remediation of oil-contaminated soils," Journal of Environmental Science and Health, Part A Toxic / Hazardous Substances and Environmental Engineering, 2008 Jul 1;43(8):876-80.

[69] Lageman R (1993). "Electro-Reclamation: Applications in The Netherlands". Environ. Sci. Technol. 27(13):2648-2650.

[70] LeVeque, R. J. (2002), Finite volume methods for hyperbolic problems.

[71] Li, H., Pan, C., and Miller, C., (2005). "Pore-scale investigation of viscous coupling effects for two-phase flow in porous media". Journal of physical review, E 72, 026705

[72] Liang L., and Lohrenz J., (1994). "Dynamic method of measuring coupling coefficients of transport equations of two phase flow in porous media". Journal of Transport in porous media, 15:71-79

[73] Lichaa P. M., Alpustun H., Abdul J. H., Nofal W. A. and Fuseni A. B. (1992), "Wettability evaluation of a carbonate reservoir rock", reviewed proceedings of the Society of Core Analysis Third European Core Analysis Symposium, P.W. Worthington and C. Chardaire-Riviere (eds.), Paris (1992).

[74] Liu M., Liu Y., Guo Q., Yang J., (2009), "Modeling of electroosmotic pumping of nonconducting liquids and biofluids by a two- phase flow method". Journal of electroanalytical chemistry, Vol 636, pages 86-92

[75] Lyklema J (1995). Fundamentals of Interface and Colloid Science. Volume II: Solid-Liquid Interfaces. San Diego: Academic Press Limited.

[76] Marinova K. G., Alargova R. G., Denkov N. D., Velev O. D., Petsev D. N., Ivanov I. B., and Borwankar R. P., (1996), "Charging of Oil-Water Interfaces Due to Spontaneous Adsorption of Hydroxyl Ions". Langmuir 1996, 12, 2045-2051.

[77] Martys N. S., and Hagedorn J. G., (2002), "Multiscale modeling of fluid transport in heterogeneous materials using discrete Boltzmann methods". Materials and StructureslMatCriaux et Constructions, Vol. 35, pp 650-659.

[78] Menon, R. M. _1996_. Numerical modeling and experimental studies on electrokinetic extraction. Ph.D. thesis, Texas A&M Univ., College Station, Texas.

[79] Muraoka, T., Ghazanfari, E., Shrestha, R., Pamukcu, S., "Electrically Induced Pore Pressures in High Salt Content Clay Slurry". Separation and Purification Technology, 79 (2011) 133–138

[80] Nelson P., (2009), "Pore-throat sizes in sandstones, tight sandstones, and shales". AAPG Bulletin, Volume 93, Issue 3, Pages 329 - 340

[81] Nernst W (1888). Zur kintetik der in losung befindlichen korper. Z. Phys. Chem 2:613–637.
Neuman V., "First report on the numerical calculation of flow problems" Collected works, Taub, A.H. (ed.), Vol 5, The MacMillan Co., New York, NY, 1963, 664-712

[82] Niessner J., and Hassanizadeh S.M., (2008), " A model for two-phase flow in porous media including fluid-fluid interfacial area". Journal of water resources research, Vol. 44, w08439

[83] Pamukcu, S., 1994. "Electrokinetic Removal of Coal Tar Constituents from Contaminated Soils". EPRI TR-103320, 65p.

[84] Pamukcu S., Filipova, I. and Wittle J.K. (1995), "The Role of Electroosmosis in Transporting PAH Compounds in Contaminated Soils". Electrochemical Technology Applied to Environmental Problems, The Electrochemical Society, PV95-12, 252-266.

[85] Pamukcu, S. and Pervizpour, M. (1998) "Electroosmotically Aided Restoration of TCE Contaminated Soil," Final Report to Lawrence Livermore National Laboratory, Environmental Restoration Division, Contract No.B3460123, University of California, Livermore, Ca, November, 52p.

[86] Pamukcu S, Weeks A, Wittle JK, (2004) "Enhanced Reduction of Cr(VI) by Direct Electric Current in a Contaminated Clay," Environmental Science and Technology, 38(4), 1236-1241,

[87] Pamukcu, S., Electrochemical Transport and Transformations. Chapter 2 in Electrochemical Remediation Technologies for Polluted Soils, Sediments and Groundwater, eds. Reddy and Camaselle; John Wiley & Sons, 2009; pp. 29-65.

[88] Pfannkuch, H. O. (1972), On the correlation of electrical conductivity properties of porous systems with viscous flow transport coefficients, in Fundamentals of Transport Phenomena in Porous Media, pp. 42‐54, Elsevier, New York.

[89] Planck M (1890). Ueber die erregung von elektricitat und warme in electrolyten. Ann. Phys. Chem. 39(ser. 3):161–186.

[90] Ramstad T., Fern P., and Bakke S. (2010), "Simulation of two-phase flow in Reservoir rocks using a lattice Boltzmann method", SPE Journal, 124617

[91] Reddy, K. R., Chinthamreddy, S., and Al-Hamdan, A. Z. _2001_. "Synergistic effects of multiple metal contaminants on electrokinetic remediation of soils," Remediation, 11(3), 85–109.

[92] Revil A. N., Linde A., Cerepi D., Jougnot S.K., Matthai S., (2007), "Electrokinetic coupling in unsaturated porous media" Journal of Colloids and Interface Science, Vol. 313, pp 315-327

[93] Rubinstein I (1990). Electro-Diffusion of Ions. SIAM Studies in Applied Mathematics, SIAM, Philadelphia, PA.

[94] Rodriguez K. Araujo M. (2006), "Temperature and pressure effects on zeta potential values of reservoir minerals", Journal of Colloid and Interface Science 300 (2006) 788–794.

[95] Santiago, J.G., (2001), "Electroosmotic Flows in Microchannels with Finite Inertial and Pressure Forces". Analytical Chemistry, 73, 10, pp. 2353-2365

[96] Sato M., Kudo N., Saito M., (1998), "Surface tension reduction of liquid by applied electric field using vibrating jet method". IEEE Transactions on Industry Applications, 34(2).

[97] Saunders J.H., Jackson M.D., Pain C.C.,"A new numerical model of electrokinetic potential response during hydrocarbon recovery," Geophysical research letters, Vol. 33, L 15316, 2006

[98] Saunders J.H., Jackson M.D., Pain C.C.,"Fluid flow monitoring in oil fields using downhole measurements of electrokinetic potential," Journal of Geophysics, 2008 Vol. 73, No. 5

[99] Senneset K., Torsater O., Lone S., Wiig T.,"Two phase flow and permeability of oil in porous media" Journal of Geoenvironment, Geotechnical special publication, 2000

[100] Shapiro, A. P. and Probstein, R.F. (1993), "Removal of contaminants from saturated clay by electroosmosis". Journal of Environmental Science and Technology, 27(2): 283-291.

[101] Sheldon J.W., Zondek B., Crdwell W.T. (1959). "One dimensional, incompressible, non-capillary two phase fluid flow in a capillary, Trans., SPE AIME Vol. 216, pp. 290-296

[102] Smoluchowski M. (1914). Handbuch der Electrizitat und des Magnetismus, II. (ed. S Graetz). 2:336. Leipzig, Germany: J.A. Barth.

[103] Stevens, S., 1999. "Enhanced oil Recovery Scoping Study". EPRI Report, CA, TR-113836.

[104] Stone H.L. and Garder A.O. (1970). "Analysis of gas cap or dissolved gas reservoir". Trans., SPE AIME Vol. 222, pp. 92-104

[105] Tao R., and Xu X., (2006), "Reducing the Viscosity of Crude Oil by Pulsed Electric or Magnetic Field", Journal of Energy & Fuels 2006, 20, 2046-2051

[106] Wang P, Chen Z, Chang HC, (2006), "A new electro-osmotic pump based on silica monoliths" Sensors and Actuators B 113, 500–509.

[107] Warburg E (1899). "Ueber das verhalten sogenannter unpolarisirbarer elektroden gegen wechselstrom," Ann. Phys. Chem, 67(ser. 3):493–499.

[108] Wayne M. Ahr, Geology of carbonate reservoirs. John Wiley & Sons, Inc., 2008

[109] Wittle J.K. and S. Pamukcu, "Electrokinetic Treatment of Contaminated Soils, Sludges and Lagoons," DOE/CH-9206, No. 02112406, US Department of Energy, Argonne National Laboratories, Argonne, Il, 45p. , 1993.

[110] Wittle, J. K., Hill, D.C., and Chilingar, G.V., (2007), "Electro-enhanced oil recovery (EEOR) using direct current ", Oil sands heavy oil technologies conference, Calgary, Canada

[111] Wittle, J. K., Hill, D.C., Chilingar, G.V., (2008), "Direct Current Electrical Enhanced Oil Recovery in Heavy-Oil Reservoirs to Improve Recovery, Reduce Water Cut, and Reduce H2S Production while Increasing API Gravity", Society of Petroleum Engineers, SPE 114012

[112] Yang G.C., Liu C.Y., (2001), "Remediation of TCE contaminated soils by in-situ EK – Fenton process". Journal of hazardous materials, 137(2):1218-1225

[113] Yao S, Santiago JG, (2003), "Porous Glass Electroosmotic Pumps: Theory," Journal of Colloid Interface Science, 268, 133-142.

[114] 10th SPE Comparative Solution Project , Society of Petroleum Engineers, online reference, " http://www.spe.org/web/csp/datasets/set02.htm".

Appendices

Appendix A

A_1. Fundamental governing equations of flux under electric field

The focus of this dissertation research will be on developing a mathematical model of electrically assisted multiphase flow of petroleum hydrocarbons in porous media. To start, we review below the governing equations of fluid flux, mass flux, and charge flux under applied electric.

Fluid flux

Fluid flux due to a hydraulic gradient is given by Darcy's law as:

$$J_w^h = -k_h \frac{\partial h}{\partial x} \tag{1}$$

The total one dimensional fluid flux (Due to hydraulic and electric gradient) is:

$$J_w = k_h \nabla.(-h) + k_{eo} \nabla.(-E) = -k_h \frac{\partial h}{\partial x} - k_{eo} \frac{\partial E}{\partial x} \tag{2}$$

Mass flux

Different coupled potential gradients cause the mass flux of chemical species relative to pore fluids in porous media. Diffusional mass flux (mass transport due to chemical concentration gradient) and migrational mass flux (mass transport of charged species due to an electric potential gradient) are the main components that contribute to the mass flux of chemical species in porous media [2]. Advection (species transport by the flowing fluid) is another component of mass flux of dissolved species.

The one- dimension steady state diffusive mass flux of chemical species in a saturated soil medium under chemical concentration gradients is described by Fick's first law as:

$$J\,(x,t) = D_i \nabla.(-C) = -D\,\frac{\partial c(x,t)}{\partial x} \tag{3}$$

Where, C is concentration, x is distance, t is time, and D is diffusion constant.

The migration mass flux of the free ionic species in the soil pore fluid due to the applied electric field was given in section 2.1(electromigration) as:

$$J\,(x,t) = \; u_i C_i \nabla.(-E) = -u_i c_i \frac{\partial E}{\partial x} \tag{4}$$

The advection mass flux due to advection of species i relative to the soil particles is:

$$J_i = c_i J_w = \; c_i\,[k_h \nabla.(-h) + k_{eo} \nabla.(-E)] \tag{5}$$

The total speicies mass flux (diffusion, migration, and advection) is given as:

$$J_i = D_i \nabla.(-C_i) + u_i C_i \nabla.(-E) + c_i\,[k_h \nabla.(-h) + \; k_{eo} \nabla.(-E)] \tag{6}$$

Further simplification results in:

$$J_i = D_i \nabla.(-C_i) + C_i(u_i + k_{eo}) \nabla.(-E) + C_i k_h \nabla.(-h) \tag{7}$$

For one dimensional flow, the total mass flux of species i is given by:

$$J_i(x) = -D_i \frac{\partial c_i(x)}{\partial x} - C_i(u_i + k_{eo}) \frac{\partial E}{\partial x} - C_i k_h \frac{\partial h}{\partial x} \tag{8}$$

Charge flux

Upon application of direct current to a saturated soil medium, electric field will be generated which causes charge transport. The main components of charge flux in a saturated soil medium are migration charge flux, and diffusion charge flux (due to the diffusion mass flux of charged species). There is no contribution of the advective fluid transport in charge transport.

The electric conductance of the soil is given by Ohm's law in the simplest form. The current density in the pore fluid due to electrical gradients is given by:

$$I = \sigma^* \nabla.(-E) \tag{9}$$

Where, σ^* is the effective electric conductivity of the porous medium given as:

$$\sigma^* = \sum_{j=1}^{N_{species}} Z_j \, F \, u_j \, C_j \tag{10}$$

The migration charge flux can be related to the migration mass flux of species by using Faraday's law for equivalence of mass flux and charge flux as:

$$I = \sum_{j=1}^{N_{species}} Z_j \, F \, u_j \, C_j \nabla.(-E) \tag{11}$$

The diffusion charge flux is given as:

$$I = \sum_{j=1}^{N_{species}} Z_j \, F \, D_j \nabla.\left(-C_j\right) \tag{12}$$

The total charge flux (migration and diffusion charge flux) is given as:

$$I = F \sum_{j=1}^{N_{species}} Z_j \; D_j \nabla.\left(-C_j\right) + \sigma^* \nabla.(-E) \tag{13}$$

For one dimensional cases, the total charge flux will be:

$$I = -F \sum_{j=1}^{N_{species}} Z_j \; D_j \frac{\partial c_j}{\partial x} - \sigma^* \frac{\partial E}{\partial x} \tag{14}$$

A_2. Electrokinetic mass transport models

Alshawabkeh and Acar [7]

This is a general model for to prediction of mass transport in soil under applied direct current. The governing equation of one dimensional mass transport due to electric, hydraulic, and chemical gradient is given as:

$$\frac{\partial n C_i}{\partial t} = D_i \frac{\partial^2 C_i}{\partial x^2} + C_i \left[(u_i + k_{eo}) \frac{\partial^2 E}{\partial x^2} + k_h \frac{\partial^2 h}{\partial x^2}\right] + \frac{\partial c_i}{\partial x}\left[(u_i + k_{eo}) \frac{\partial E}{\partial x} + k_h \frac{\partial h}{\partial x}\right] + n \, R_i \tag{15}$$

The mass conservation equation is given as:

$$\frac{\partial n C_i(x)}{\partial t} = -\nabla.(J_i) + n R_i \quad (16)$$

Where, n is porosity of the media, J_i is the total mass flux of species, and R_i is the production rate of the ith aqueous chemical species per unit fluid volume due to chemical reactions such as sorption, precipitation-dissolution, oxidation/reduction, and aqueous phase reactions.

Shapiro and Probstein [100]

The model is one dimensional model developed for removal of contaminants from saturated clay. The governing equation of the resulting convective-diffusion equation is given as:

$$\frac{\partial C_i}{\partial t} = \frac{D_i}{\tau^2}\frac{\partial^2 C_i}{\partial x^2} - \frac{\partial}{\partial x}[C_i[u_{ei} + u_c] + R_i \quad (17)$$

with τ an empirical constant describing the tortuosity of the porous medium. u_c is convection velocity (the bulk electroosmotic velocity) given as:

$$u_c = \frac{1}{\tau^2}\frac{\varepsilon\xi}{\mu}(\xi\frac{\partial E}{\partial x}) \quad (18)$$

And u_{ei} is electromigration velocity given as:

$$u_{ei} = -v_i Z_i F \frac{1}{\tau^2}\frac{\partial E}{\partial x}\frac{1}{\tau^2} \quad (19)$$

Cao and Pamukcu [24]

The model was developed to investigate multispecies transport under transient electric field as an extension to the Alshawabkeh and Acar model. The governing equation of mass transport in this model is given as:

$$\frac{\partial nC}{\partial t} = D^* \frac{\partial^2 C}{\partial x^2} - E[v_m + k_{eo}]\frac{\partial C}{\partial x} - C[v_m + k_{eo}]\frac{\partial E}{\partial x} + n\,r \quad (20)$$

Where, D* is effective diffusion coefficient, K_{eo} is effective electroosmosis mobility, v_m is effective electromigration mobility, E is electric field, r is the term of chemical reaction rate.

A_3. Two phase flow in porous media

The simplest form of multiphase flow is the flow of two immiscible fluids. Consider three phases: Porous solid (R), aqueous fluid (W), and non-aqueous fluid (N). Assuming Darcy's law holds for both flows and considering the mass conservation in the system, the simplified flow equations are [5]:

$$\frac{\partial}{\partial t}(\Phi S_w \rho^w) = \nabla.\left[\rho^w \frac{k_{rw}k}{\mu_w}(\nabla P_w - \rho^w g \nabla z)\right] \quad (21)$$

$$\frac{\partial}{\partial t}[\Phi(1 - S_w)\rho^N] = \nabla.\left[\rho^N \frac{k_{rN}k}{\mu_N}(\nabla P_N - \rho^N g \nabla z)\right] \quad (22)$$

Where,

n is the porosity of the solid (i.e., porous rock) $\quad n = 1 - n_R = n_w + n_N \quad (23)$

S is fluid saturation $\quad S_w = \frac{n_w}{n}\ ,\ S_N = \frac{n_N}{n}\ ,\ S_w + S_N = 1 \quad (24)$

ρ^i is mass density of fluid i

∇ is differential operator

μ_i is dynamic viscosity of the fluid i

k is intrinsic permeability

k_{ri} is relative permeability of fluid i(coefficient describing the effect of other fluid in obstructing the flow of fluid

$$\Lambda_i = \frac{k_{ri}k}{\mu_i} \quad \text{(Mobility of fluid i)} \tag{25}$$

P_i is mechanical pressure in fluid i

$$P_{CNW} = (P_N - P_W)S_w \quad \text{(Capillary pressure)} \tag{26}$$

g is gravitation

Z is elevation

The flow equations are obviously nonlinear. Nonlinearity is a characteristic feature of multiphase porous-media flows, since the permeability of the medium to one fluid varies with the saturation of any other fluid.

A_4. Multi phase flow in porous media

In multiphase flow we could consider three phases of flow: water, oil and gas. To get the governing equation of simultaneous flow of water, oil, and air the flow equation and the mass conservation equation for individual phases should be combined.

Although Darcy's law is developed for single phase flow, flow equations could be derived by extending Darcy' law with the following assumptions [5]:

6) The gradient in phase pressure of the individual phases is a driving force of that specific force.
7) The effective permeability for the individual phases is a function of saturation of the phases involved

The governing differential equation for phase i (in an incompressible medium with constant fluid densities) could be simplified as:

$$n\frac{\partial S_i}{\partial t} = \nabla.\left[\frac{k_{ri}k}{\mu_i}(\nabla P_i - \rho_i g \nabla z)\right] \tag{27}$$

In this study, we are investigating two phase flow of immiscible fluids and we assume that there is no exchange of chemical species among the fluid phases.

A_5. Multiphase flow models in enhanced oil recovery

In the following sections some of the most accepted multiphase flow models in porous media developed for enhanced oil recovery applications are described.

Buckley-Leverett model:

The simple model is developed for two-phase flow in porous medium. The model has been used frequently in petroleum engineering since gas and water injection are among the common methods in oil recovery. The simplest multiphase flows in porous media are those in which two fluids flow simultaneously but do not exchange mass or react with the solid matrix. There are three basic assumptions associated with the model:

1) The total flow rate of oil and water (as displacing fluid) remains constant
2) The rock matrix and fluids are incompressible
3) The effect of capillary pressure gradients on the flow field are negligible compared with the pressure gradient through pumping

Buckley-Leverett saturation equation for water is given as [43]:

$$\frac{\partial S_W}{\partial t} + \frac{\partial}{\partial x}\left(\frac{q f_W}{\Phi}\right) = 0 \tag{28}$$

Where,

S_W is water saturation

q is the total flow rate $\quad q = q_W + q_O$ (29)

$f_w = \frac{\Lambda_w}{\Lambda_N + \Lambda_w}$ is the fractional flow of water (Λ_i is mobility of phase i)

(Φ) is porosity

f_W depends on the unknown water saturation(S_W). Similar flow equation for oil phase could be derived as well. Although the model is simple and useful in some cases, the assumptions associated with the model inhibit widespread application of the model in many cases.

Black oil model:

Black oil model is a multiphase fluid flow model through porous media. The model is special cases of general compositional equations that allow limited inter-phase mass transfer. The premise of the black oil model is that a highly simplified three species system could be implemented as a model representing complex mixtures of brine and hydrocarbon in oil reservoirs. The main assumptions considered in the model are [13]:

a) there are three phases: water (w), oil (o) and gas (g)
b) porous matrix and fluids are slightly compressible
c) oil phase consists of two components: non volatile oil and dissolved gas, while the water and gas phases are pure, i.e., they are compound for only one component respectively
d) diffusion will be neglected for all phases
e) it is considered that the porous medium is fully saturated, but the phases are separated in the pore space

Three black oil model equations are:

$$\Phi \frac{\partial}{\partial t}\left(\frac{S_w}{B_w}\right) + \nabla.\left(\frac{1}{B_w}u_w\right) = q_w \tag{30}$$

$$\Phi \frac{\partial}{\partial t}\left(\frac{S_o}{B_o}\right) + \nabla.\left(\frac{1}{B_o}u_o\right) = q_o \tag{31}$$

$$\Phi \frac{\partial}{\partial t}\left(\frac{S_g}{B_g} + \frac{R_{so}S_o}{B_o}\right) + \nabla.\left(\frac{1}{B_g}u_g\frac{R_{so}}{B_o}\right) = q_g \tag{32}$$

where u_α represents the volumetric phase velocity, which can be expressed by the Darcy law as:

$$v_\alpha = \frac{k_{r\alpha}k}{\mu_\alpha}(\nabla P_\alpha - \rho_\alpha g_z) \quad (33)$$

Where, n is the porosity, k is the absolute permeability of the porous system, S_α is the saturation phase, μ_α is viscosity, ρ_α is density, P_α is pressure, u_α is Darcy velocity, B_α is formation volume factor, $k_{r\alpha}$ is relative permeability, and q_α is external source term for each phase (g, o, w). R_{so} is the gas solubility, and g_z is the gravitational downward-pointing constant vector.

There are six unknowns in the equation ($P_g, P_o, P_w, S_g, S_o, S_w$). The following three equations are used to solve the system of equations.

$$S_g + S_o + S_w = 1 \quad (34)$$

$$P_{cgo}(S_g) = P_g - P_o \quad (35)$$

$$P_{cow}(S_w) = P_o - P_w \quad (36)$$

Where, P_{cgo} is gas-oil capillary pressure and P_{cow} is water-oil capillary pressure.

EEOR model:

The model is a three dimensional reservoir simulator that models the electrically enhanced oil recovery process [63]. The basic assumption in the model is that upon application of electric current to two adjacent wells the conductive oil bearing formation between the wells is heated due to electrical dissipation and results in oil viscosity reduction. The model is a non-isothermal, mulitcomponent, multiphase reservoir simulator that solves for temperature, saturation, mole fraction, pressure, and electric potential in the reservoir. The model results in a total of N independent equations to be solved.

For applied direct current: $N = N_p + N_c + 3$ (37)

Where, N_p is the number of phases and N_c is the number of components. The phases are referred by the index or subscript j (j=1 for liquid water, j=2 for oil, j=3 for gas, and j=4 for the solid phase) and the components are referred by the index or subscript i (i=2 for heavy oil component , i=3 for gaseous component, i=4 for coke if a solid component is present ; gaseous or oil component if solid component is not present)

There are five set of equations to be solved. These equations are:

a) Mass balance of components (i=1, 2, …, N_c) :

$$\frac{V}{\nabla t}\delta_t\left(n\sum_{j=1}^{N_p}\rho_j S_j X_{ij}\right)=\sum_{j=1}^{3}\nabla\tau\,\rho_j X_{ij}\frac{k_{rj}}{\mu_j}\left(\nabla P+\nabla P_{cj}-\gamma_j\nabla Z\right)-q_i \qquad (38)$$

Where, V is the finite difference cell volume, Δ is finite difference analog of Laplacian, t is time, δ_t is temporal finite difference operator, n is porosity of the reservoir, ρ_j is density of phase j, S_j is saturation of phase j, X_{ij} is mole fraction of component i in phase j, τ is fluid flow transmissibility, k_{rj} is relatve permeability of phase j, μ_j is viscosity of phase j, P is pressure of gas phase, P_{cj} is capillary of phase j, γ_j is specific weight of phase j, Z is finite difference cell depth, q_i is production rate of component i.

b) Energy balance

$$\frac{V}{\nabla t}\delta_t[\Phi\sum_{j=1}^{N_p}\rho_j S_j U_j+(1-n)M_f(T-T_i)]+\sum_{j=1}^{3}\nabla[\tau\,\rho_j\frac{k_{rj}}{\mu_j}H_j\left(\nabla P+\nabla P_{cj}-\gamma_j\nabla Z\right)+$$

$$(\tau_c\nabla T)-Q_H-Q_{HL}-Q_E \qquad (39)$$

Where, U_j is internal energy of phase j, M_f is reservoir rock heat capacity(BTU/ft^3 °F), T is temperature (°F), T_i is initial reservoir temperature (°F), H_j is enthalpy of phase j (BTU/Ib$_m$ mol), τ_c is thermal conductance, Q_H is production rate of enthalpy (BTU/D), Q_{HL} is overburden and underburden heat loss (BTU/D), Q_E is electric dissipation (BTU/D).

c) Electric current balance

For direct current $$0 = \nabla(\tau_e \nabla E) + q_e \quad (40)$$

Where, τ_e is electrical conductance of formation, E is electrical potential, and q_e is current source.

d) Saturation constraint

$$\sum_{j=1}^{N_p} \delta_t S_j = 0 \quad (41)$$

e) Mole fraction constraints (for j=1, 2, …, N_p):

$$\sum_{i=1}^{N_c} x_{ij} = 1 \quad (42)$$

By definition: $$x_{ij} = k_{vij} x_i \quad (43)$$

Where k_{vij} are equilibrium k values and x_i is the mole fraction of component i in phase j. The unknowns in the equations are :$\delta S_1, \delta S_2, \ldots, \delta S_{N_p}$; $\delta x_1, \delta x_2, \ldots, \delta x_{N_p}, \delta p, \delta T, \delta E$ (δ is finite difference operation at iteration level).

Although the model incorporates the applied direct current on the reservoir, it does not incorporate the flow phases due to electric gradient. The model mostly considers the role of applied electric field as heating the reservoir and reducing oil viscosity which results in oil production enhancement and not focus on the mass transport resulting from applied electric gradients.

A_6. Electrokinetic with single and multiphase flow in porous media

The most general relations between the fluxes of electric current density (I) and fluid volume flow density (J), and the forces of electric potential gradient ∇E and fluid pressure gradient ∇P are [56]:

$$I = -L_{ee}\nabla E - L_{ev}\nabla P \quad (44)$$

$$J = -L_{ve}\nabla E - L_{vv}\nabla P \quad (45)$$

Where, L_{ab} are the phenomenological coefficients .The term $L_{ee}\nabla E$ represents Ohm's law, and the term $L_{vv}\nabla P$ represents Darcy's law. The terms $L_{ev}\nabla P$ and $L_{ve}\nabla E$ correspond to the coupling effect.

Ishido and Mizutani model

In order to give explicit expressions of L_{ab} for a general porous medium, Ishido and Mizutani [57] took a capillary model. The model has a cross-sectional area of A (in square meters) and an overall length L (in meters) in the direction of general flow. The length of a tortuous pore channel is L_f, where $L_f > L$. The free cross- sectional area available to flow is A_f. The porosity (n) , tortuosity (t), the specific internal area S (m^{-1}), and the hydraulic radius h (m) of the sample are given as the followings:

$$n = \frac{A_f L_f}{AL} \quad ; \quad t = \frac{L_f}{L} \quad ; \quad S = \frac{S_f}{AL} \quad ; \quad h = \frac{A_f L_f}{S_f} = nS^{-1} \quad (46)$$

Where, S_f is the total internal pore surface area (m^2). The specific conductivity of the sample is given as [87]:

$$L_{ee} = nt^{-2}\sigma_f + t^{-2}S\sigma_s \quad (47)$$

Where, σ_f and σ_s are the specific conductivity of the fluid in the capillaries ($\Omega^{-1}m^{-1}$) and the specific surface conductivity respectively.

The coefficient L_{ev} (= L_{ev}) is given as [56, and 57]

$$L_{ev} = L_{ve} = -nt^{-2}\varepsilon\xi/\mu \tag{48}$$

Where, ε is the dielectric constant of the fluid (Farads per meter), μ is the viscosity of the fluid (Pascal seconds) and ξ is the zeta potential at the slipping plane in DDL (volts).

The term of L_{vv} is given by Darcy's law:

$$L_{vv} = \frac{k}{\mu} \tag{49}$$

Where, k is the permeability (m^2). Substituting the coefficients in the equation, we get:

$$I = -(nt^{-2}\sigma_f + t^{-2}S\sigma_s)\nabla E + nt^{-2}\varepsilon\xi/\mu\nabla P \tag{50}$$

$$J = (nt^{-2}\varepsilon\xi/\mu)\nabla E - (\frac{k}{\mu})\nabla P \tag{51}$$

Jackson model

The model is extension of the bundle of capillary tubes approach of Ishido and Mizutani [57]. Each capillary can have a different radius (r_c) and all capillaries have the same orientation and there is no intersection between capillaries. The model assumption is that the small capillaries are occupied by the wetting phase and large capillaries are occupied by the non-wetting phase, because the capillary entry pressure for the non-wetting phase increases with decreasing capillary radius. Also, the model assumes that the surface charge is constant in capillaries occupied by a given phase.

In this model $m(r_c)dr_c$ defines the number of capillaries of radius between r_c and $r_c + dr_c$ such that:

$$\int_{r_{min}}^{r_{max}} m(r_c)dr_c = N \tag{52}$$

The porosity (n), permeability (k), saturation of wetting phase (S_w), and relative permeability of the wetting phase (k_{rw}) are given as:

$$n = \frac{\pi t}{A}\int_{r_{min}}^{r_{max}} {r_c}^2\, m(r_c)dr_c \tag{53}$$

$$k = \frac{n}{8t^2}\frac{\int_{r_{min}}^{r_{max}} {r_c}^4 m(r_c)dr_c}{\int_{r_{min}}^{r_{max}} {r_c}^2 m(r_c)dr_c} \tag{54}$$

$$S_w = \frac{\int_{r_{min}}^{r_{w\,max}} {r_c}^2 m(r_c)dr_c}{\int_{r_{min}}^{r_{max}} {r_c}^2 m(r_c)dr_c} \tag{55}$$

$$k_{rw} = \frac{\int_{r_{min}}^{r_{w\,max}} {r_c}^4 m(r_c)dr_c}{\int_{r_{min}}^{r_{max}} {r_c}^4 m(r_c)dr_c} \tag{56}$$

Where, t is tortuosity ($t_c = \frac{L_c}{L}$), and $r_{w\,max}$ is the radious of the largest capillary occupied by the wetting phase. The conductivity of the model is the sum of the bulk and surface electrical conductivity through each capillary given as:

$$\sigma = \frac{n}{t^2}\left[\sigma_w S_w + 2\,\sigma_{sw}\frac{\int_{r_{min}}^{r_{w\,max}} r_c m(r_c)dr_c}{\int_{r_{min}}^{r_{max}} {r_c}^2 m(r_c)dr_c} + \sigma_{nw}S_{nw} + 2\,\sigma_{snw}\frac{\int_{r_{w\,max}}^{r_{max}} r_c m(r_c)dr_c}{\int_{r_{min}}^{r_{max}} {r_c}^2 m(r_c)dr_c}\right] \tag{57}$$

The streaming current is given as:

$$I_{\xi} = -\frac{\Delta P}{8tL}\left[\frac{Q_w}{\mu_w}\int_{r_{min}}^{r_{wmax}} {r_c}^4\, m(r_c)dr_c + \frac{Q_{nw}}{\mu_{nw}}\int_{r_{wmax}}^{r_{max}} {r_c}^4\, m(r_c)dr_c\right] \quad (58)$$

Where, Q_w and Q_{nw} are the excess charge per unit volume of wetting and nonwetting phases respectively. The magnitude of streaming current generated by a given fluid potential is given as:

$$j = -\sigma C \nabla P \quad (59)$$

Substituting the conductivity and streaming current, the coupling coefficient will be determined as:

$$C = \left[\frac{Q_w}{\mu_w}\int_{r_{min}}^{r_{wmax}} {r_c}^4\, m(r_c)dr_c + \frac{Q_{nw}}{\mu_{nw}}\int_{r_{wmax}}^{r_{max}} {r_c}^4\, m(r_c)dr_c\right]\{8[\sigma_w \int_{r_{min}}^{r_{wmax}} {r_c}^2\, m(r_c)dr_c +$$

$$2\,\sigma_{sw}\int_{r_{min}}^{r_{wmax}} r_c\, m(r_c)dr_c + \sigma_{nw}\int_{r_{wmax}}^{r_{max}} {r_c}^2\, m(r_c)dr_c + 2\,\sigma_{snw}\int_{r_{wmax}}^{r_{max}} r_c\, m(r_c)dr_c \quad (60)$$

Saunders model

Assuming that a single fluid is saturating the pores, the fluid flow (given by Darcy's law) and charge flow equations [97] are given as:

$$q = -\frac{k}{\mu}\nabla P - L\nabla E \quad (61)$$

$$J = -\sigma_r \nabla E - L\nabla P \quad (62)$$

Where, k is permeability of the rock, μ is the viscosity of the fluid, σ_r is the conductivity of the rock-fluid system, and the coupling term (L) is given by:

$$L = \frac{\varepsilon_f \xi}{\mu F} \quad (63)$$

Where, ε_f is fluid permittivity, ξ is zeta potential, and $F = \frac{\sigma_f}{\sigma_r}$ is the formation factor [92]

When J=0 (In steady state, when the electrical current caused by advection is balanced by electrical current caused by conduction), the streaming potential coupling coefficient is defined as:

$$C = \frac{\nabla E}{\nabla P} = \frac{L}{\sigma_r} = \frac{\varepsilon_f \xi}{\mu \sigma_f} \tag{64}$$

For two phase flow of immiscible fluids, the flow equations for the wetting and non-wetting phase are given as (without considering the contribution of the electrical potential to fluid flow):

$$J_w = -\frac{k_{rw} k}{\mu_w} (\nabla P_w - \rho_w g_z) \tag{65}$$

$$J_{nw} = -\frac{k_{rnw} k}{\mu_{nw}} (\nabla [P_w - P_c] - \rho_{nw} g_z) \tag{66}$$

Where, J_w and J_{nw} are the fluid velocity of the wetting and non wetting phases, k_{rw} and k_{rnw} are relative permeability of wetting and non-wetting phases, P_w and P_c are the pressure of wetting phase and capillary pressure, and g_z is the gravitational acceleration.

The conservation equation which considers incompressible fluids is given as:

$$\frac{\partial (n S_\alpha)}{\partial t} + \nabla J_\alpha = Q_\alpha \tag{67}$$

Q is source /sink term.

The electrical term is coupled to fluid term using the electrokinetic coupling term (L) as [92]:

$$J = -\sigma_r \nabla E - L L_r \nabla (P_w - \rho_w g_z) \tag{68}$$

Where L_r is saturation dependent relative coupling term. The L_r term is incorporated in the equation to account for partial saturation of the wetting phase.

Saunders and coworker [97] used the finite element method to solve the fluid flow and charge flow equations with no external current source.

Vita

Ehsan Ghazanfari was born in 1980 in Qom, Iran. After finishing Moalem High school in Qom, he left his father, Gholamali Ghazanfari and his mother, Khadijeh Elmi, and moved to Tehran where he attended K.N.Toosi University of Technology and received a bachelor of science in Civil Engineering in 2001.

Ehsan received his Master of Science in Geotechnical Engineering from Iran University of Science and Technology in 2004 and worked in consulting for several years before joining Lehigh University to pursue his doctoral study in 2009. He pursued his study at Lehigh for four years and received his PhD in Civil Engineering in September 2013. In addition to his PhD, Ehsan received an MCE (Master in Civil Engineering) degree from Lehigh University in January 2013.

Ehsan has been appointed as teaching assistant and adjunct instructor for different courses in civil and environmental engineering at Lehigh University. He joined the faculty of Civil and Environmental Engineering Department at University of Vermont in September 2013.